1-1-2002

Phase behavior of polyelectrolyte solutions.

Vivek M. Prabhu
University of Massachusetts Amherst

PHASE BEHAVIOR OF POLYELECTROLYTE SOLUTIONS

A Dissertation Presented

by

VIVEK M. PRABHU

Submitted to the Graduate School of the
University of Massachusetts Amherst in partial fulfillment
of the requirements for the degree of

DOCTOR OF PHILOSOPHY

February 2002

Polymer Science & Engineering

PHASE BEHAVIOR OF POLYELECTROLYTE SOLUTIONS

A Dissertation Presented

by

VIVEK M. PRABHU

Approved as to style and content by:

Murugappan Muthukumar, Chair

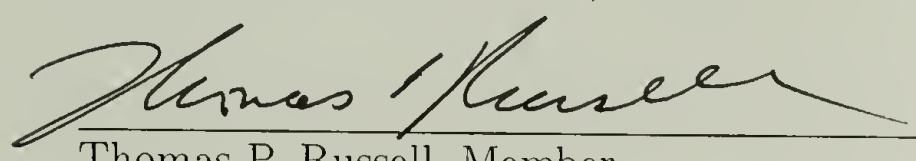

Thomas P. Russell, Member

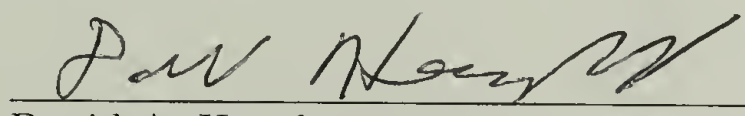

David A. Hoagland, Member

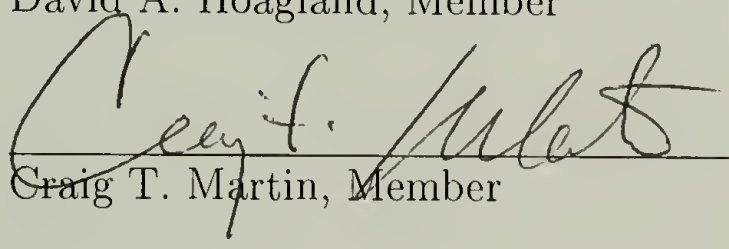

Craig T. Martin, Member

Thomas J. McCarthy, Department Head
Polymer Science & Engineering

Dedication

To my Mother for all her encouragement and to the wonderful living memory of my father, Manohar S. Prabhu.

ACKNOWLEDGMENTS

My deepest thanks go to Muthu for his patience and encouragement throughout these years. I have had an exciting five years and many rewarding experiences including course work, conferences, experimental trips to O.R.N.L, Oak Ridge, Tennessee, N.I.S.T., Gaithersburg, Maryland, and Forschungszentrum, Juelich, Germany, and stimulating discussions. I thank him for being not just an advisor, but a friend. My thanks go to Professors David Hoagland, Craig Martin and Tom Russell for serving on my committee and for their time, patience, and input regarding this dissertation.

Sincere gratitude goes to our collaborators from Oak Ridge National Laboratory, George Wignall and Yuri Melnichenko. They have taken much time and effort to introduce me to the field of neutron scattering. I learned significant lessons on neutron scattering and experimentation from them.

My fellow group members, both past and present, need to be thanked as they have provided fun both in and outside of the lab: Yvonne Akpalu, B. Ashok, Gustavo Carri, Kingshuk Ghosh, Yashodhan Hatwalne from RRI, Sonoko Kanai, Lars Kielhorn, Chester Liu, Shulan Liu, Radu Mondescu, Dirk Petera, Paul Welch. Also, those from other groups, in particular, Rick Beyer, Matt Dunbar, Heather Hayes, Vijayakumar Ramachandrarao, Sanaul Siddiquee, and Chris Stafford.

I would like to thank the N.I.H. sponsored Chemistry-Biology Interface traineeship at the University of Massachusetts for funding and providing a glance at the current challenges through course work and chalk talks.

Particular thanks go to the Materials Research Science and Engineering Center at the University of Massachusetts Amherst for providing such extensive central facilities.

ABSTRACT

PHASE BEHAVIOR OF POLYELECTROLYTE SOLUTIONS

FEBRUARY 2002

VIVEK M. PRABHU, B.S., VIRGINIA POLYTECHNIC INSTITUTE &S.U.

PH. D., UNIVERSITY OF MASSACHUSETTS AMHERST

Directed by: Professor M. Muthukumar

Due to the presence of long-ranged electrostatic interactions, polyelectrolyte solutions are characterized by a length scale in addition to the radius of gyration and the correlation length, the Debye screening length. Contrasted to the behavior observed in neutral polymer solutions in which miscibility is controlled by molecular weight and temperature, the inverse-square Debye length additionally controls polyelectrolyte phase behavior.

This thesis project experimentally investigated the influence of added barium chloride on both the collective and configurational properties of a model polyelectrolyte, sodium-poly(styrene sulfonate). Regarding the collective properties the crossover from mean field to Ising criticality close to the precipitation phase boundary was measured. This crossover was demonstrated for both salt-dependent and temperature-dependent thermodynamics. A mean field model qualitatively describes the collective behavior in polyelectrolyte solutions as a competition between a short-ranged chemical mismatch, governed by a Flory-Huggins interaction parameter, that disfavors miscibility and a repulsive screened-Coulombic interaction between monomers that favors miscibility. The addition of salt screens the

electrostatic interaction such that it becomes short-ranged, leading to the observed precipitation at fixed temperature. Similarly, for a fixed salt concentration, the solvent quality is tuned and precipitation is observed upon lowering temperature.

The configurational properties of labeled chains were also examined as a function of molecular weight, polymer concentration, and salt concentration. In solutions without any added salts, we observe scaling laws for low-ionic strength semidilute polyelectrolyte solutions in agreement with the double screening theory. These scaling laws, along with the adequate fits of the labeled chain structure factor with the Debye structure factor, highlight the concept of screening in semidilute solutions and polyelectrolytes obeys Gaussian chain statistics on length scales of the order of a renormalized Kuhn length. Significant coil contraction is measured upon the addition of the multivalent salt. Upon comparing the correlation length, the radius of gyration, and the Debye length, the radius of gyration remains the dominant length scale in the system, until a crossover is observed as the correlation length diverges and surpasses the labeled chain dimension with increased ionic strength.

The double screening theory was applied to understand the dependence of size of the labeled chains as functions of polymer concentration and added multivalent salt. It was necessary to include the influence of ion-pairing into a salt-concentration dependent degree of ionization. Such ion-pair formation is also necessary to calculate phase diagrams with better qualitative agreement with experimental data. These initial efforts should foster strong theoretical and simulation studies and further experimentation in the area of polyelectrolyte solutions.

TABLE OF CONTENTS

LIST OF TABLES

LIST OF FIGURES

CHAPTER 1

GENERAL INTRODUCTION

The influence of charges on the configurational and collective behavior of polyelectrolytes is an important subject matter which crosses all scientific and engineering disciplines. The importance of polyelectrolytes in the biological sciences in borne out in the nature of the single cell which is a "Coulomb Soup[1];" polypeptides, polynucleotides, polysaccharides, and lipids typically bear ionizable groups either along the backbone, such as the phosphates in polynucleotides, or as pendant side groups such as glutamic acid in polypeptides. The collective behavior of polyelectrolytes in the biological context sustains life through cooperative coupled transitions such as in cell division in which the charged microtubules orient in solution undergoing a persistent polymerization-depolymerization process to separate sister chromatids[2]. Such behavior may be understood as a coupling between the isotropic-nematic transition and polymerization kinetics[1].

Collective behavior also has disastrous events in biology. Our attention is drawn to the problems of aggregation and precipitation of proteins linked to neurodegerative disorders such as Creutzfeldt-Jakob disease (CJD) and Alzheimer's. In the class of disease related to CJD is prion disease. One aspect of this disease involves secondary structure in which prion proteins in a "healthy" form are dominated by α-helices and are monomeric, but these proteins may become rich in β-structure and aggregate[3].

In disease such as Alzheimer's the collective behavior of proteins leads the uncontrolled self-assembly of β-Amyloid proteins into β-Amyloid plaques which are essentially protein deposits occurring between nerve cells and entangled proteins inside nerve cells between tau proteins and tubulin; the same protein which polymerizes to form microtubules. The formation of these plaques and tangles in the brain are related to Alzheimer's disease[4].

Due to molecular biology and genetics advancements, the genes of the dominant role-players, to some degree of certainty, have been pinpointed. However, the cure or treatment of the disease is yet to be found. A strategy is to either design a drug which will break up the β-Amyloid plaques to reduce the risk of continued neurodegerative disorder, or to block the ability of the formation of the β-Amyloid protein fragments which are chemically cleaved from a high molecular weight precursor.

Admittedly, the complexity of biological problems requires a systematic study with a relevant model system, under physiological conditions. However, it is clear that both the configurational properties determined by primary, secondary, and tertiary structure and the collective properties in the form of quaternary structure and uncontrolled aggregation are key ingredients to understand. In the context of polymer physics we make an attempt to understand these classes of problems by investigating model systems in which the dominant physics is parameterized in terms of hydrophobicity, degree of ionization, and ionic strength; essentially ignoring the cascade of events which leads to the defective polymers.

In polymeric mixtures χN determines the state of miscibility, where N is the degree of polymerization and χ is the Flory-Huggins interaction parameter. Thus, the connectivity of the monomers controls the miscibility in an equivalent manner as inverse temperature. Due to this fact, uncharged model polymer mixtures have

been extensively investigated to explore the critical exponents, experimental ranges of dominance of concentration fluctuations, and the nature of the crossover from the mean field to Ising behaviors[5, 6, 7]. On the other hand, there has been little experimental study on critical phenomena of polyelectrolyte solutions, where the potential interactions among monomers are long-ranged. In systems with long-range interactions, even the nature of the universality class is not known [8, 9, 10, 11]. In addition to molecular weight, the range of the electrostatic interaction is an important variable in dictating the phase behavior of polyelectrolyte solutions.

In an effort to explore the phase behavior of polyelectrolyte solutions, we have studied experimentally, solutions of sodium-poly(styrene sulfonate) in water at different ionic strengths by controlling the amounts of added barium chloride. First, we have identified the salting out phase boundaries for a given temperature as a function of added salt and polymer concentration as well as a given salt concentration and as functions of the temperature and polymer concentration. We have then investigated using small-angle neutron scattering (SANS) the radius of gyration (Rg) of labeled polymers, the correlation length (ξ) of concentration fluctuations, and the osmotic compressibility ($\sim$I(0), scattered intensity extrapolated to zero-angle) in the homogeneous phase as the unstable phase boundary is approached.

By considering the influence of added salt ions and counter-ions of the polyelectrolyte in terms of a Debye length(κ^{-1})[12], our SANS data show that ξ and I(0) diverge as the phase boundary is approached by tuning the added salt. Similarly, for a fixed Debye length, apparent critical phenomena is observed as the phase boundary is approached by decreasing temperature. The divergence is quantified as a crossover from mean field to Ising criticality, close to the salt or temperature-dependent phase boundary. The divergence is made with respect to a critical inverse-square Debye length κ_c^2 and temperature. The solution thermodynamics is

examined by a mean field theory.

The rest of the dissertation is organized as follows; Chapter 2 contains relevant theoretical discussion. Chapter 3 describes the phase diagrams and collective behavior for salt-dependent and temperature-dependent thermodynamics. Chapter 4 contains a brief description of the labeling methodology, followed by the main results for low and high ionic strength. Chapter 5 includes opportunities for future work.

This dissertation attempts to understand the simplest case of phase behavior for a linear flexible homopolyelectrolyte; where complexities of primary and secondary structure are avoided. These issues are necessary ingredients to understand complex biological polyelectrolytes, namely nucleic acids, proteins, lipids and polysaccharides. Both experimentally and theoretically, this area of soft matter physics proves to be exciting. This dissertation is a natural first attempt to understand these things.

CHAPTER 2

MEAN FIELD THEORIES

2.1 Introduction

The present problem is one of a multi-component solution containing polymers, solvent, and added low molar mass electrolytes. In order to bring understanding and highlight essential physics, we have taken the multi-component solution as a quasi two-component system consisting of the polymer and an effective solvent. The influence of the added electrolytes is captured by the Debye length (κ^{-1}) associated with the solvent. In the presence of a bathing electrically neutral ionic medium, the bare Coulomb interaction between two point charges separated by a distance r is screened and takes on the Debye-Hückel form[12],

$$V(r) \sim \frac{1}{r} \longrightarrow \frac{e^{-\kappa r}}{r} \tag{2.1}$$

For separation distances larger than κ^{-1} the electrostatic interaction is screened. Since κ^2 is proportional to the solution ionic strength, under high salt conditions the screening length becomes short, indicating a weak electrostatic effect. This screening effect becomes coupled to the usual short-ranged excluded volume interactions. In order to understand this problem, we use the calculation of Muthukumar[19, 14] to include the effect of a screened Coulombic repulsion between monomers in addition to the usual short-ranged excluded volume interaction. It will be shown how

this Coulombic repulsion influences the scattering properties using the main results from the random phase approximation and how the Flory-Huggins chi parameter is modified to understand the spinodal phase diagrams as predicted by a Flory-Huggins theory. The premise is that we utilize the concept of screening based upon the calculations of Debye-Hückel which linearizes the Poisson-Boltzmann equation and is an exact limiting law in infinite dilution[12]. It is understood that for high concentrations of added electrolytes the Debye-Hückel theory is not applicable. However, we maintain its use to keep the problem on a conceptual basis. Any attempts to quantify the results or present qualitative remarks must bear in mind these approximations.

2.2 Random Phase Approximation

The model[13, 14]for understanding the monomer-monomer correlations begins with the potential, $V(r)$, between Kuhn segments,

$$\frac{V(r)}{k_B T} = w\delta(r) + w_c l_k^3 \frac{e^{-\kappa r}}{r} \tag{2.2}$$

The first term is the short-ranged excluded volume pseudo-potential and the second term the long-ranged electrostatic contribution. w represents the pseudo-potential strength and is equivalent to $(1/2 - \chi)l_k^3$, where χ is the Flory-Huggins interaction parameter which describes the chemical mismatch between monomer and solvent. l_k is the Kuhn statistical segment length. $\delta(r)$ is the Dirac delta function. The strength w_c is a result of modeling the polymer with a uniform charge, where each monomer is treated as a point-like object,

$$w_c = \frac{4\pi Z^2 \alpha^2 l_B}{l_k^3}, \tag{2.3}$$

where Z is the Kuhn segment valence, α is the degree of ionization, and the Bjerrum length l_B is given by $e^2/4\pi\epsilon\epsilon_o k_B T$. e is the electronic charge, ϵ and ϵ_o are the solvent dielectric constant and permittivity, respectively. Knowing the monomer valence, one can scale the theoretical valence of the Kuhn segment by the ratio of Kuhn length to monomeric contour length.

Within the Debye-Hückel approximation the dominant range of the interaction is dictated by the inverse-square Debye length κ^2,

$$\kappa^2 = 4\pi l_B N_A (Z_c^2 \alpha C_c + \sum_\gamma Z_\gamma^2 C_\gamma), \tag{2.4}$$

where N_A is Avogadro's number, Z_c and C_c are the counter-ion valence and concentration, respectively, and Z_γ and C_γ are the added salt valence and concentration, respectively, of the γ added salt ion. We have introduced the influence of the polymer counter-ions to the total solution ionic strength. This is motivated by including all randomly distributed ions which may include a fraction(αC_c) of dissociated counter-ion species. Within this description the only measure for polymer-salt interactions, such as counter-ion condensation and dissociation equilibria are parameterized by a degree of ionization of the chain through α. The concentrations C_c and C_γ are in molar units.

Upon Fourier transform of the model potential and in the limit of high salt, such that $\kappa^2 >> q^2$, where q is the scattering wavevector, the model potential becomes short-ranged[14, 15] and only modifies the understanding of the pseudopotential w. As a direct consequence of the high salt limit the Flory-Huggins interaction parameter is modified such that,

$$(1/2 - \chi) \rightarrow (1/2 - \chi_o) + \frac{w_c}{\kappa^2} \tag{2.5}$$

The new Flory-Huggins interaction parameter (χ_{Eff}) is composed of a neutral chemical mismatch (χ_o, related to the pseudopotential strength w) between monomer and solvent and an electrostatic contribution which is a function of the ionic strength (w_c/κ^2),

$$\chi_{Eff} = \chi_o - \frac{w_c}{\kappa^2} \tag{2.6}$$

χ_o is a function of temperature, usually of the form $A/T+B$ and the electrostatic term is temperature independent. Thus the temperature dependence and ionic strength dependence are separate.

Using the main results of the random phase approximation (RPA)[14, 16, 17, 18, 19, 20, 21, 22] for the effective two-component system, the form for the structure factor is,

$$S_t(q)^{-1} = \frac{1}{\phi S_D(q)} + \frac{1}{1-\phi} - 2\chi_{Eff} \tag{2.7}$$

Where ϕ is the polymer volume fraction and $S_D(k)$ is the Debye structure factor. We then introduce the effective Flory-Huggins interaction parameter, Eq.2.6 and use the Debye structure factor in $qR_G < 1$ limit. The result is,

$$S_t(q)^{-1} = \frac{1}{\phi N} + \frac{1}{1-\phi} - 2\chi_o + \frac{q^2 R_G^2}{3\phi N} + \frac{2w_C}{\kappa^2} \tag{2.8}$$

This formula reproduces the Ornstein-Zernike form,

$$S_t(q)^{-1} = A[\kappa^2][1 + \xi^2 q^2]$$

$$A[\kappa^2] = \frac{1}{\phi N} + \frac{1}{1-\phi} - 2\chi_o + \frac{2w_C}{\kappa^2} \tag{2.9}$$

$$\xi^2 = \frac{\frac{R_G^2}{3\phi N}}{A[\kappa^2]}$$

Thus one may extract the correlation length (ξ) and scattered intensity to zero angle ($I(0) \sim S(0)$) from the Ornstein-Zernike plot. Which is the analysis performed Chapter 3.

2.3 Relation to Critical Phenomena

As discussed earlier the universality class of polyelectrolyte solutions is poorly understood. We will illustrate using the mean field model that one may experimentally observe a unique situation of salt-induced criticality in addition to temperature-induced criticality. Returning to the neutral polymer case RPA predicts the correlation length to diverge,

$$\xi^2 \sim (A[T])^{-1}$$

where,

$$A = \frac{1}{\phi N} + \frac{1}{1-\phi} - 2\chi_o \tag{2.10}$$

$$A \sim 2(\chi_s - \chi_o) \sim \left(\frac{1}{T_s} - \frac{1}{T}\right) \tag{2.11}$$

where χ_s is value of the Flory Huggins interaction parameter at the spinodal temperature. As the system is brought closer to the spinodal curve by lowering temperature, ξ and $I(0)$ diverge with mean field critical indices of $\nu = 0.5$ and $\gamma = 1.0$[23].

$$\xi^{-2} \sim \left(\frac{1}{T_s} - \frac{1}{T}\right)^{2\nu} \quad \text{and} \quad S_t(0)^{-1} \sim \left(\frac{1}{T_s} - \frac{1}{T}\right)^{\gamma} \tag{2.12}$$

However, very close to the critical temperature the critical indices take on the values of the three-dimensional Ising model; $\nu = 0.63$ and $\gamma = 1.24$[23]. This crossover is observed as a deviation from the linear mean-field plot of $\xi^{-2}(\text{or} I(0)^{-1})$ versus $1/T$ where the slope is negative.

In the presented mean-field model for polyelectrolyte solutions, the Flory-Huggins interaction parameter becomes modified as given in Eq. 2.6, such that,

$$A = 2\left(\chi_s - \chi_o + \frac{w_c}{\kappa^2}\right) \sim \left(\frac{1}{T_s} - \frac{1}{T} + \frac{w_c}{\kappa^2}\right) \tag{2.13}$$

Upon replacing the expected temperature dependence for χ_o and χ_s with $1/T$ and $1/T_s$, respectively, we ignore dimensional prefactors to illustrate the dominant variables. Given the expression for A,

$$\xi^{-2} \sim \left(\frac{1}{T_s} - \frac{1}{T} + \frac{w_c}{\kappa^2}\right)^{2\nu} \quad \text{and} \quad S_t(0)^{-1} \sim \left(\frac{1}{T_s} - \frac{1}{T} + \frac{w_c}{\kappa^2}\right)^{\gamma} \tag{2.14}$$

Thus, in this case a plot of $\xi^{-2}(\text{or} S_t(0)^{-1})$ versus $1/\kappa^2$ will yield a straight line with a positive slope. Equivalently, for a fixed $1/\kappa^2$ a plot of $\xi^{-2}(\text{or} S_t(0)^{-1})$ versus $1/T$ will yield a straight line with a negative slope. Any deviation near the phase transition is attributed to the crossover from mean field to the Ising universality class as the role of fluctuations become important. This is the expected behavior in the limit of high salt where the electrostatic interactions become short-ranged. The above arguments will be used to provide a minimal quantitative measure for the solution behavior and to understand the universality class of high-salt polyelectrolyte solutions.

2.4 Limitations

The above simple theory lacks several features which increases the complexity of the problem. The first ingredient is the entropy of mixing of the added salt ions and the total electrostatic free energy. In the event of specific interactions between added salt and polymer, such as the formation of ionic bridges, several points need to be considered; any type of ion-polymer formation will reduce the number of free ions that are randomly distributed in the solution. Thus the Debye screening length will be a function of the ion-pair concentrations. Assuming a uniformly charged chain, ion-pairs will also modify the charge density of the chain, since each ion-pair will modify the local charge. For example, if a divalent cation were to bind with a monovalent anion, then the monomer charge is effectively inverted, contrasted with the case of a divalent cation bridging two anionic monomers; the charge of the chain is reduced. The formation of any stable ion-pair comes at a strong penalty of the loss of chain entropy. Thus, the configurational properties strongly couples to the underlying distribution of salt ions, through ion-pair formation. This remains an unsolved theoretical and experimental problem. A zeroth-order mean field theory to include the influence of ion-pair formation is left for Chapter 5.

2.5 Conclusions

The main results for the scattering properties of a semidilute solution of polyelectrolytes is presented based upon the random phase approximation of Edwards and introduction of the screened Coulombic interaction between Kuhn segments, as result from the double screening theory[14] consistent with the Debye-Hückel theory[12]. The introduction of the screened Coulombic interaction demonstrates

that miscibility is reduced upon the addition of salt, which screens the interaction. Thus the long-ranged effect of electrostatics, which favors the miscibility, is in competition with the Flory-Huggins interaction parameter that opposes miscibility. This competition predicts trends in the structure factor measurable by small-angle scattering, to be exploited in Chapter 3. The Flory-Huggins theory modified by introducing χ_{Eff} predicts trends observable in the phase diagrams of polyelectrolytes also demonstrated in Chapter 3.

CHAPTER 3

COLLECTIVE PROPERTIES

3.1 Introduction

In general, the structure factor ($S_t(q)$) measured in a total scattering experiment is the Fourier transform of the pair-correlation function[16] which is calculated using a random phase approximation[17]. The final form of the general scattering equation in terms of the absolute differential coherent neutron scattering cross section, I(q), is,

$$I(q) = (\frac{b^2}{v_m})S_t(q) \tag{3.1}$$

$$b = (b_m - \overline{b_s}\frac{v_m}{v_s}) \tag{3.2}$$

This form chooses the molecular volume of the monomer, v_m, as the reference volume. b, the contrast factor, is defined by Eq. 3.2, b_m is the coherent scattering length of the monomeric anion, $\overline{b_s}$ is the average coherent scattering length of the solvent, which includes the monomer counter-ions and added salt ions,and v_s is the molecular volume of the solvent. To calculate the scattering length for a given monomer one sums the coherent neutron scattering length for each atom which constitutes the monomer of interest. Examples of this are given in Appendix C.

3.2 Experimental

The polymers used throughout the study were prepared using methods described in Appendix B. The phase diagrams presented for 120,000gmol^{-1} and 56,000gmol^{-1} were poly(styrene sulfonate) standards purchased from Scientific Polymer Products, Inc and subsequently purified by dialysis, or ion-exchange. All samples used for scattering experiments were sulfonated in our laboratories. The protonated polystyrenes of molecular weight 25,000gmol^{-1}, 60,000gmol^{-1}, and 100,000gmol^{-1} were anionically prepared by Chris Stafford from the research groups of Professors T.J. McCarthy and T.P. Russell. The rest of the protonated and deuterated samples were purchased from Polymer Laboratories and Polymer Source. All characterization details are in Appendix A.

The neutron scattering experiments in this Chapter are without selective labeling. The protocol uses a fully protonated polymer in heavy water to maximize the scattering contrast and minimize contribution from incoherent scattering arising primarily from the protons. All these experiments are within the homogeneous phase. In order to examine the density-density correlations the macroscopic phase behavior was examined by visual inspection or light scattering. Thus, the salient results of the macroscopic phase behavior is discussed first, which sets up the discussion of the main experimental results.

3.3 Salt-Induced Macroscopic Phase Behavior

The following are the precipitation maps, for a fixed temperature of 294K, with barium chloride concentration (C_s) versus polymer concentration (C_p) for molecular weights 16k, 56k, 120k, and 200kgmol^{-1} in Figs. 3.1, 3.2, 3.3, and 3.4 respectively.

The filled circles indicate precipitation; the open circles a homogeneous phase. These C_s-C_p diagrams represent a convenient map for understanding the miscibility of polyelectrolytes with added salts. It is observed that these diagrams are weakly dependent on the molecular weight, as in the low salt concentration-low polymer concentration region. The C_p-independent salting-out line is a function of the molecular weight, 0.02M for 16kgmol^{-1} and 0.008M for the 200kgmol^{-1}, indicating that the high molecular weight will precipitate with slightly lower added salt at equivalent monomer concentration. In the very dilute polymer solution region, a region of miscibility is observed, particularly for 16kgmol^{-1}. In the higher polymer concentration region, a salting out line is observed, which is weakly dependent on the molecular weight. By assembling the apparent phase boundaries on a single plot, Fig. 3.5, the molecular weight dependencies of the C_s-C_p diagrams is clearly observed and the weak dependence in the semidilute region is also observed.

Similar diagrams can be constructed for other salts, such as magnesium chloride, potassium chloride, and sodium chloride for the poly(styrene sulfonate) system. These salts do not show precipitation at 294K for salt concentrations, up to saturation. Salts including lanthanum chloride[25] and calcium chloride do show precipitation. For the case of calcium chloride the precipitation is observed for added salt concentrations near the saturation limit of 6.7M. For barium chloride and lanthanum chloride the precipitation is observed well below saturation. One of the reasons for examining the miscibility of polyelectrolytes with added salt well below the saturation limit is minimize the influence of salt miscibility competing for polyelectrolyte miscibility.

The experimental observation of precipitation of polyelectrolytes is well documented in the literature, such as the work by Michaeli[26] on poly(methacrylic acid) with added divalent salt. Also the work by Delsanti et al.[25] shows added

features for sodium-poly(styrene sulfonate) with added trivalent salt. Delsanti observes an apparent envelope of immiscibility at a fixed temperature. This envelope is bordered by a salting-out line at low salt concentrations and a salting-in line at higher salt concentrations.

These macroscopic phase behaviors from the literature, and our own data, are for both monovalent and multivalent salts. Table 3.1 shows a summary of the current literature on the precipitation behavior of synthetic and natural polyelectrolytes. It illustrates that not only multivalent salts are required for precipitation. Thus the property of multivalence does not always lead to precipitation, at least under ambient conditions. The role of temperature is important to understand the phase behavior of polyelectrolytes.

3.4 Temperature-Induced Phase Behavior

Precipitated polyelectrolyte solutions were heated and found to exhibit a clearing temperature in which the precipitate dissolves leaving a homogeneous solution as shown in Figure 3.6 with a molecular weight of 120,000gmol^{-1}. For a given salt concentration these clearing temperatures for the respective monomer concentration show phase behavior similar to an upper critical solution. We will refer to them as phase diagrams even though their construction does not constitute true binodal or spinodal lines, but only as a reference, similar to cloud-point experiments.

It can be seen that the effect of increasing the level of salt concentration shifts the clearing temperatures to higher temperatures with no noticeable shift along the monomer concentration. This can be understood from the influence of the added salt is to make the solvent quality poorer, thus a higher temperature is necessary in order to enhance the miscibility. This is captured by the form of

the effective Flory-Huggins parameter, Eq.2.6. It is to be noted that for a fixed level of salt, the maximum clearing temperature for a given salt concentration is in the dilute solution limit of monomer concentration $\sim$ 0.002M. The estimation of the overlap concentration, assuming rod-like conformation yields 0.003M. Since the system has added salt due to screening of the electrostatic interaction, the true overlap concentration should be expected to be larger than 0.003M. So, the concentration for which there is a maximum in the clearing temperature is below the theoretical overlap limit. Solutions with salt concentration greater than 0.05M did not clear, even near the boiling point of water.

As a note, another diagram can be constructed by systematically cooling the samples from the homogeneous state. Upon cooling the mixtures the solutions takes on a uniformly cloudy appearance and then with time settle, at constant temperature. Once the solution becomes cloudy we then define this as the demixing temperature upon cooling. We found that the demixing temperatures upon cooling were systematically at lower temperatures than those defined by heating by $13°C$ for the peak temperatures. The meaning of this difference is unclear as the role of kinetics of precipitation remain to be explored in this system, preliminary data are given in Chapter 5.

The temperature dependence was similarly determined by Eisenberg and Mohan[27] for poly(vinyl sulfonic) acid, in the presence of added monovalent sodium chloride salt. This system demonstrates an upper critical solution temperature. Again, the role of the valence of the salt is not the only factor in the miscibility of polyelectrolytes.

3.4.1 Concluding Remarks

These macroscopic phase diagrams illustrate the importance of salt concentration, polymer concentration, and temperature. The salient features, such as the influence of salt concentration on the temperature-dependent behavior is captured by the simple model presented earlier. However, a comparison of phase diagrams is left for Chapter 5, in which the trends are easily compared from calculated and experimental phase diagrams. Quantitative agreement is lacking at this point as many issues are unresolved in particular the role of specific ion interactions and the lack of a meniscus between the precipitated phase and the clear aqueous phase upon. UV spectroscopy indicates a finite polymer concentration in the upper phase, however, the precipitated phase does not represent a classic liquid phase as one would observe in the liquid-liquid phase separation in neutral polymers such as polystyrene-cyclohexane.

3.5 SANS Results

3.5.1 Homogeneous Phase: Low Ionic Strength

Under the conditions of low ionic strength, polyelectrolyte solutions exhibit a peak in the scattering structure factor at finite wavevector. This feature is absent in neutral polymer solutions. Several theories and simulations have been proposed to describe this feature[24, 32, 33, 19, 14, 21, 20, 34, 35]. However, common to most approaches the physical origin may be qualitatively understood to be due to a balance between two types of correlations. Since, all monomers are similarly charged, they will tend to have a bare repulsion as understood from Coulomb's law (or the screened Coulombic potential). However, due to the polymeric nature

monomers are chemically connected, hence correlated. The bare repulsion and the connectivity which is described, for instance in ideal neutral polymer solutions by the Debye structure factor, gives rise to the correlation peak.

A random phase approximation that approximates the monomer-monomer density correlations predicts a correlation peak for low ionic strength polyelectrolyte solutions. In addition RPA predicts the peak shifts to lower wavevectors with decreasing polymer concentration and the peak shifts to lower wavevectors with an increase in ionic strength. However, both predictions fail to capture the correct scaling laws observed by experiment. The reason for the discrepancy is due to the nature of the RPA which does not account properly for fluctuations. The double screening theory which includes fluctuations recovers the correct scaling laws between the correlation length and polymer concentration for low ionic strength semidilute solutions. A scaling argument for the concentration dependence of the correlation length is in agreement with most experimental data in the semidilute limit as originally proposed within the isotropic model of de Gennes et al. [24]. They demonstrated first the predicted scattering peak and produced scaling arguments which agree with current experimental data[36, 37, 38] in the semidilute regime.

RPA Predictions

Using the main results from the RPA presented earlier, we may directly write the structure factor $S(q)$, and keeping the wavevector dependence of the screened Coulombic repulsion,

$$S(q)^{-1} = \frac{1}{\phi N}\frac{1}{S_D} + \frac{1}{1-\phi} - 2\chi_o + \frac{2w_C}{\kappa^2 + q^2} \tag{3.3}$$

Solving for $S(q)$ and using the Debye structure factor in the high-q, and taking $\kappa^2 < q^2$, we arrive at the following asymptotic limits that describe the essential feature.

$$S(q) = \frac{q^2}{(1/(1-\phi) - 2\chi_o)q^2 + 2w_c)} \sim q^2 \text{ at small-q} \tag{3.4}$$

$$S(q) = \frac{q^2}{\frac{q^2}{2w_c} + (\frac{Rg^2}{3\phi N})q^4} \sim \frac{1}{q^2} \text{ at high q} \tag{3.5}$$

The low q limit inspects the longer length scales, or the long-ranged Coulombic repulsion between any two monomers and tends to go as q^2. The high q limit probes the local correlations defined by the connectivity. Solving for the peak position by determining the maximum in the the structure factor, and maintaining the κ^2 dependence the following scaling argument results[34] for the peak position which defines the correlation length as functions of the polymer concentration and inverse-square Debye screening length ($\sim$ ionic strength).

$$q_{max}^2 = \left(\left(\frac{6w_C\phi N}{R_g^2} \right)^{1/2} - \kappa^2 \right) \tag{3.6}$$

In the limit of low salt, or κ^2 tending to zero,

$$q_{max}^{-1} \equiv \xi \sim \phi^{-1/4} \left(\frac{Nw_c}{R_g^2} \right)^{-1/4} \tag{3.7}$$

.

This result of $\xi \sim \phi^{-1/4}$ disagrees with the experimental facts for the correlation length in semidilute solutions. Thus, even though RPA captures the essential physics of low ionic strength semidilute polyelectrolyte solutions, it is unable to capture the correct scaling behavior. Another problem with this approach is that

it suggests that the correlation length is a function of molecular weight, which is not observed experimentally in the semidilute regime.

Scaling Predictions

The correlation length may be understood using the scaling analysis in terms of the infinite dilute solution results and the cross over function from dilute to semidilute solution, a function of $(C/C^{\star})$, where $C^{\star}$ is the "overlap"concentration which is the concentration at which the polymer chains just touch as if forming a close-packed structure. In the limit of semidilute solution the crossover function displays a power-law in which the exponent is yet to be determined. The overlap concentration is proportional to N/R_g^3 and using the scaling between molecular weight and radius of gyration simplifies the scaling ansatz to,

$$\xi \sim Rf(\frac{C}{C^{\star}}) \sim N^{\nu}(N^{3\nu-1}C)^{y} \tag{3.8}$$

Since the correlation length is independent of the molecular weight($\sim N^0$) in the semidilute limit, we obtain the following result solving for the unknown scaling exponent,y, for varying values of ν,

$$y = \frac{-\nu}{3\nu - 1} \tag{3.9}$$

The value for ν will depend upon the solvent quality and the main results are in Table 3.2. These are the predicted scaling laws for semidilute polyelectrolyte solutions. Comparison to our experimental and literature data are made in the following section.

3.5.2 Experimental Results

One data set for molecular weight 120,000gmol^{-1} is shown in Fig.3.7 to demonstrate the polyelectrolyte peak for four polymer concentrations. The data are not corrected for the flat incoherent background, as this does not change the peak position. It can easily be seen that the peak shifts to smaller q as the concentration is decreased. The low q data also show the anomalous excess scattering not predicted by theory. The discussion for this phenomena will be deferred to a later section.

The polyelectrolyte peak has been measured by various groups for a variety of highly charged synthetic polymers and biopolymers, as shown in Table 3.3. Recent work by Essafi et al.[39, 40] has demonstrated that the chemical charge density is correlated to the polyelectrolyte peak position. The experimental scaling law leads to $q_{max}^{-1} \sim \alpha^{-0.9}$. The experimental trend is in qualitative agreement with the RPA predictions, but fails with the scaling law that predicts $\xi \sim \alpha^{-1/2}$, by Eq.3.7.

We examined several molecular weights and polymer concentrations, without any added salts. At the maximum intensity of the polyelectrolyte peak, we define the inverse wavevector q_{max}^{-1} and plot versus C_p for all molecular weights and concentrations in Fig. 3.8. These experimental data clearly demonstrate the semidilute nature, under no added salts, since the correlation length is independent of the molecular weight and varies with polymer concentration as $q_{max}^{-1} = 72.6 C_p^{-0.473 \pm 0.02}$. This also suggests, experimentally the proper experimental ranges in which configurational properties may be investigated in the semidilute limit. However, with the addition of salt the calculated overlap concentration will change and possibly shift the conditions for semidilute solution.

We can further interpret these data using a scaling ansatz; since each molecular weight has a different value for the overlap concentration the experimental data

can be reduced on a dimensionless plot of ξ/L versus $C/C^\star$ as suggested by the ansatz,

$$\xi \sim N^\nu \left(\frac{C}{C^\star}\right)^y \tag{3.10}$$

Using a value for ν of 1.0 we are able to calculate $C^\star$ using the rod-like limit for the radius of gyration and nondimensionalize the abscissa. The ordinate is made dimensionless by dividing by the contour length leads to Fig.3.9. The quality of the fits over a wide range in molecular weight and concentration demonstrates the validity of the scaling ansatz.

These experimental data are without any added salts and at a fixed temperature. In the context of the state of miscibility such solutions are far from precipitation phase boundaries. As these solutions can be heated to near boiling and cooled to freezing without any onset of phase separation. In a significant and simple study, Boue et al.[46], demonstrated that the polyelectrolyte peak (magnitude of ξ) was *independent* of temperature. This is expected since the range of correlations will only increase in the proximity of the phase boundary. Hence, the correlations remain on the mesh-size length scale, familiar to neutral polymers.

Apart from the temperature independence, we have shown that with the addition of salt ξ increases consistent with previously documented experimental results [41]. However, the peak position loses the baseline resolution and broadens significantly. The experimental data taken for molecular weight 50kgmol^{-1} is shown in Fig.3.10, where the variation in q_{max}^{-1} with salt concentration and polymer concentration is shown.

These data compliment the values of the correlation length taken from the Ornstein-Zernike type correlations under high salt conditions. This brings to light

that a crossover from electrostatic dominated phase behavior to Ornstein-Zernike correlations, interpreted from the scattering structure factor under high salt. The typical scenario for polyelectrolytes which do not precipitate under the addition of salt leads to no significant increase in the correlation length. Once the polyelectrolyte peak is absent due to electrostatic screening, the only correlation length remains at the length scale of the mesh size. Preliminary data on sodium-poly(styrene sulfonate) with added sodium chloride demonstrate this behavior.

The next step is to move onto the interpretation of the small-angle scattering data to obtain the correlation length and susceptibility in the limit of high salt as the phase boundary is approached.

3.6 Homogeneous Phase: High Ionic Strength

3.6.1 Salt-Dependent Thermodynamics

We will demonstrate the salt-dependent thermodynamics for a molecular weight of 56,000 $gmol^{-1}$. Then we will show the main results for different molecular weights. The first experimental observation is that the scattered intensity is strongly dependent on the addition of barium chloride salt. The variation in the total scattering, in absolute units cm^{-1}, shown in Fig.3.11, where the increase in scattered intensity with added salt is clearly seen. The lowest salt concentration corresponding to added salt 0.125M is sufficiently high such that the expected peak at finite wavevectors is absent. In the inset the lower salt concentrations, on a logarithmic scale, illustrates the polyelectrolyte peak and influence of added salt at lower concentrations.

We quantify the scattered intensity to zero angle, I(0), and the correlation

length, ξ, using the following equation,

$$S_t(q)^{-1} = S_t(0)^{-1}(1 + \xi^2 q^2) \tag{3.11}$$

The Ornstein-Zernike plot is shown in Fig.3.12, for salt concentrations 0.125, 0.188, 0.250, 0.300, 0.325, and 0.330M. An incoherent-scattering background of 0.15cm^{-1} was subtracted as a flat background from the total scattering data. This is an estimated incoherent background from the protonated NaPSS in D_2O.

Upon investigation of the Ornstein-Zernike plots, one notices the familiar q^2 dependence similar to that observed in neutral polymers as the temperature approaches the critical temperature. Also, it is easily seen that at the lowest wavevectors a significant downturn is apparent, particularly the lower salt concentration data. This deviation (upturn on I-versus-q, downturn on Ornstein-Zernike plot) has been observed before for low-ionic strength polyelectrolyte solutions[47, 44] and neutral polymers in good solvents[48], with physical interpretation as a form factor for large aggregates. Recent SANS and osmotic pressure experiments by Horkay et al. on sodium polyacrylate hydrogels with added salts demonstrates that an analysis similar to ours was used to successfully overlap independent osmotic pressure and SANS measurements of the isothermal osmotic compressibility[49]. Theory and simulation have not explained the presence of this excess scattering. Since we are interested in the monomer-monomer correlations the experimental data was fit away from the strong excess scattering at the lowest q. $I(0)$ and ξ diverge as shown in Fig.3.13 and Fig.3.14, respectively. This divergence becomes significant close to the precipitation phase boundary. ξ increased from 5.0$\pm$1.0Å to 160$\pm$17Å between salt concentrations 0.125M and 0.330M, respectively. The divergence in $I(0)$ and ξ with increasing salt concentration is similar to that seen for neutral polymer solu-

tions on approach to the spinodal curve by varying temperature. Thus added salt in this system enhances concentration fluctuations.

3.6.2 Crossover from Mean Field to Fluctuation Regime: Divergence in ξ & I(0)

We have analyzed the divergence of $I(0)$ and ξ in the spirit of the Landau-Ginsburg theory. In a direct analogy for critical phenomena for the divergence of $I(0) \sim \epsilon^{-\gamma}$ and $\xi \sim \epsilon^{-\nu}$, where ϵ is the reduced temperature, $|(T - T_c)/T|$. We present the divergence, not with temperature, but with the solution ionic strength quantified by the inverse-square Debye length, κ^2. κ^2 is given by the experimentally convenient form, Eq. 3.12 for the 1:2 electrolyte barium chloride and sodium counter-ion. The monomer and salt concentrations, C_m and C_{salt}, respectively, are given in moles per liter of solution.

$$\kappa^2 = 4\pi l_B 1000 N_A \left(\alpha C_m + 6 C_{salt}\right) \tag{3.12}$$

As described earlier, plotting ξ^{-2} and $I(0)^{-1}$ versus $1/\kappa^2$ is a mean field plot and should reveal a straight line with positive slope if the mean field model is correct. This is precisely what is observed with the experimental data as shown in Figs 3.15 and 3.16. However, a significant deviation is seen at high salt, close to the phase boundary. This deviation signifies the importance of fluctuations, hence, a crossover to the Ising criticality. This concludes that high salt polyelectrolyte solutions are in the same universality class as neutral polymer solutions.

3.6.3 Results for 120,000gmol^{-1}

An example of the variation in scattered intensity versus wavevector as a function of added salt is given in Fig. 3.17. The main results for the three concentrations

investigated are shown in Fig. 3.18. We did not achieve significant divergence in ξ or $I(0)$ as we did not approach the precipitation boundary closely enough. However, it can be seen that the correlation length increases with added salt for all three polymer concentrations investigated. These data compliment the measurements of the radius of gyration to be presented in the next chapter.

3.6.4 Temperature-Dependent Thermodynamics

We discovered that at elevated temperatures a typical semidilute polyelectrolyte solution of the current system will appear homogeneous upon visual inspection. However, as the solution is slowly cooled a blue opalescence is observed with no signs of precipitation. Such observations are characteristic of a system with correlation length on the order of 100 nm, however, it does not tell us if the system is forming particulate matter, or experiencing strong concentration fluctuations as that observed with true critical opalescence.

Two types of experiments were performed; keeping the polymer and salt concentration fixed and monitoring the homogeneous phase as a function of temperature. Repeating this experiment for different levels of salt concentration was also performed. We have examine three molecular weights, 56,000gmol^{-1}, 120,000gmol^{-1}, and 200,000gmol^{-1}. Due to the strong dependence of both salt concentration and polymer concentration on the clearing temperature, the phase diagrams were roughly mapped using a hot plate, and in the more recent experiments an aluminum hot stage with temperature control from a re-circulating heating/cooling bath was built that accepts the quartz cells used in the SANS experiments. These experiments proved useful as the same sample could be used, rather than preparing a new sample for each experiment, which reduced the supply of polymer.

The phase diagram on the temperature-composition plane was also investigated

using both SALS and SANS. The phase diagram is shown in Fig. 3.19. This phase diagram was explored using small-angle light scattering and neutron scattering. Since, our interests lie within the semidilute solution limit and the evolution of the density correlations, it was experimentally determined a convenient range of salt concentrations and polymer concentrations to maintain temperatures within reasonable limits. From Fig. 3.19, it is observed that the precipitation temperatures continuously increase with decreasing polymer concentration. Even in the limit of dilute solution of $0.2 gL^{-1}$ the clearing temperature is near the boiling point of pure water, hence we were unable to explore this high level of salt, in the dilute solution regime of optically homogeneous solutions.

Similarly, maintaining the polymer concentration fixed, we may determine the influence of the salt concentration on the precipitation temperatures. The increase in the precipitation temperatures with increasing level of added salt is qualitatively captured by the mean field model described earlier. Fig.3.20 illustrates this discovery for a polymer concentration of $103 gL^{-1}$ and molecular weight $M_w = 200{,}000 gmol^{-1}$. Similar data have been taken for low molecular weight of $56{,}000 gmol^{-1}$ shown in Fig.3.21 as prepared using the hot plate method.

We performed a systematic study in the high polymer concentration region using SANS, these results will be presented below. In addition, we attempted to follow the increase in scattering using a small-angle light scattering. Small-angle light scattering was observed and is typically weak until the phase boundary was reached. From which the intensity rises strongly and becomes time-dependent. It is the demarcation of the rise in intensity which defines the phase boundary that is probed by SANS. We observed that the temperatures which are extrapolated by SANS are roughly 1 to 2 degrees higher than those defined by the SALS experiment. The SALS experiment involved cooling in decrements of 1-2K and waiting for 30

minutes for equilibration. Preliminary experiments are shown regarding the kinetics in Chapter 5.

3.6.5 Main Results:56,000gmol^{-1}

The experimental data of scattered intensity versus temperature are shown for a fixed salt concentrations of 0.38M in Fig.3.22. Notice the strong increase in scattering as the temperature approached the phase boundary. These observations agree with the measured salt-dependent thermodynamic behavior.

The next step to quantifying the results is from the Ornstein-Zernike plots, consistent with the salt-induced behavior. This is demonstrated in Figs.3.22. It is clearly seen that deviation occurs in the small-q region, similar in the case of salt-induced behavior. Thus, we will again restrict the experimental data fitting to the linear in q^2 region to extract the correlation length and scattered intensity to zero angle. The divergence behavior for I(0) and ξ is summarized in Figs. 3.23 and 3.24, respectively. Notice the quantitative increase from the order of 10Å to more than 200Å in ξ.

3.6.6 Crossover from Mean Field to Fluctuation Regime

The mean field plots for the 56kgmol^{-1} samples are demonstrated in Fig.3.25 and 3.26 for the three different fixed salt concentration all data show a deviation from the mean field to Ising close to the phase transition. Similarly, for 120,000gmol^{-1} in Fig. 3.27. An extensive data set were collected for 200,000gmol^{-1} as a function of different levels of added salt. One result is shown in Fig.3.28 clearly demonstrating the cross over in $I(0)$ versus $1/T$.

3.7 Long-Wavelength fluctuations

We examined a sample of molecular weight 200,000gmol^{-1} with concentration 206gL^{-1} and no added salt using a series of scattering techniques. Figure 3.29 demonstrates an important puzzle for semidilute polyelectrolyte solutions. Light scattering and neutron scattering were performed on this sample which is able to extend the wavevector range significantly. We were able to take small-angle and ultra-small angle neutron scattering data in absolute units of intensity and then use static and small-angle light scattering to complete the scattering spectrum. Similar experiments were performed by overlapping small-angle neutron scattering and static light scattering[44]. In our case the ultra small-angle neutron scattering was performed and did not reveal the Guinier region at lowest q, then small-angle light scattering clearly reveals the Guinier regime in which the cluster size is order of 4 microns. The origin of this cluster remains a strong experimental and theoretical challenge as it is the origin of the observed excess scattering. The origin of the samples is from our laboratory. The samples were purified by ion-exchange and filtered through membrane filter units of porosity 0.45 microns, then subsequently lyophillized and redissolved at the given concentration. The semidilute solution of this concentration is not readily filterable.

3.8 Concluding Remarks

In the limit of low ionic strength, evidence for screening in polyelectrolyte solutions is found. This is demonstrated by the scaling of the correlation length with polymer concentration (in gL^{-1}) leading to the main result of $\xi = q_{max}^{-1} = 72.6 C_p^{-0.473 \pm 0.02}$. The exponent of 0.47 is in comparison with the scaling result of

1/2. With the addition of salt we observed polyelectrolyte phase diagrams. By exploring the homogeneous phase we measured by SANS the divergence in the correlation length and susceptibility are consistent with Ising criticality. This is based on the experimental observation of the divergence even in regions of the phase diagram, not defined by the critical point commonly found in neutral polymer solutions. The presence of the Ising criticality is demonstrated by the non-mean field behavior very close to the precipitation phase boundary in the temperature-dependent thermodynamics study. It was demonstrated that opalescence is observed for a wide range in concentrations, in the semidilute limit, and molecular weight and is thus a general phenomena discovered first in this system. Contrast this result with the behavior of sodium chloride added salt, which displays none of this behavior. The next chapter which deals with the labeled chains will describe the special efforts used to separate the intra and intermolecular correlations, thus extracting the configurational properties of the labeled chains.

Table 3.1: Polyelectrolyte Systems Exhibiting Precipitation.

Polyelectrolyte	Added Salt	T[°C]
poly(vinylsulfonic acid)[27]	NaCl,KCl,RbCl,KI,KBr,KCl	0 to 50
poly(methacrylic acid)[26]	CaX,SrX,BaX, X=$(OH)_2$ and Cl_2	25
poly(methacrylic acid)[28]	$CuCl_2$	25
poly(acrylic acid)[29]	NaCl, $MgCl_2$,$BaCl_2$	25
Na-poly(styrene sulfonate)[30]	$BaCl_2$, $AlCl_3$	25
Na-poly(styrene sulfonate)[25]	$CaCl_2$,$LaCl_3$,$Th(NO_3)_4$	25
Polycarboxylate[31]	$CaCl_2$,$CuCl_2$,$MnCl_2$,$MgCl_2$	25
Quaternized-poly(4-vinylpyridine)[15]	NaBr	20

Table 3.2: Semidilute Solution Scaling Exponents.

ν	y	Solvent Quality
1	-1/2	Rod-like
1/2	-1	θ Solvent
3/5	-3/4	Good Solvent

Table 3.3: Low-ionic strength polyelectrolytes solutions.

Polyelectrolyte	Reference
poly(styrene sulfonate)	Nierlich[37]
poly(styrene sulfonate)	Ise[41]
t-RNA, BSA, lysozyme, chondroitin sulfate	Matsuoka[42]
Xanthan, semi-flexible polymer	Milas[43]
poly(N-methyl-2-vinyl pyridine chloride)	Ermi[44]
DNA	Borsali[45]

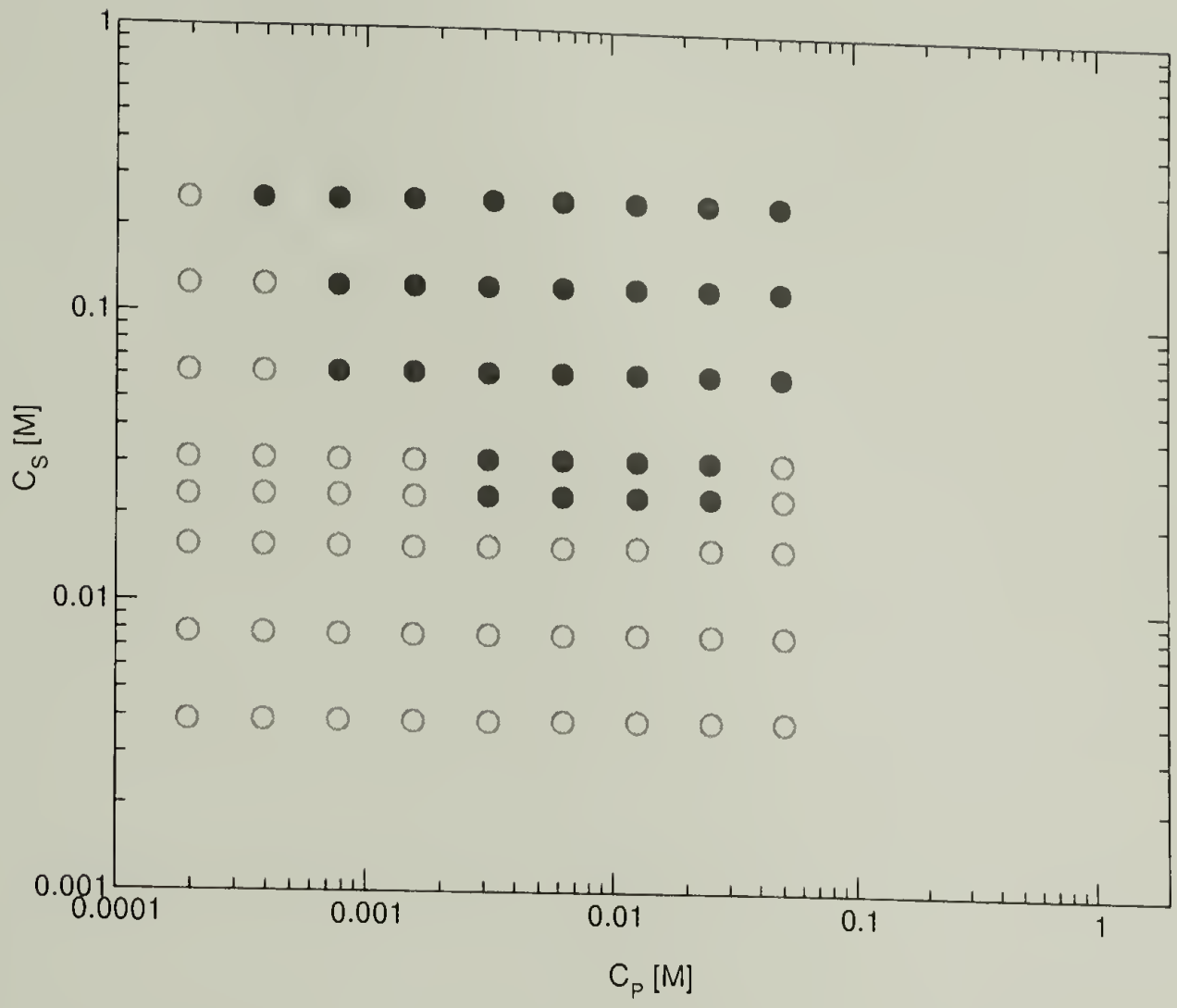

Figure 3.1: Precipitation phase diagram for 16kgmol^{-1} NaPSS with added barium chloride salt at 294K. Concentrations are in moles of monomer per liter of solution and moles of barium chloride salt per liter of solution. Filled circles homogeneous phase and open circles precipitation.

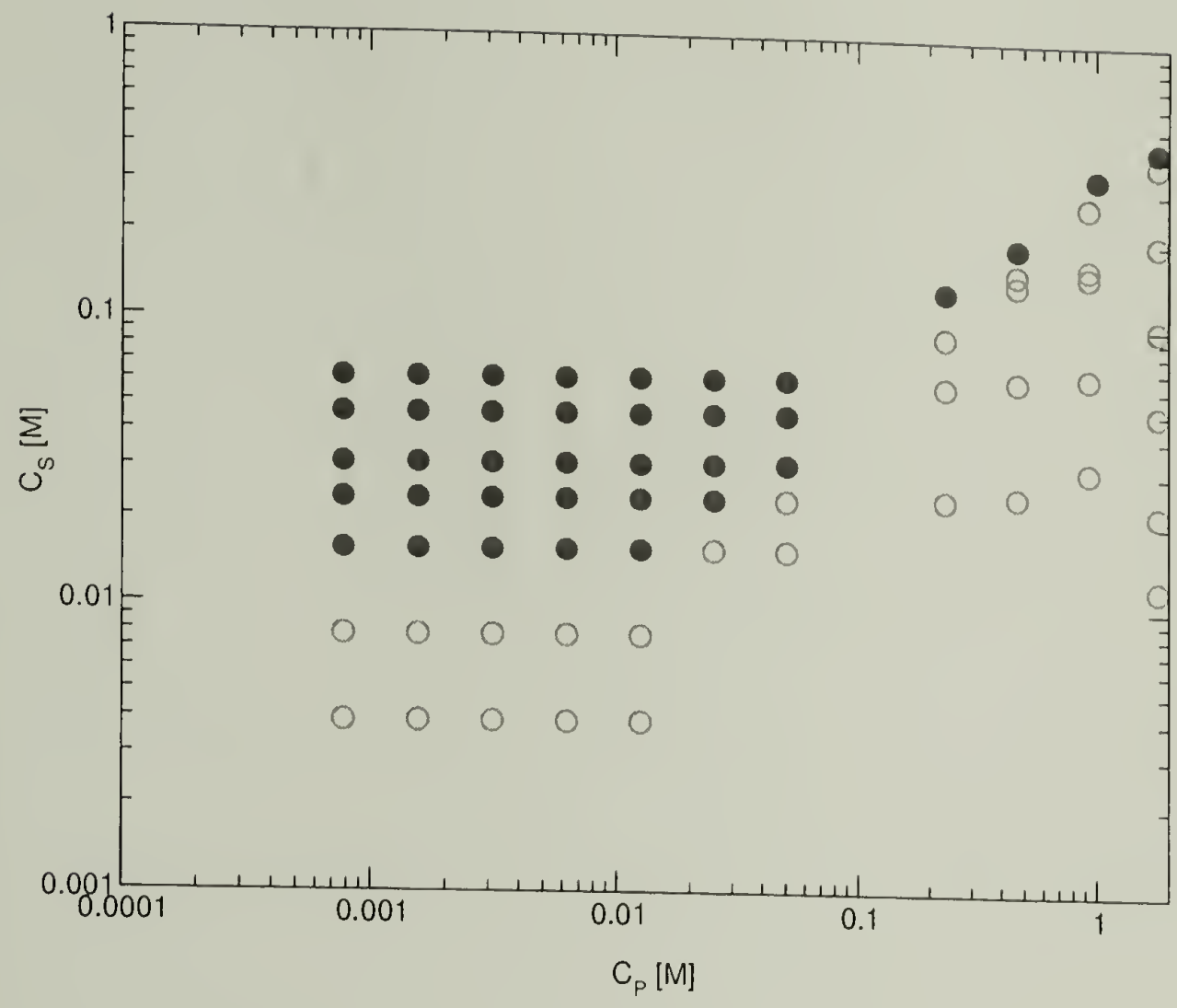

Figure 3.2: Precipitation phase diagram for 56,000gmol^{-1} NaPSS with added barium chloride salt at 294K. Concentrations are in moles of monomer per liter of solution and moles of barium chloride salt per liter of solution. Filled circles homogeneous phase and open circles precipitation.

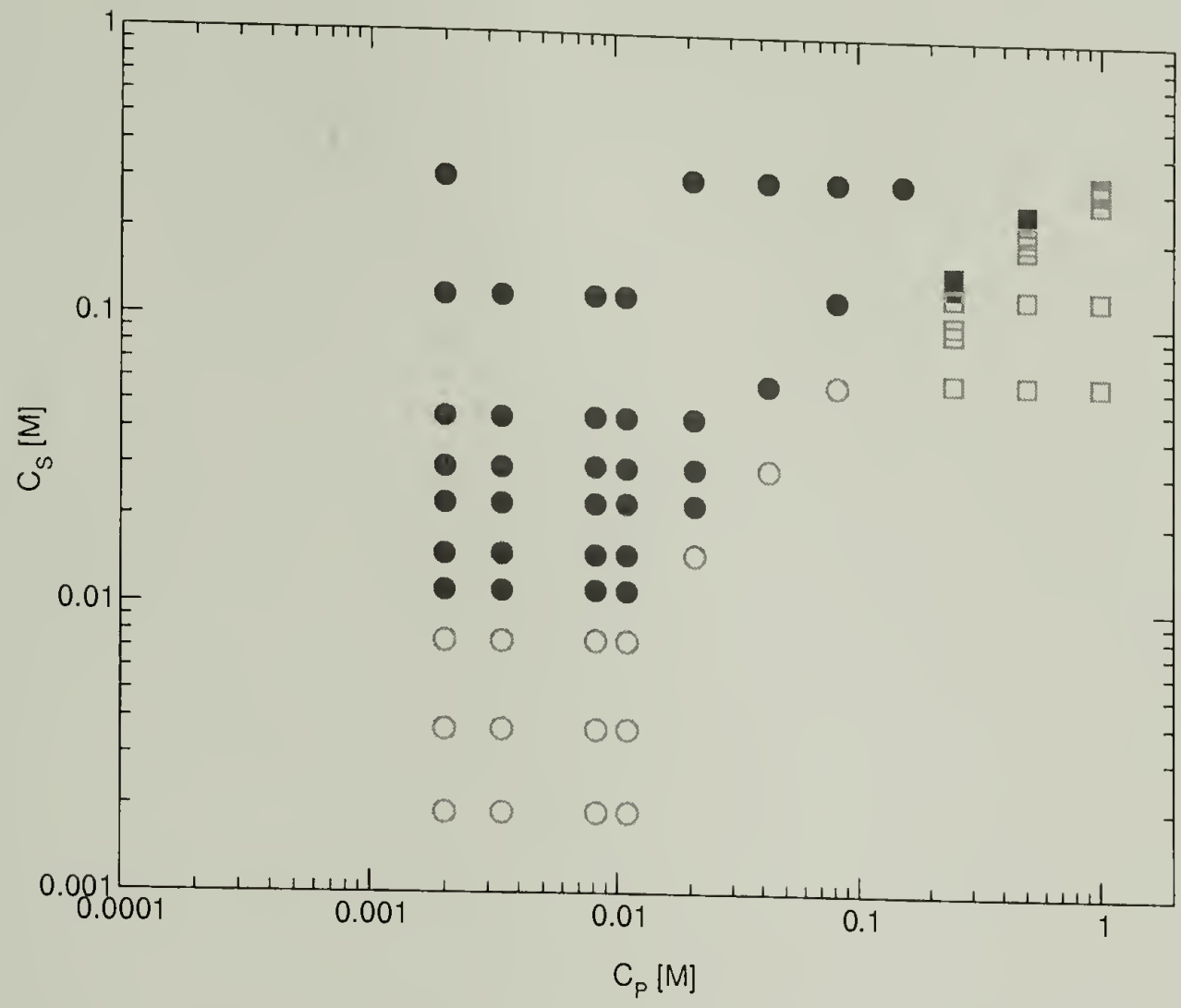

Figure 3.3: Precipitation phase diagram for 120,000gmol^{-1} NaPSS with added barium chloride salt at 294K. Concentrations are in moles of monomer per liter of solution and moles of barium chloride salt per liter of solution. Filled circles homogeneous phase and open circles precipitation.

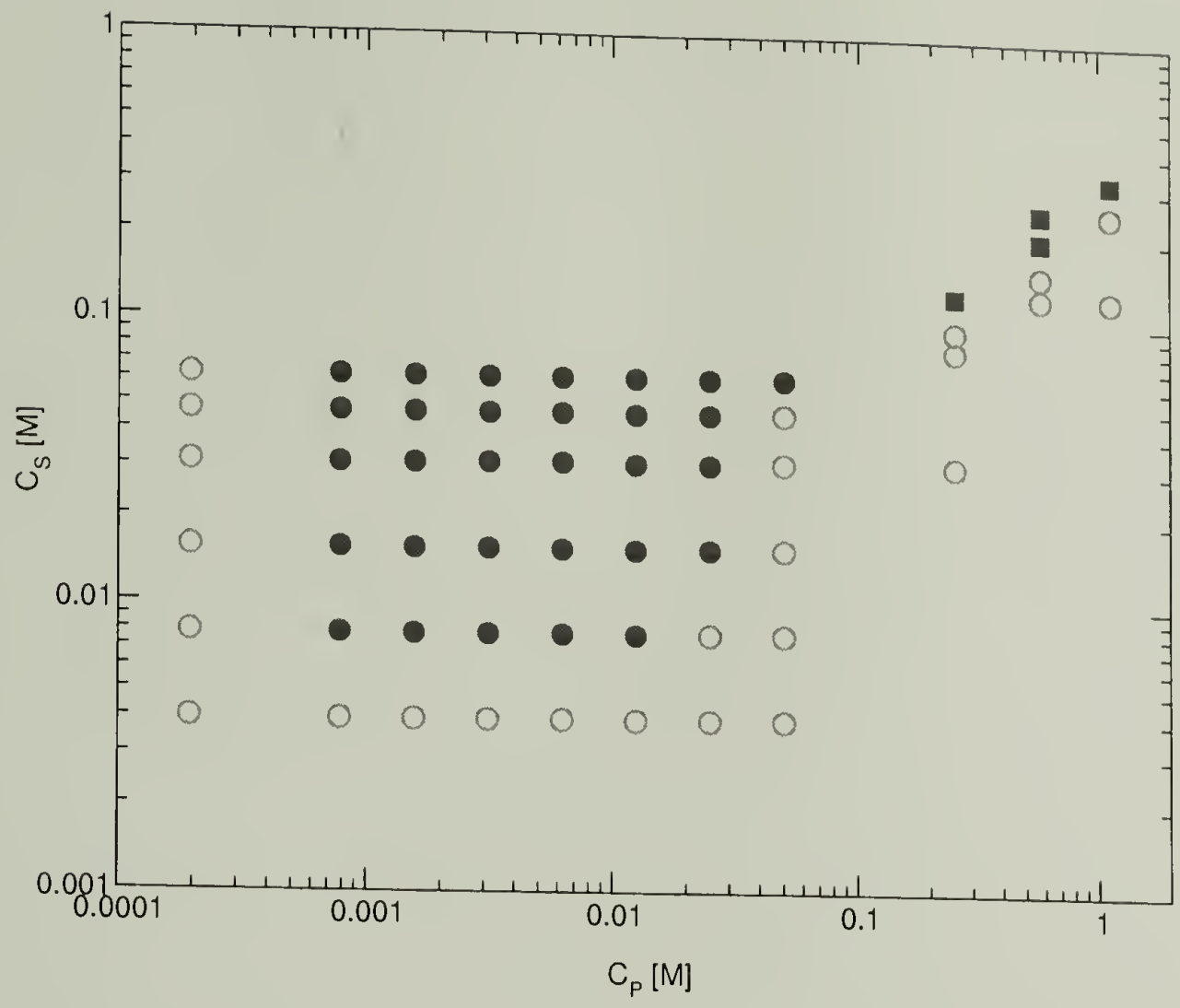

Figure 3.4: Precipitation phase diagram for 200,000gmol^{-1} NaPSS with added barium chloride salt at 294K. Concentrations are in moles of monomer per liter of solution and moles of barium chloride salt per liter of solution. Filled circles homogeneous phase and open circles precipitation.

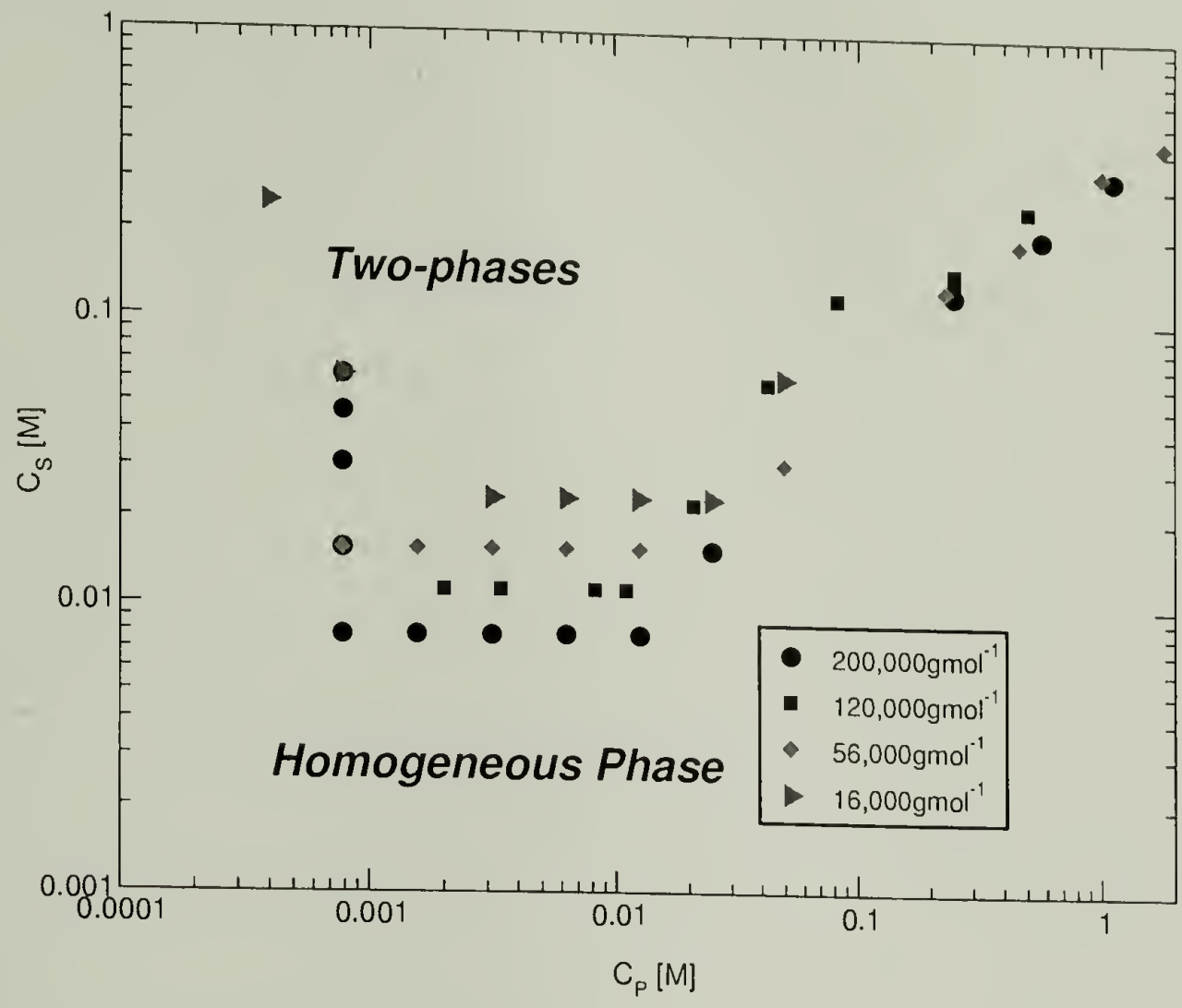

Figure 3.5: Composite plot of all molecular weights studied showing only the observed phase boundaries. The weak molecular weight dependence is observed regarding the salt concentration independent salting out line.

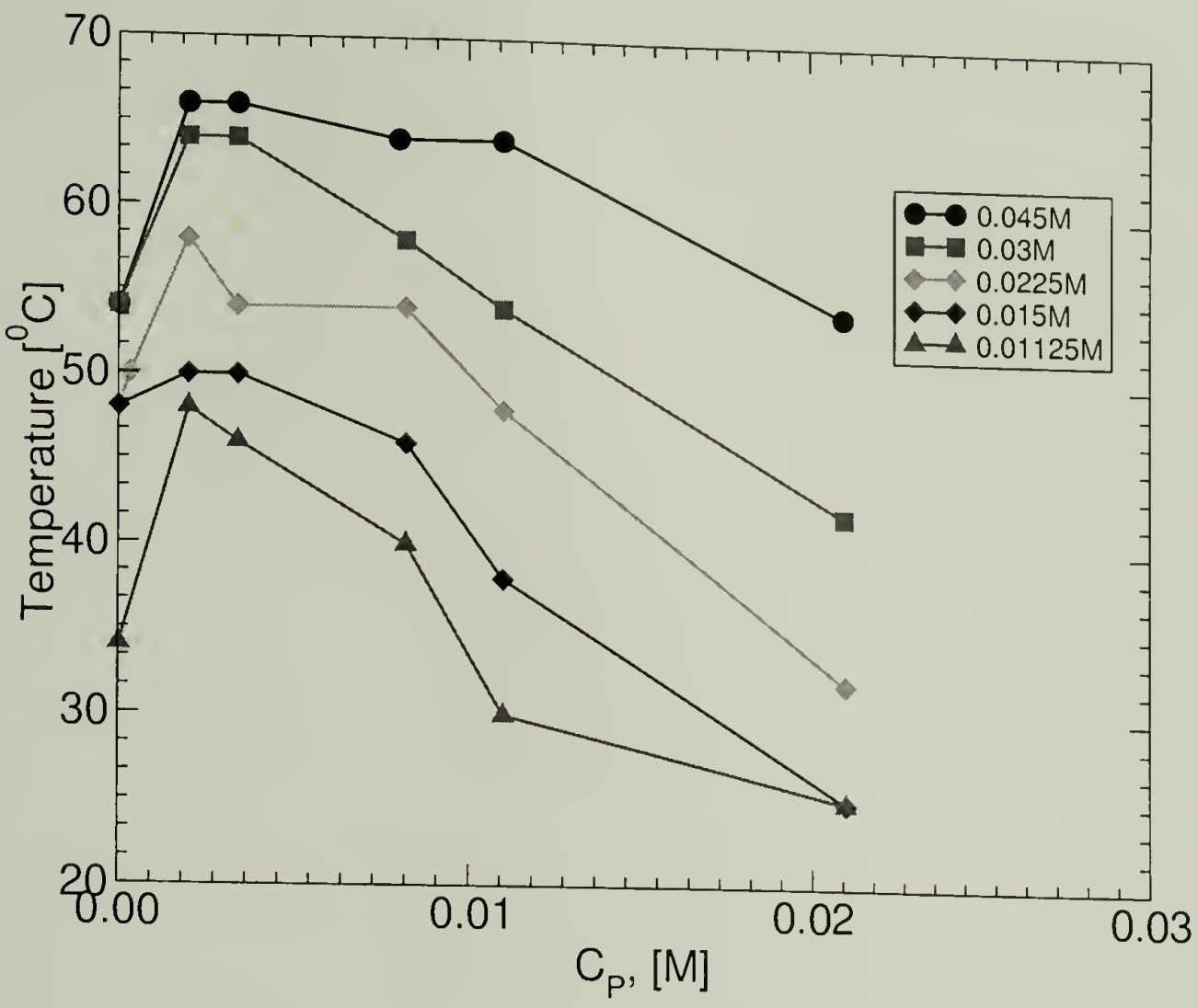

Figure 3.6: Temperature-polymer concentration phase diagram for molecular weight 120,000gmol^{-1}, NaPSS/$BaCl_2$ system. Above the line a homogeneous solution, below a precipitated phase, illustrated for different levels of added salt concentration as shown in the legend. It is demonstrated that increasing levels of added salt increase the clearing temperatures.

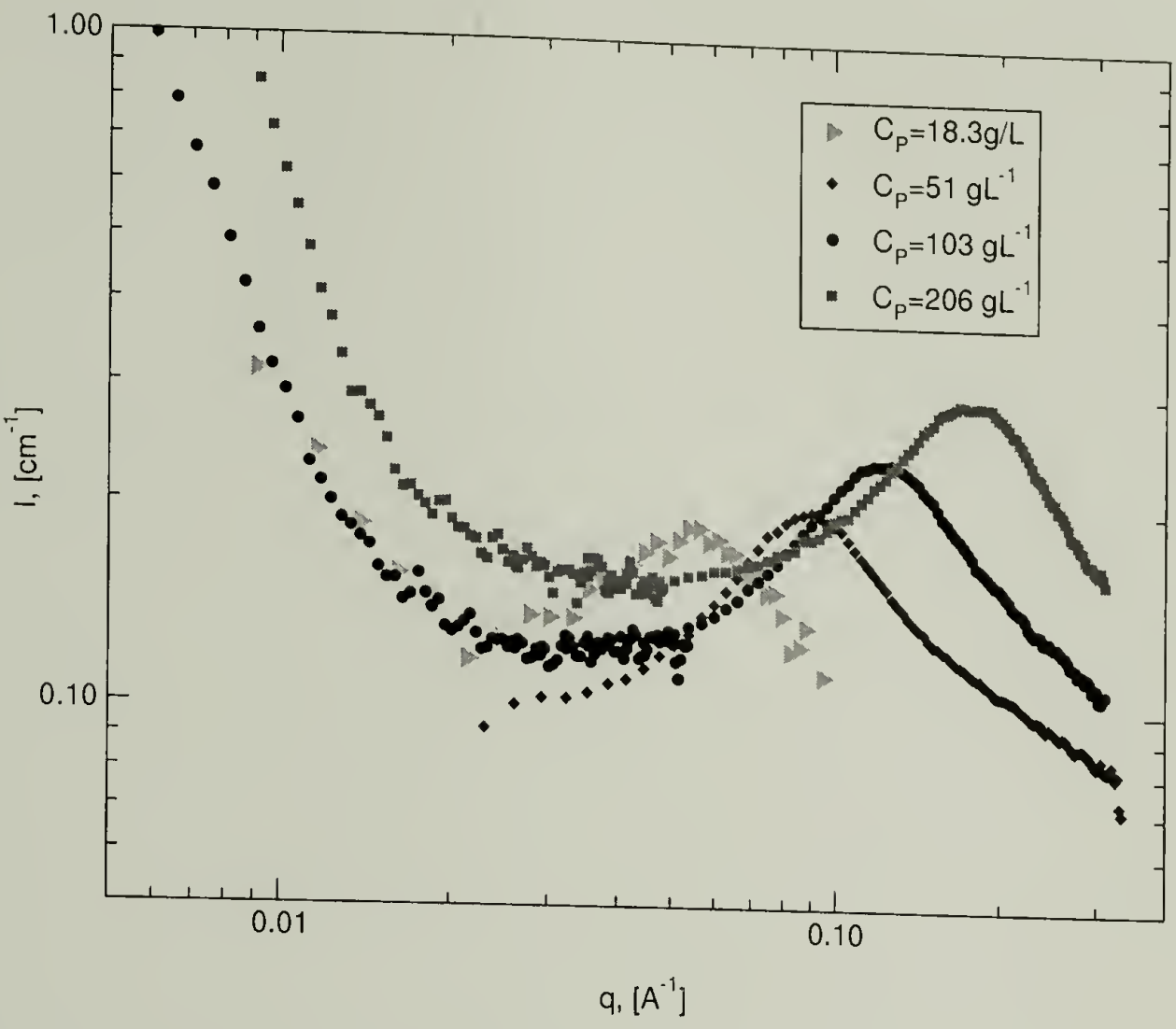

Figure 3.7: Plot of total scattering by molecular weight 120,000gmol^{-1} NaPSS for four polymer concentrations, shown in the legend, with no added salt. The polyelectrolyte peak at ($q \neq 0$) is well resolved, also the upturn at low q is observed. These data are not corrected for a flat incoherent background.

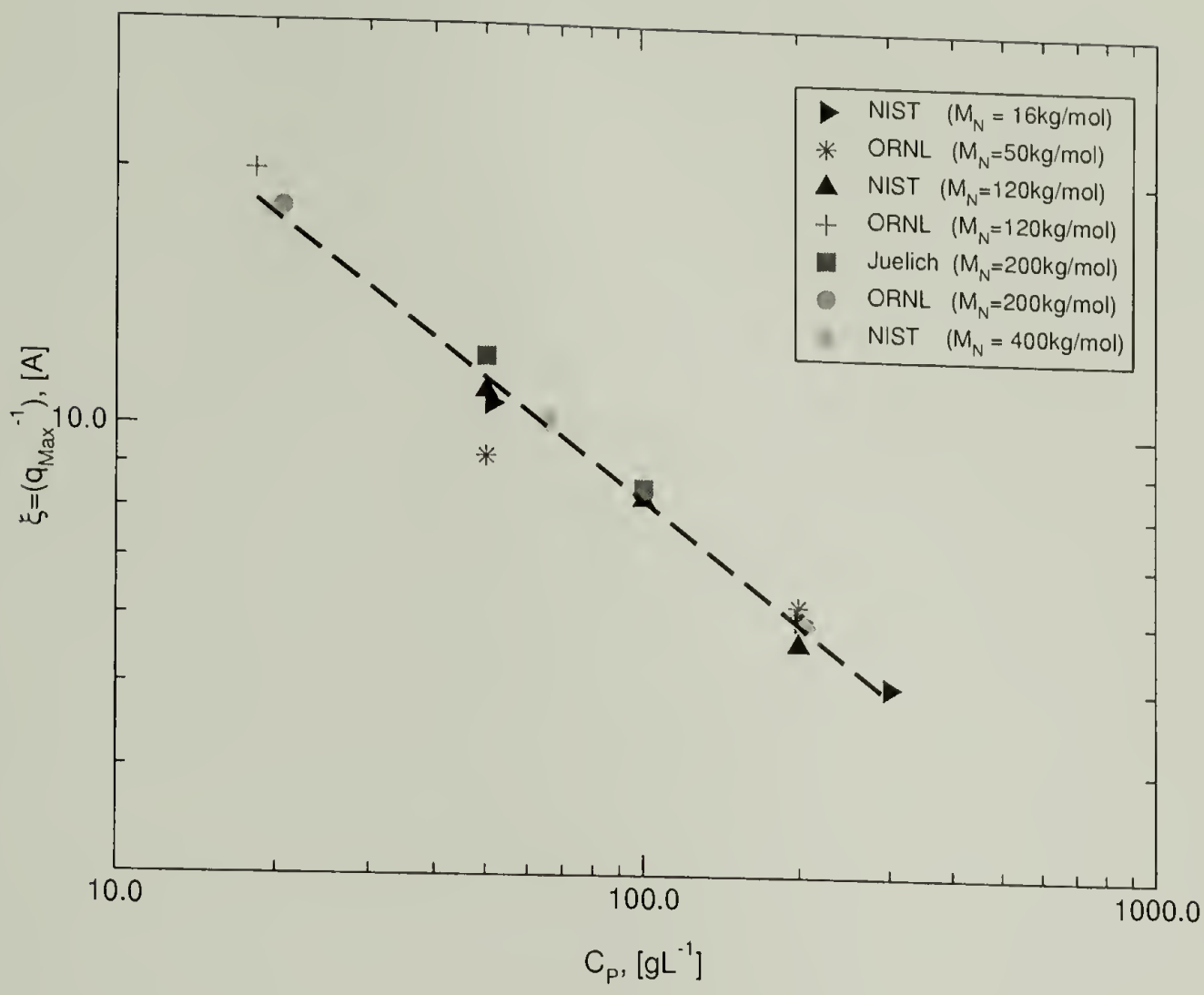

Figure 3.8: Plot of inverse polyelectrolyte high-q peak position versus polymer concentration, with no added salt. Peak position is independent of molecular weight and scales with polymer concentration: $q_{max}^{-1} = 72.6 \mathrm{C}_p^{-0.473 \pm 0.02}$.

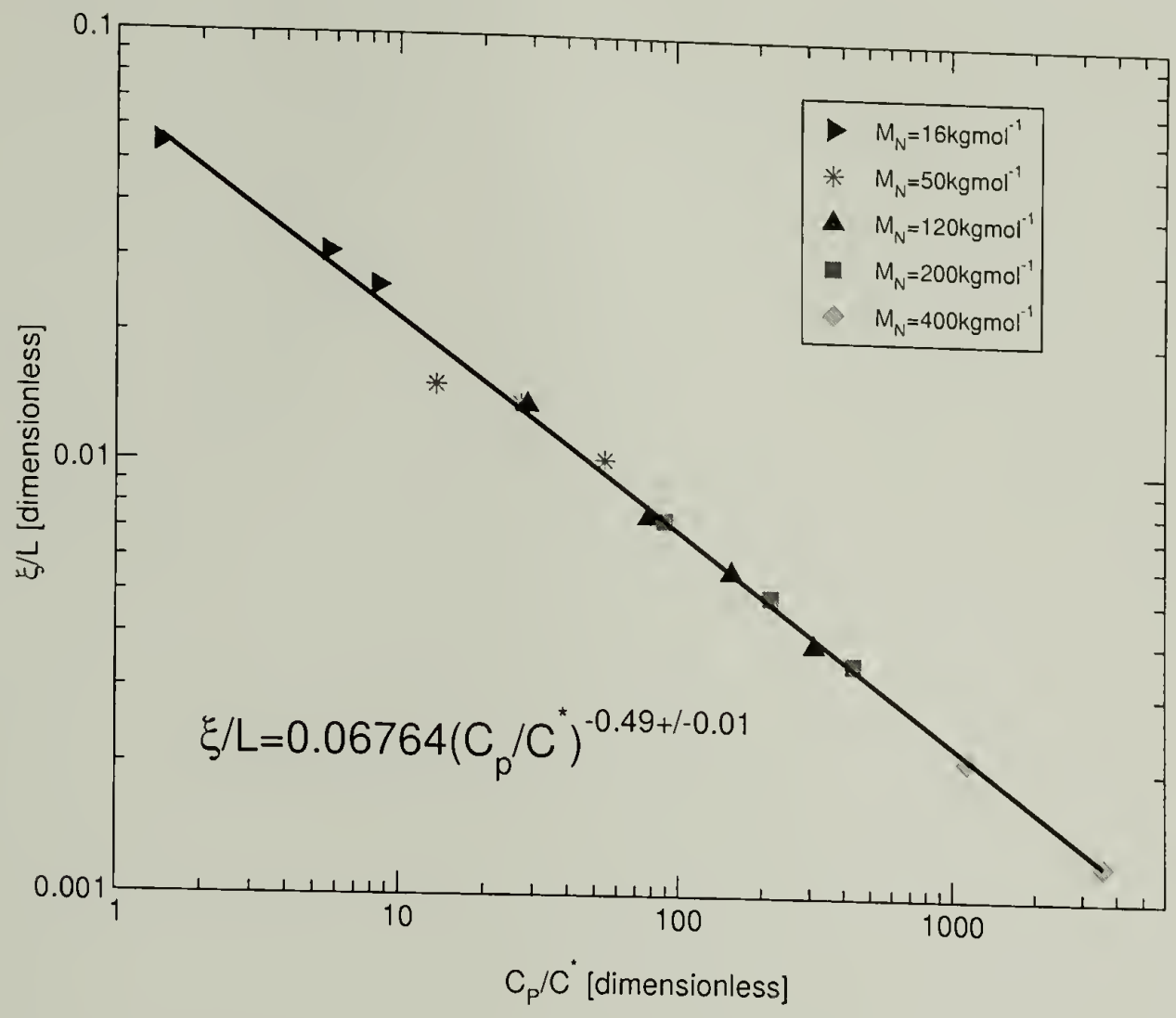

Figure 3.9: Dimensionless plot of ξ/L versus $C/C^{\star}$, where L is the calculated contour length and C* the over lap concentration, using a value of 1.0 for ν of 1.0. Regression over the entire range illustrates ξ/L =$0.0676C/C^{\star-0.49\pm0.01}$, in agreement with the theory.

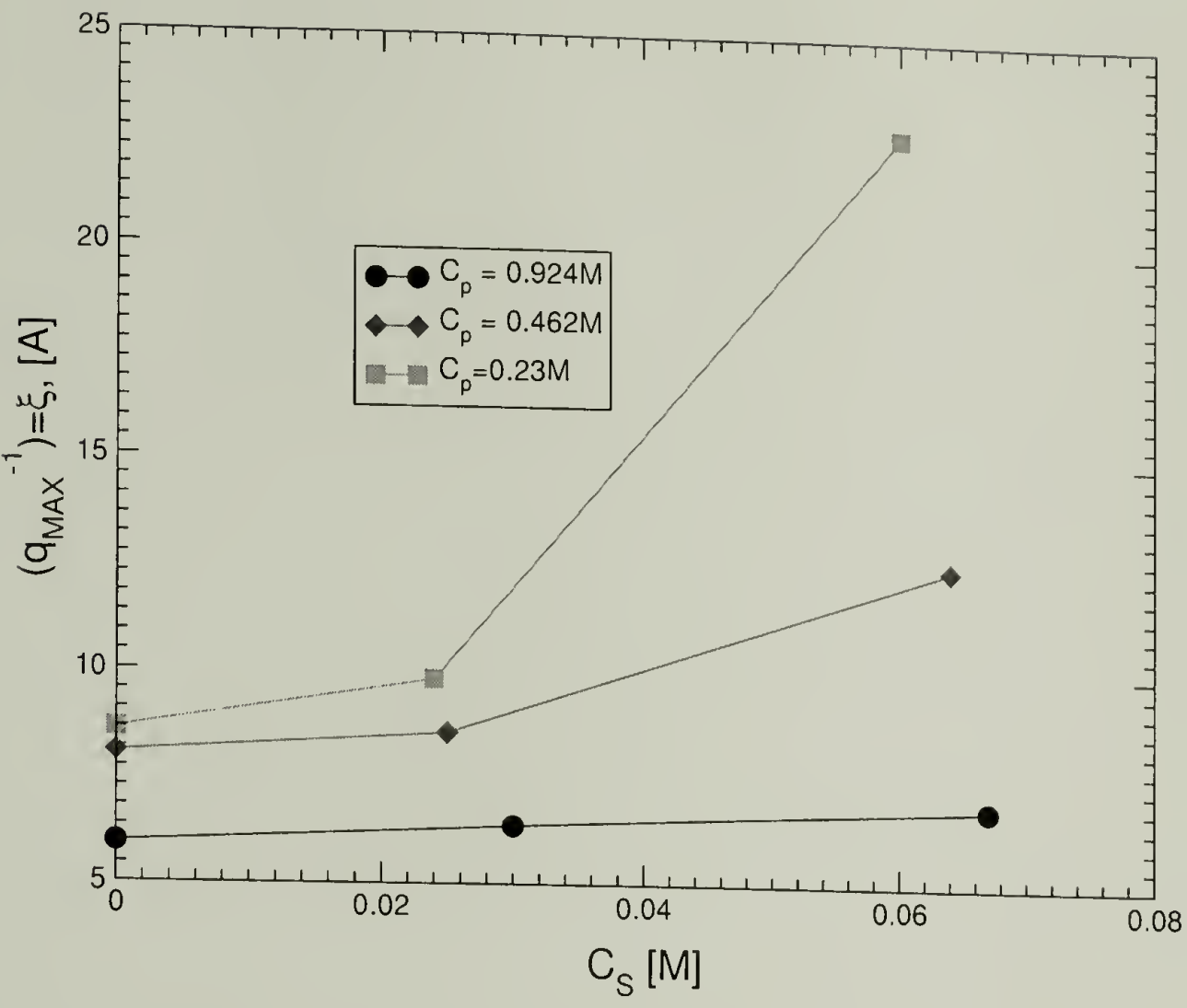

Figure 3.10: Variation in peak position with salt concentration for molecular weight 50,000gmol^{-1} for three different polymer concentrations given in the legend.

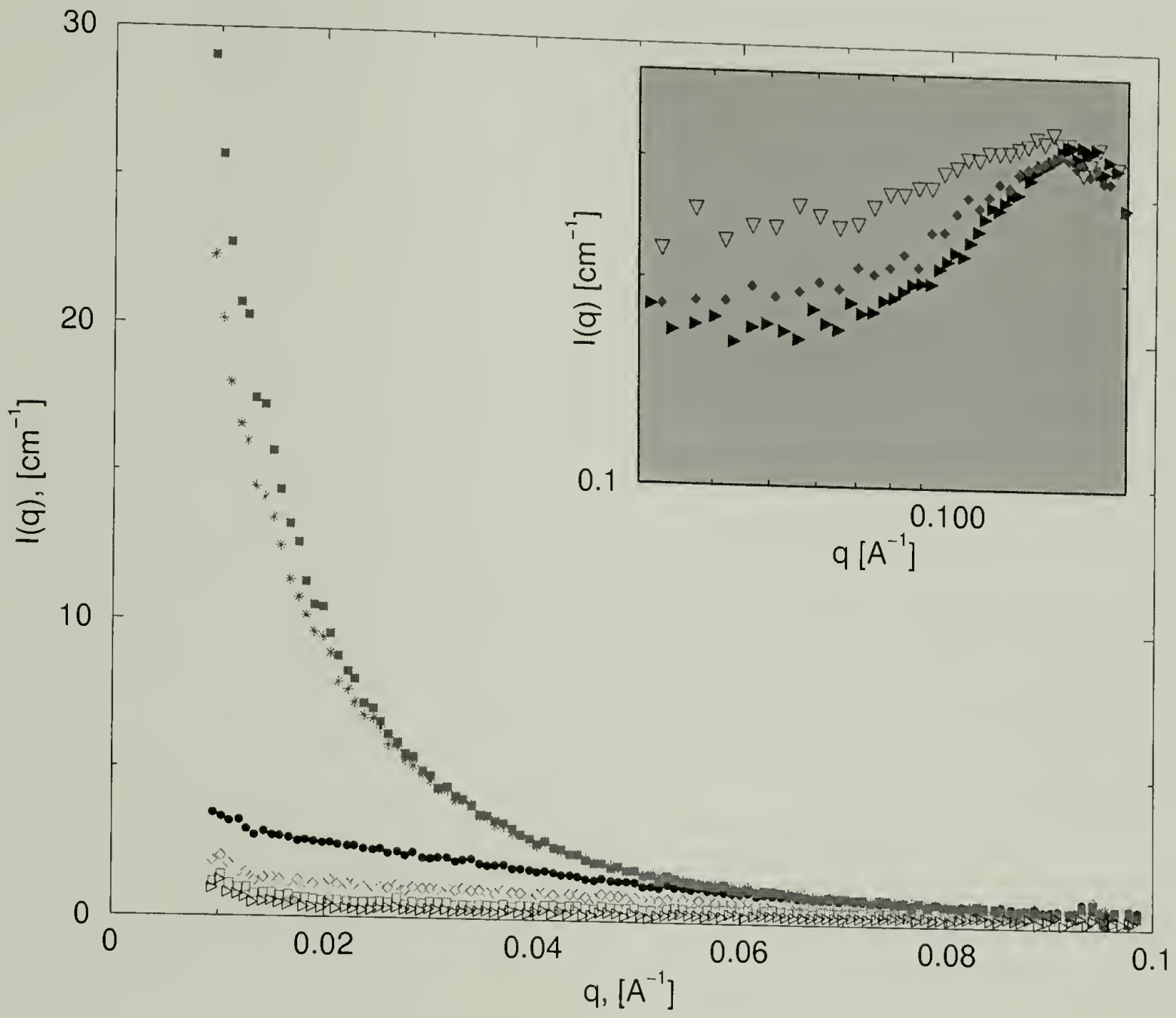

Figure 3.11: Total scattering for increasing levels of added barium chloride salt for 56,000gmol^{-1} sodium-poly(styrene sulfonate). Legend for barium chloride salt concentration is ▷ 0.125M, □ 0.188M, ◇ 0.250M, • 0.300M, ∗ 0.325M, ■ 0.330M. Inset legend ▶ 0.0M,◆ 0.03M, ▽ 0.067M.

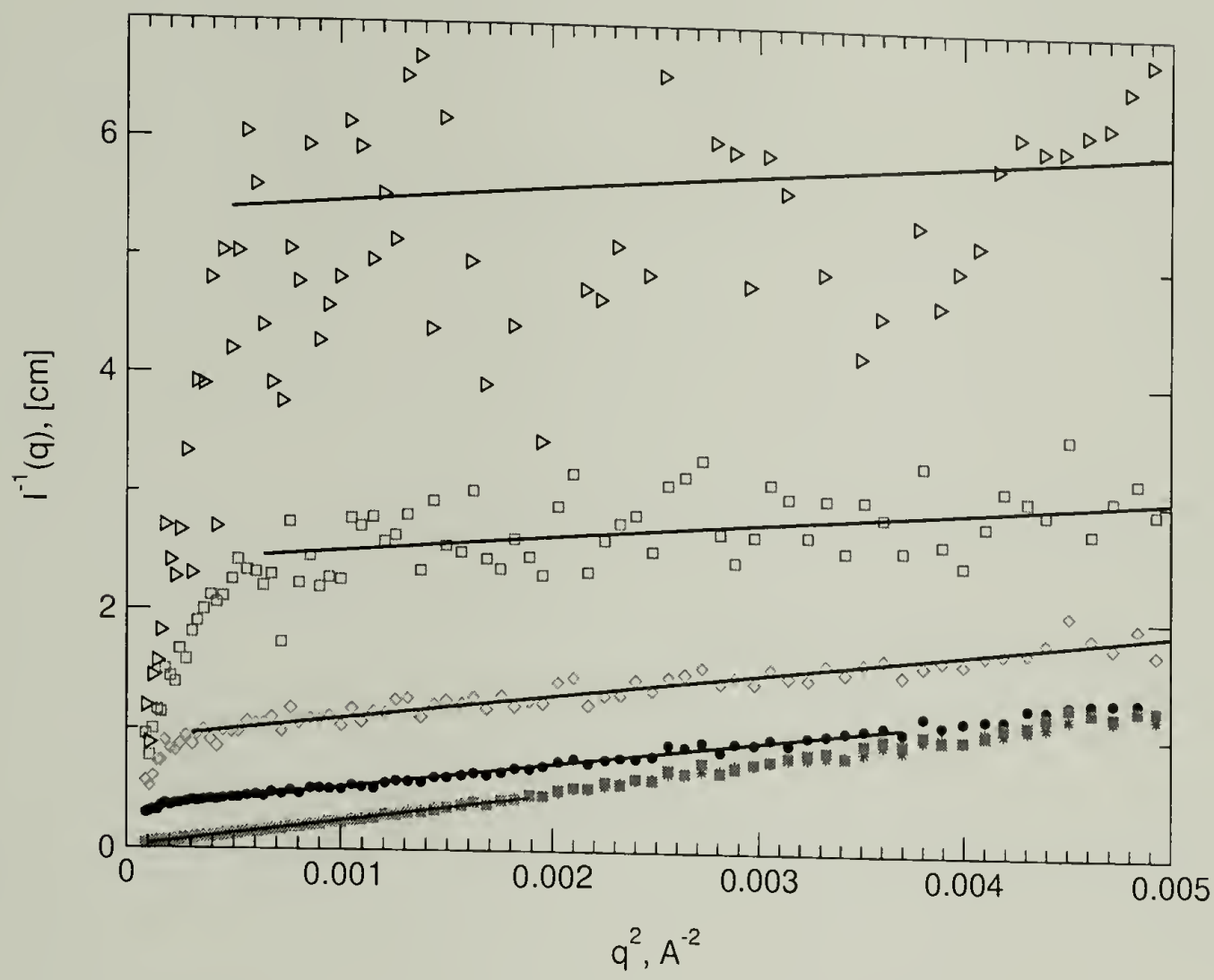

Figure 3.12: Ornstein-Zernike Plot for increasing levels of added barium chloride salt for 56,000gmol^{-1} sodium-poly(styrene sulfonate). Legend for barium chloride salt concentration is $\triangleright$ 0.125M, $\square$ 0.188M, $\Diamond$ 0.250M, $\bullet$ 0.300M, $*$ 0.325M, $\blacksquare$ 0.330M. The excess scattering leading to the downturn is not fit.

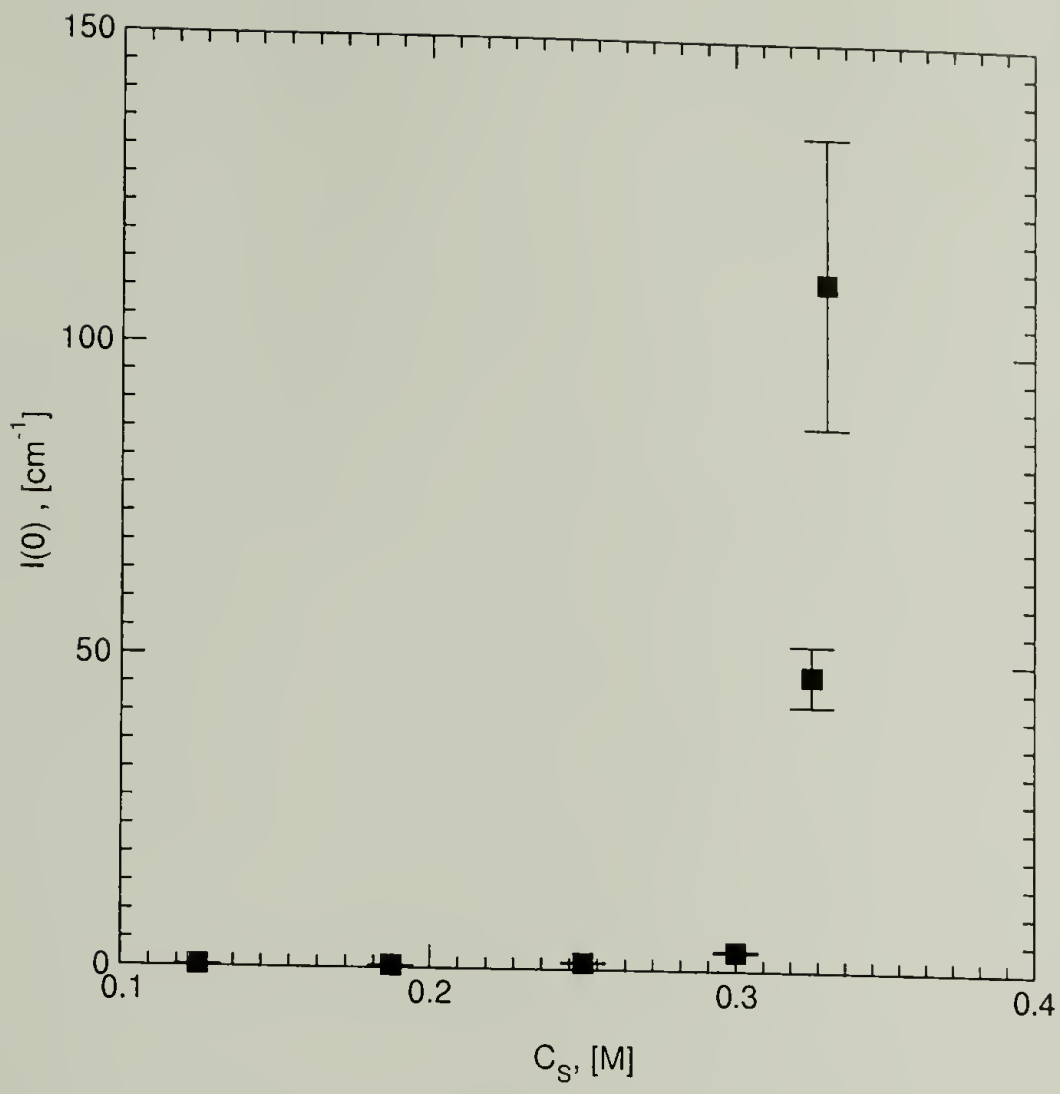

Figure 3.13: Total scattering for 56,000gmol^{-1} sodium-poly(styrene sulfonate), extrapolated scattered intensity to zero angle from Ornstein-Zernike plot as a function of added barium chloride salt concentration.

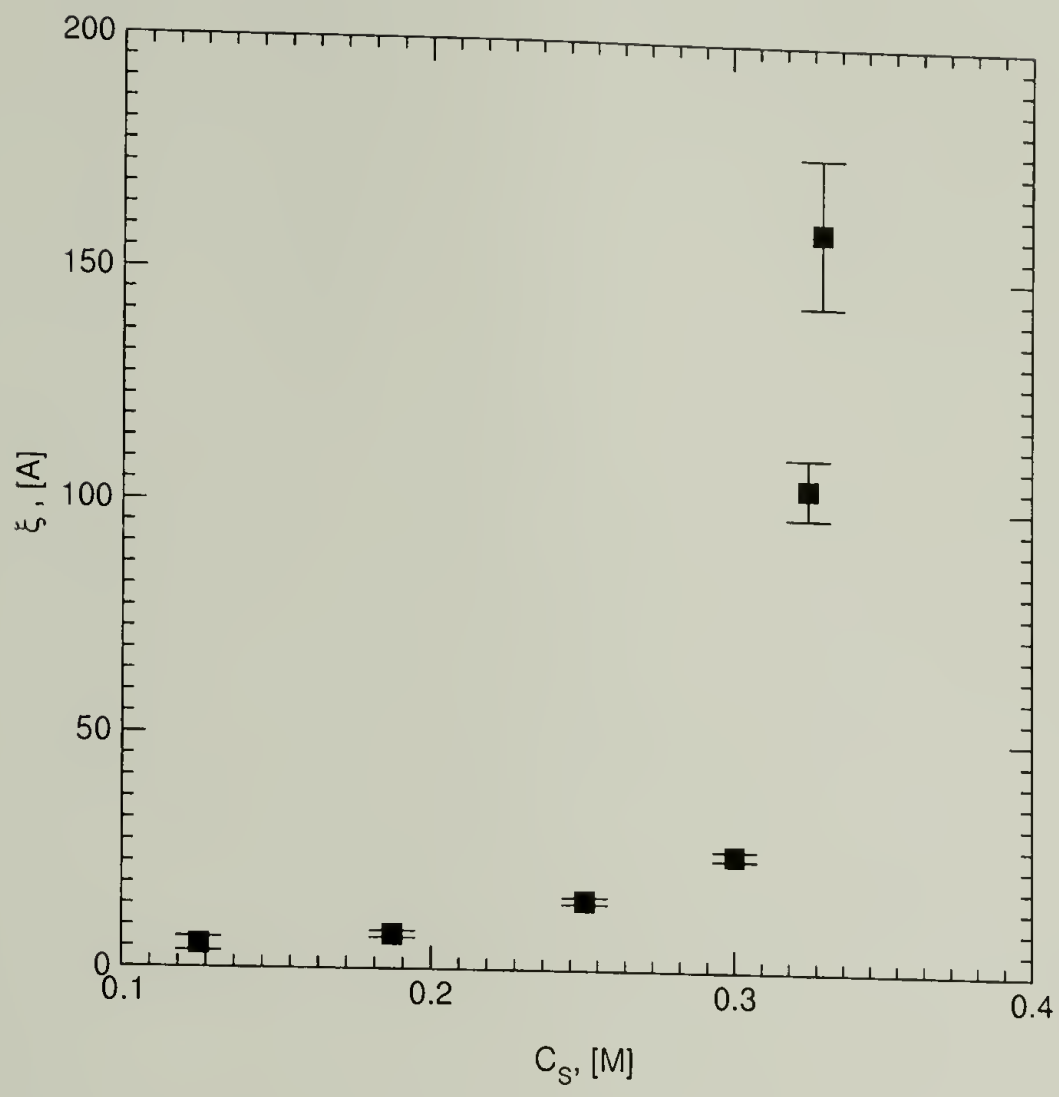

Figure 3.14: Total Scattering for 56,000gmol^{-1} sodium-poly(styrene sulfonate), correlation length from Ornstein-Zernike plot as a function of added barium chloride salt concentration.

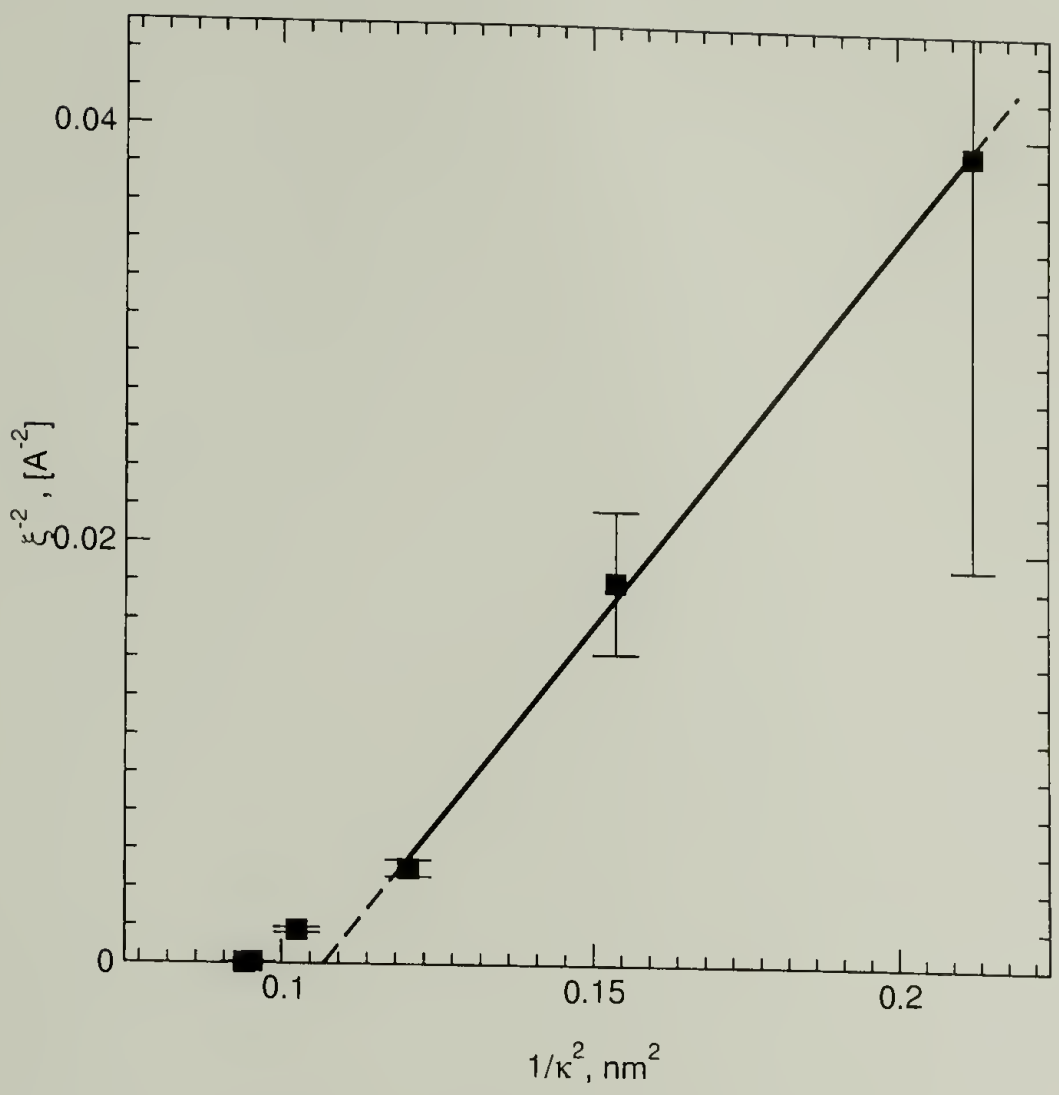

Figure 3.15: Demonstration of crossover from mean field to Ising criticality for ξ^{-2} versus $1/\kappa^2$ for 56,000gmol^{-1} sodium-poly(styrene sulfonate) .

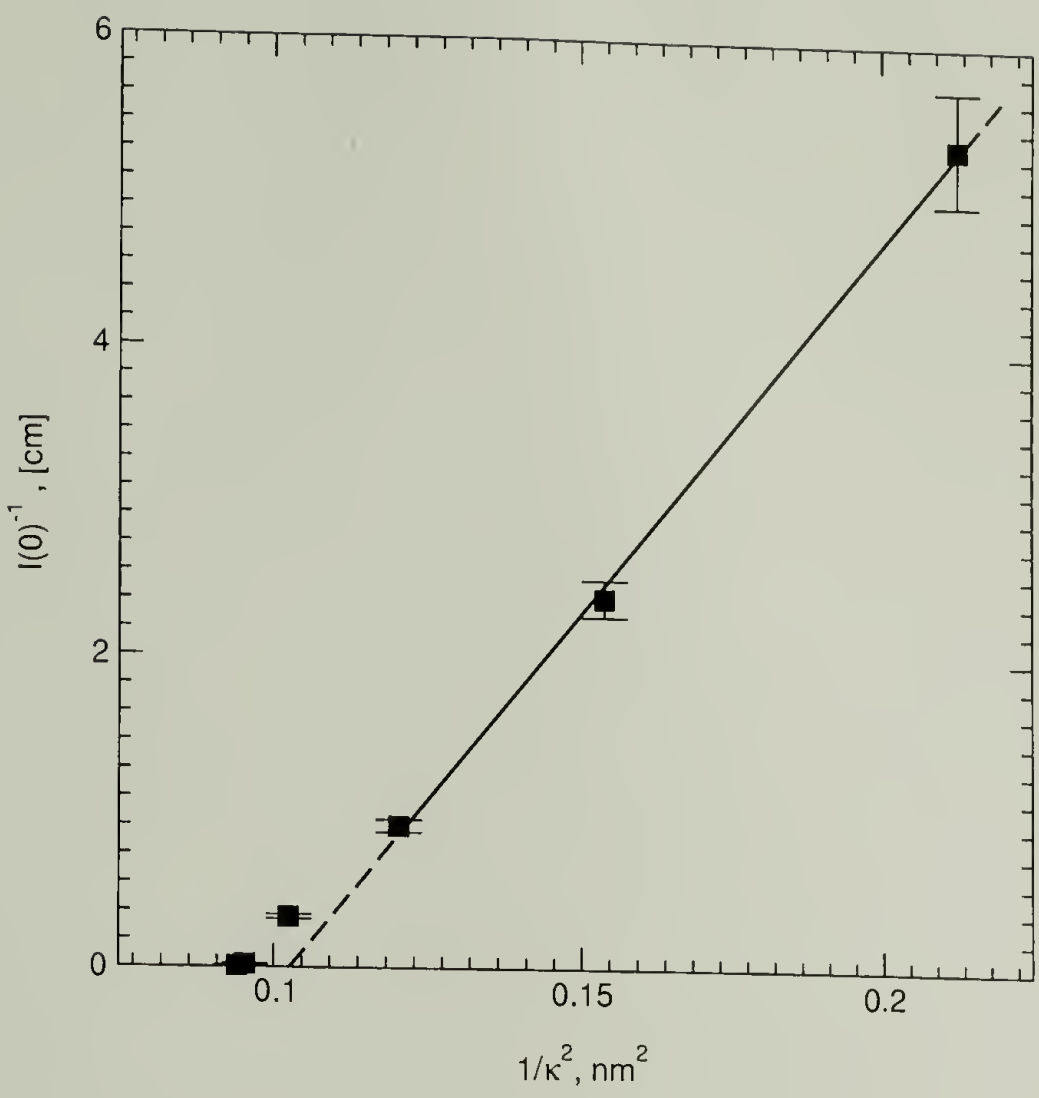

Figure 3.16: Demonstration of crossover from mean field to Ising criticality for $I(0)^{-1}$ versus $1/\kappa^2$ for 56,000gmol^{-1} sodium-poly(styrene sulfonate).

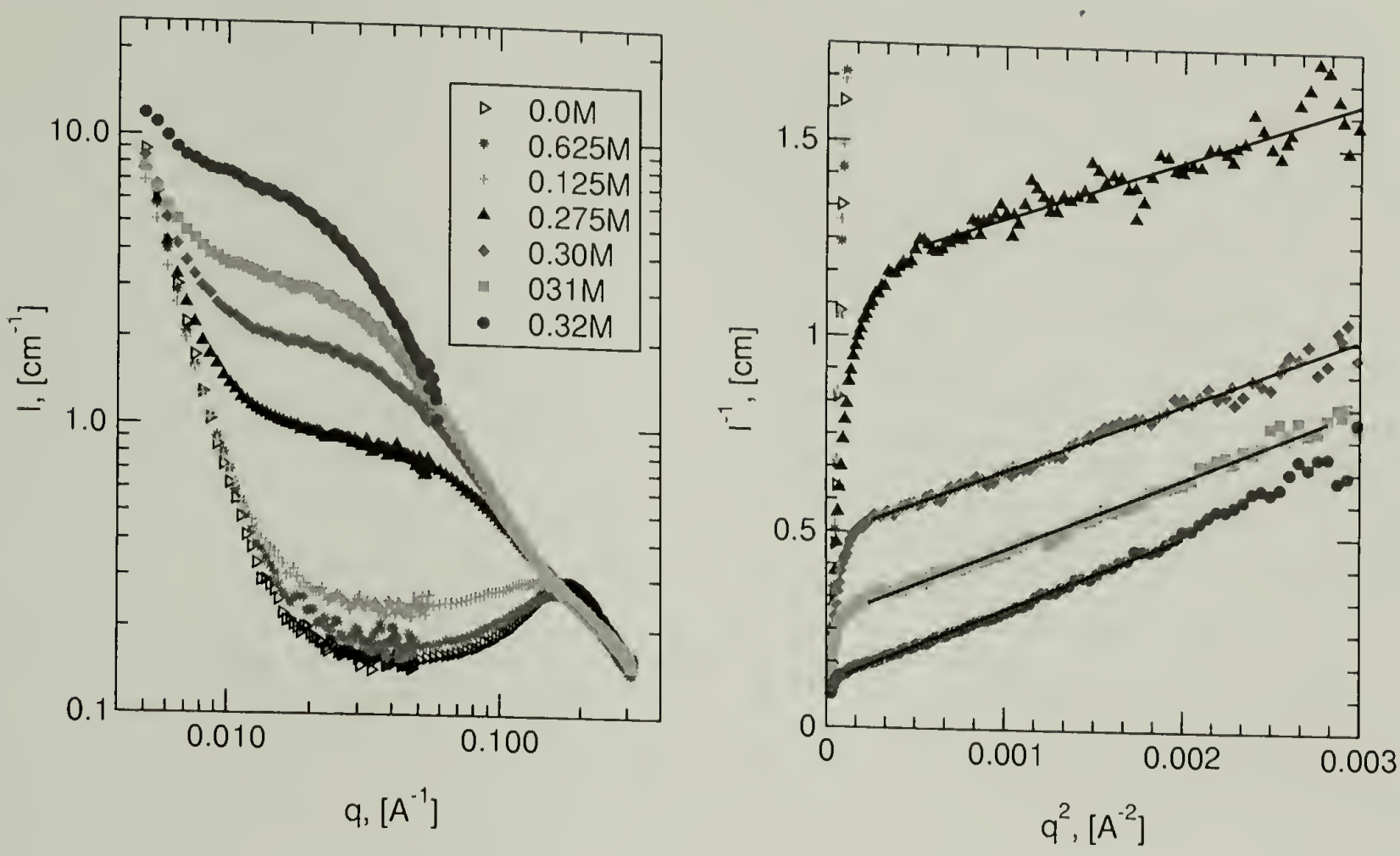

Figure 3.17: Demonstration of the scattered intensity versus wavevector as a function of salt for a fixed polymer concentration of 206gL^{-1} for 120,000 gmol^{-1} sodium-poly(styrene sulfonate). The corresponding Ornstein-Zernike plot is also shown from which ξ and I(0) are obtained.

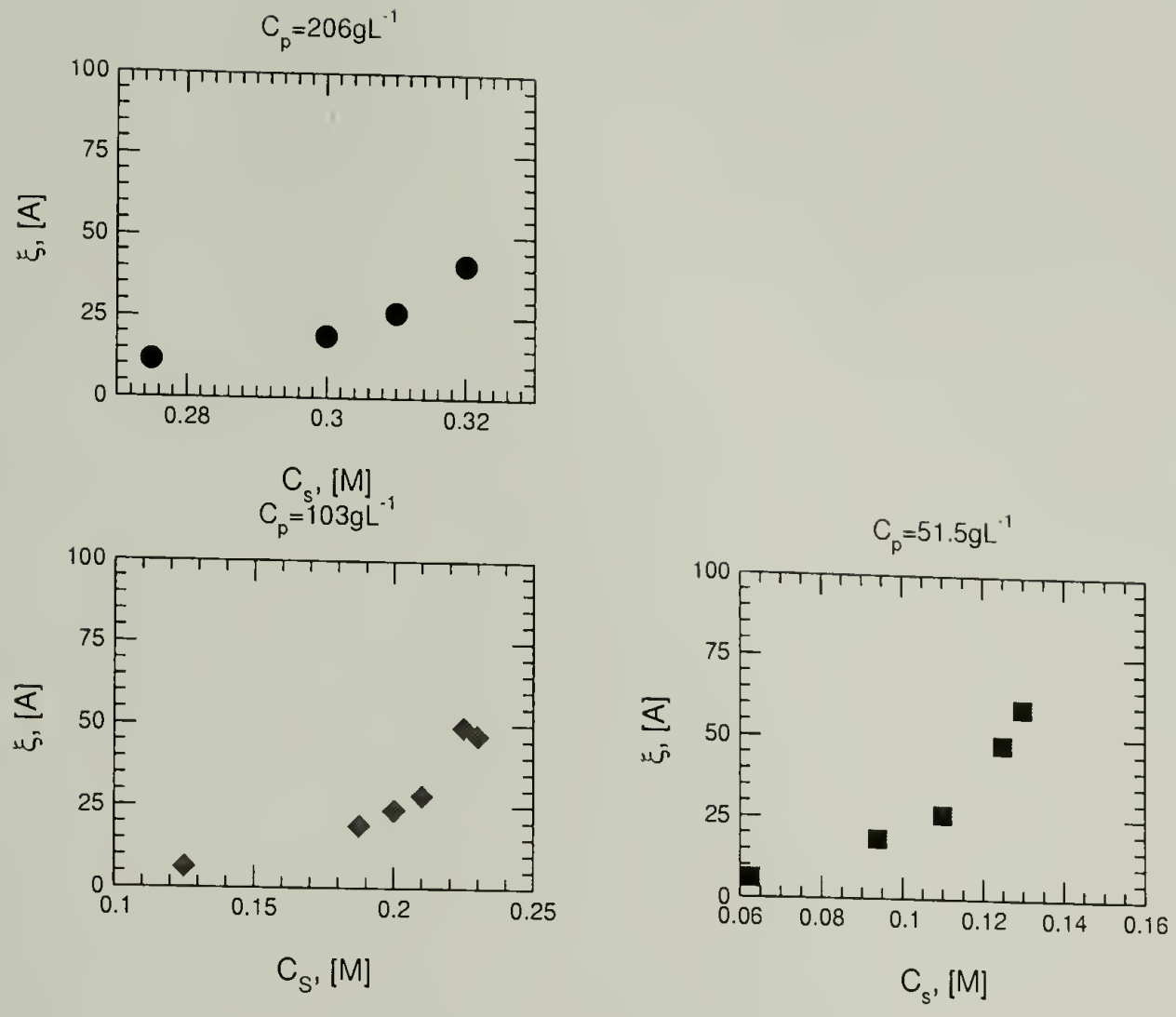

Figure 3.18: Demonstration of divergence in correlation length with increasing level of salt for three different polymer concentrations for 120,000 $gmol^{-1}$ sodium-poly(styrene sulfonate).

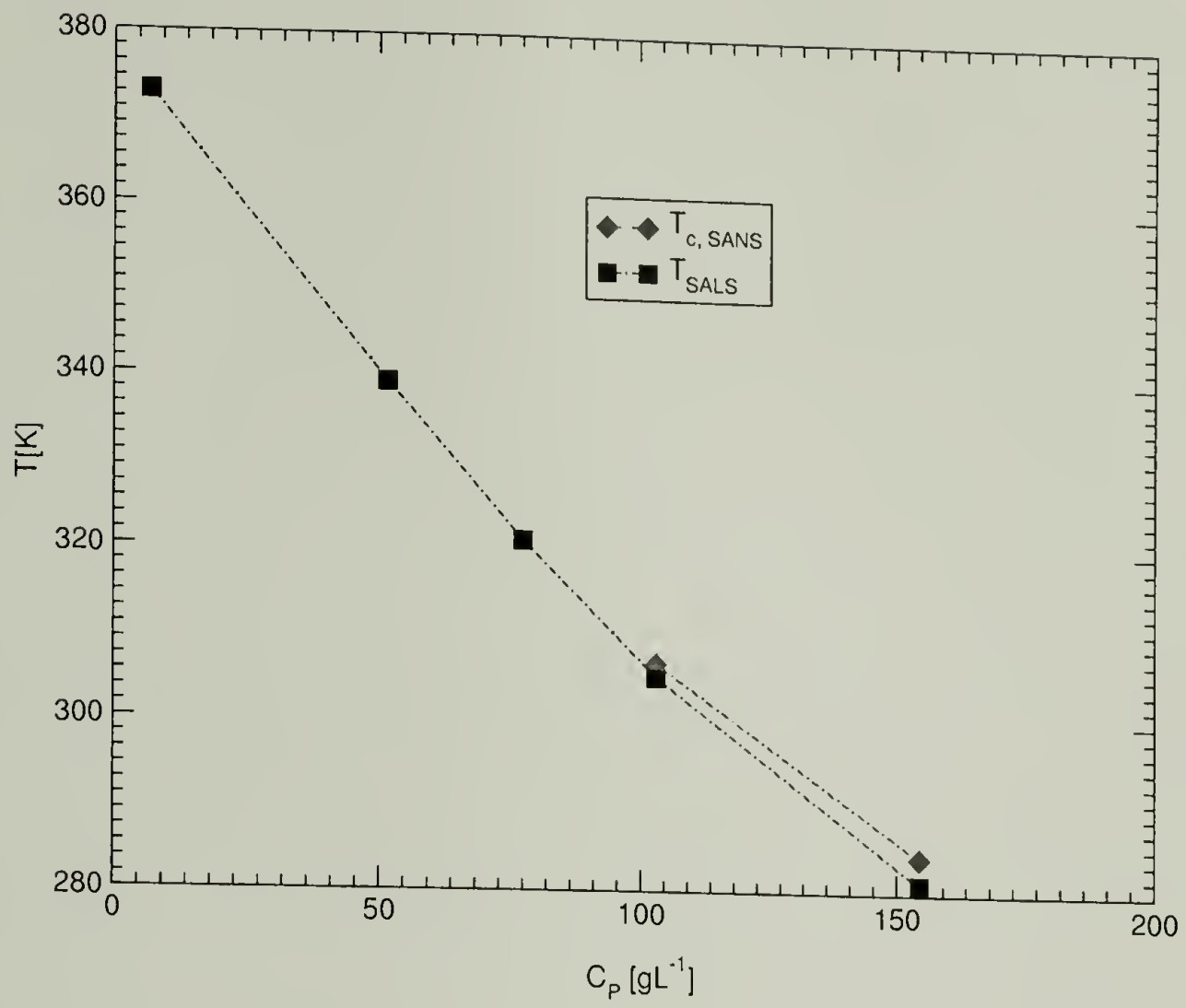

Figure 3.19: Phase Diagram for $M_w = 200{,}000 gmol^{-1}$ with a fixed salt concentration level of $C_s = 0.19M$. Below the line indicates precipitation, above a clear solution.

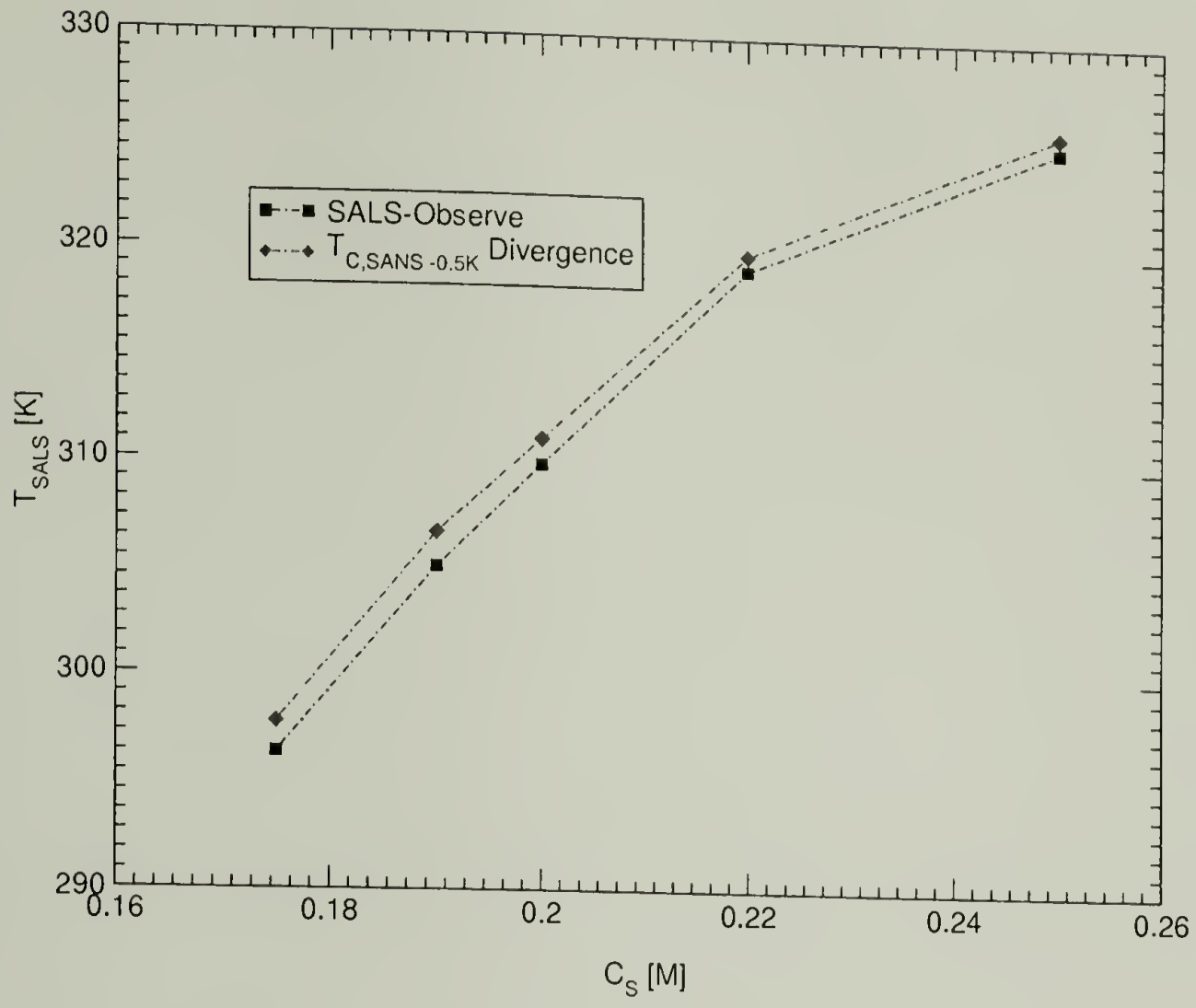

Figure 3.20: Influence of salt concentration on precipitation temperature for a fixed polymer concentration of $C_p = 103 gL^{-1}$. Examine for $M_w = 200{,}000$ $gmol^{-1}$. The cloud point temperatures determined by SALS are systematically at lower temperature than the SANS data. These data are of high confidence as the temperature stability was better than 0.5K. The phase boundary by SALS were determined upon observation of the kinetics of the phase separation.

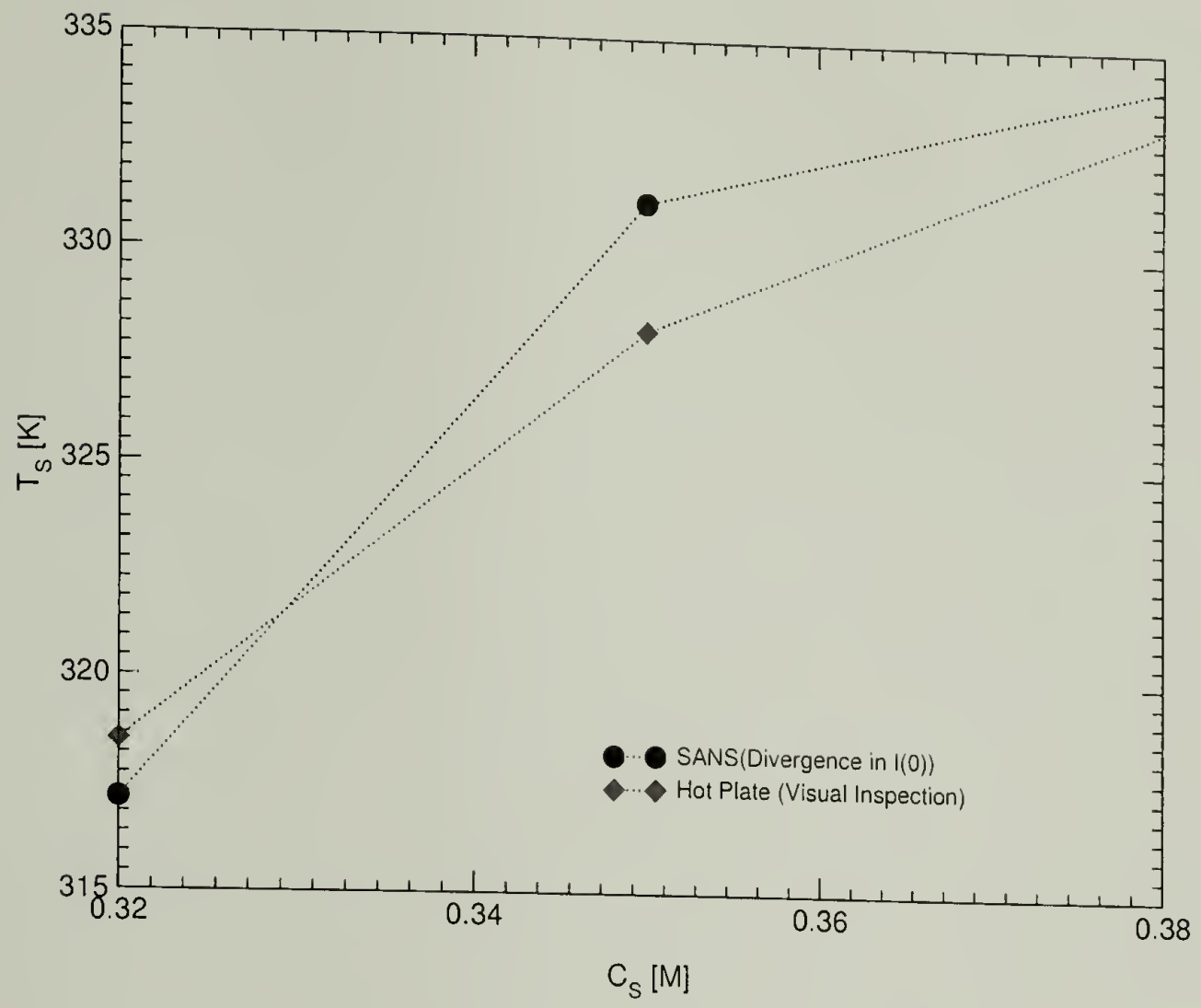

Figure 3.21: Influence of salt concentration on precipitation temperature for a fixed polymer concentration of C_p= 206gL^{-1}. Examine for M_w = 56,000 gmol^{-1}. The original estimates for the cloud point temperatures were coarsely determined using a hot plate. The SANS data are of better thermal stability and trustworthy, the hot plate only an estimate.

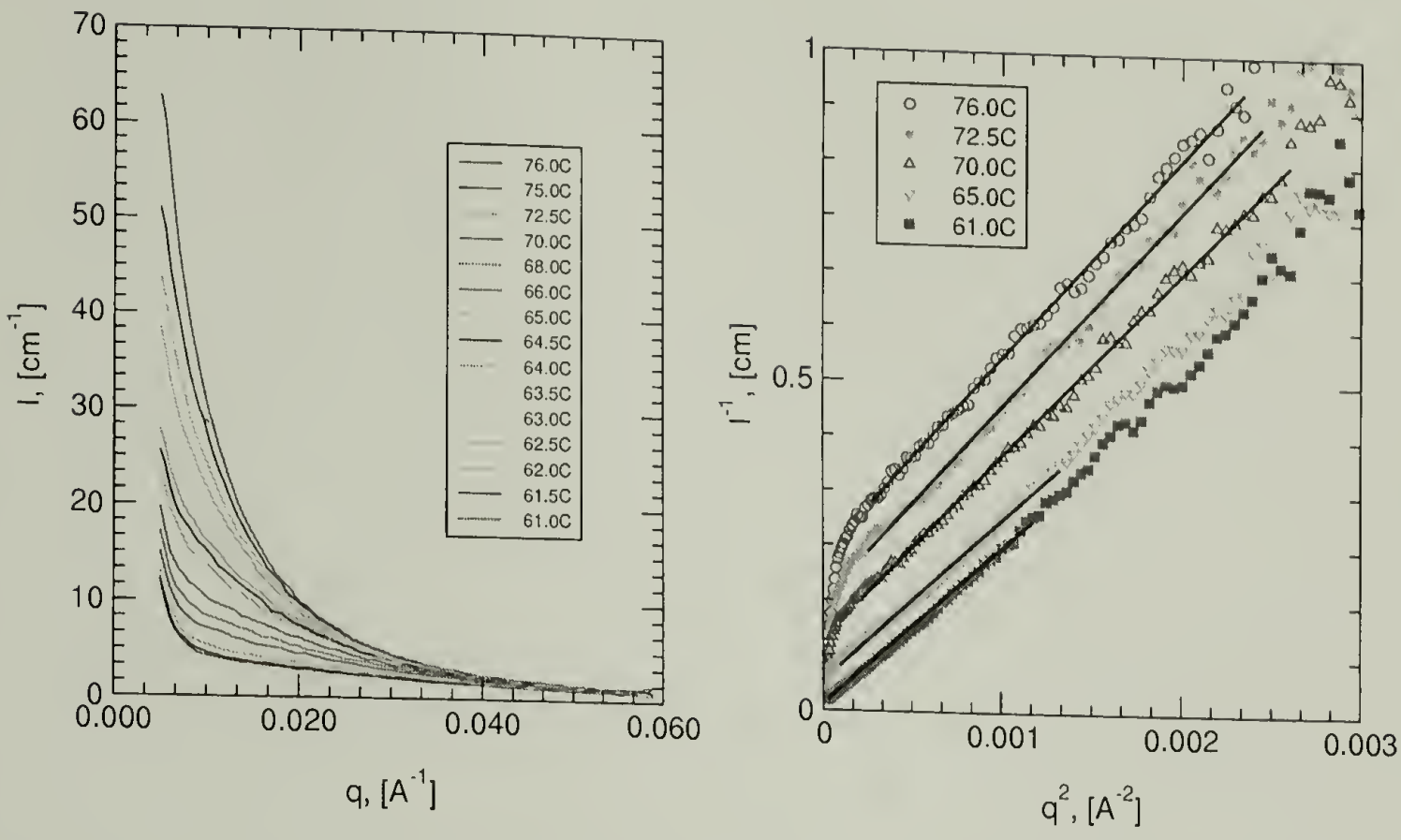

Figure 3.22: Left: Typical scattered intensity versus wavevector as a function of decreasing temperature to phase boundary for a fixed NaPSS polymer concentration of 206gL^{-1} and barium chloride salt concentration 0.38M for 56,000gmol^{-1}.Right: Corresponding Ornstein-Zernike plot from which ξ and I(0) are extracted avoiding the fit to the downturn excess scattering.

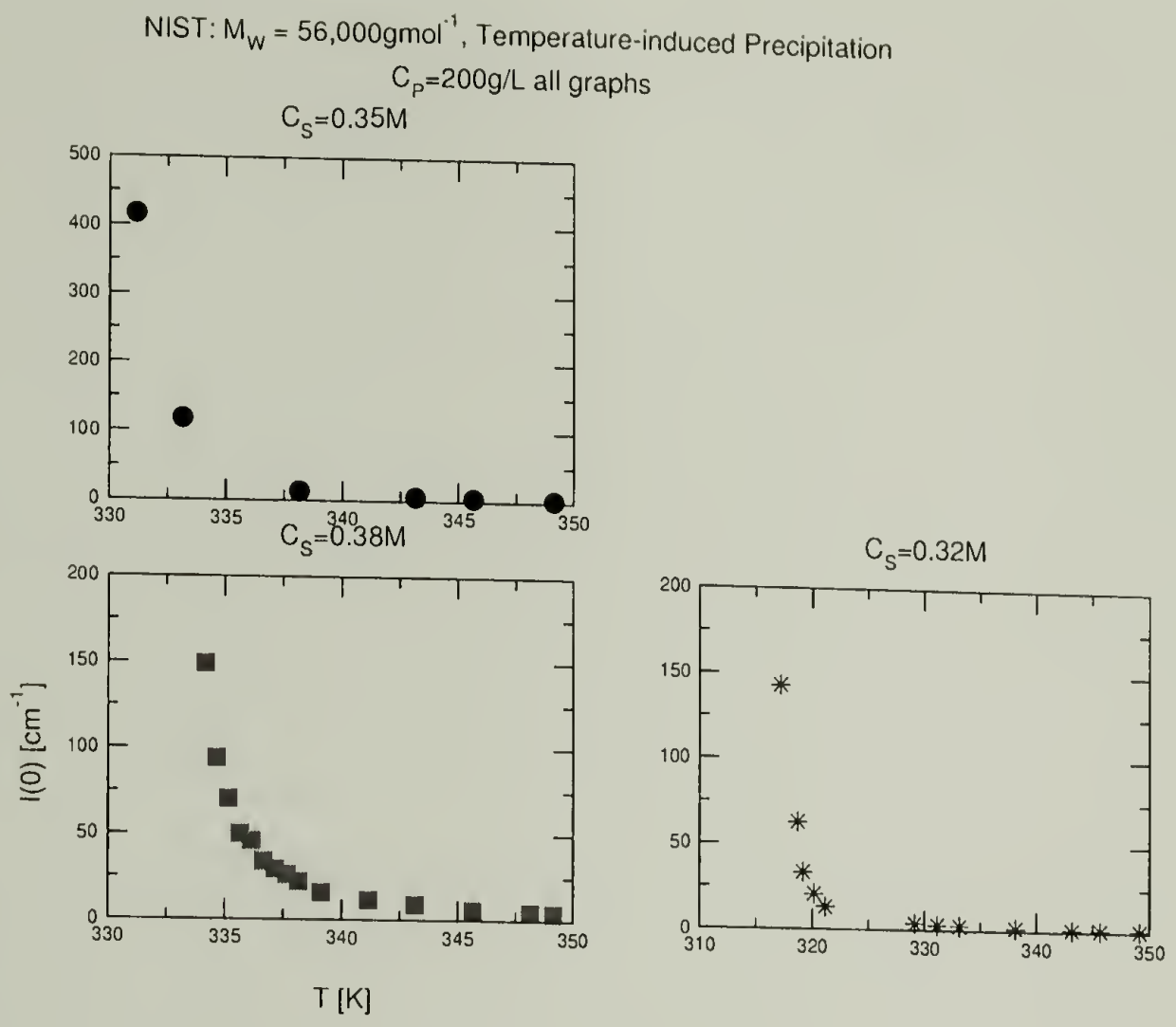

Figure 3.23: Summary of Divergence of I(0) for molecular weight 56,000gmol^{-1} and three salt concentrations given above each figure.

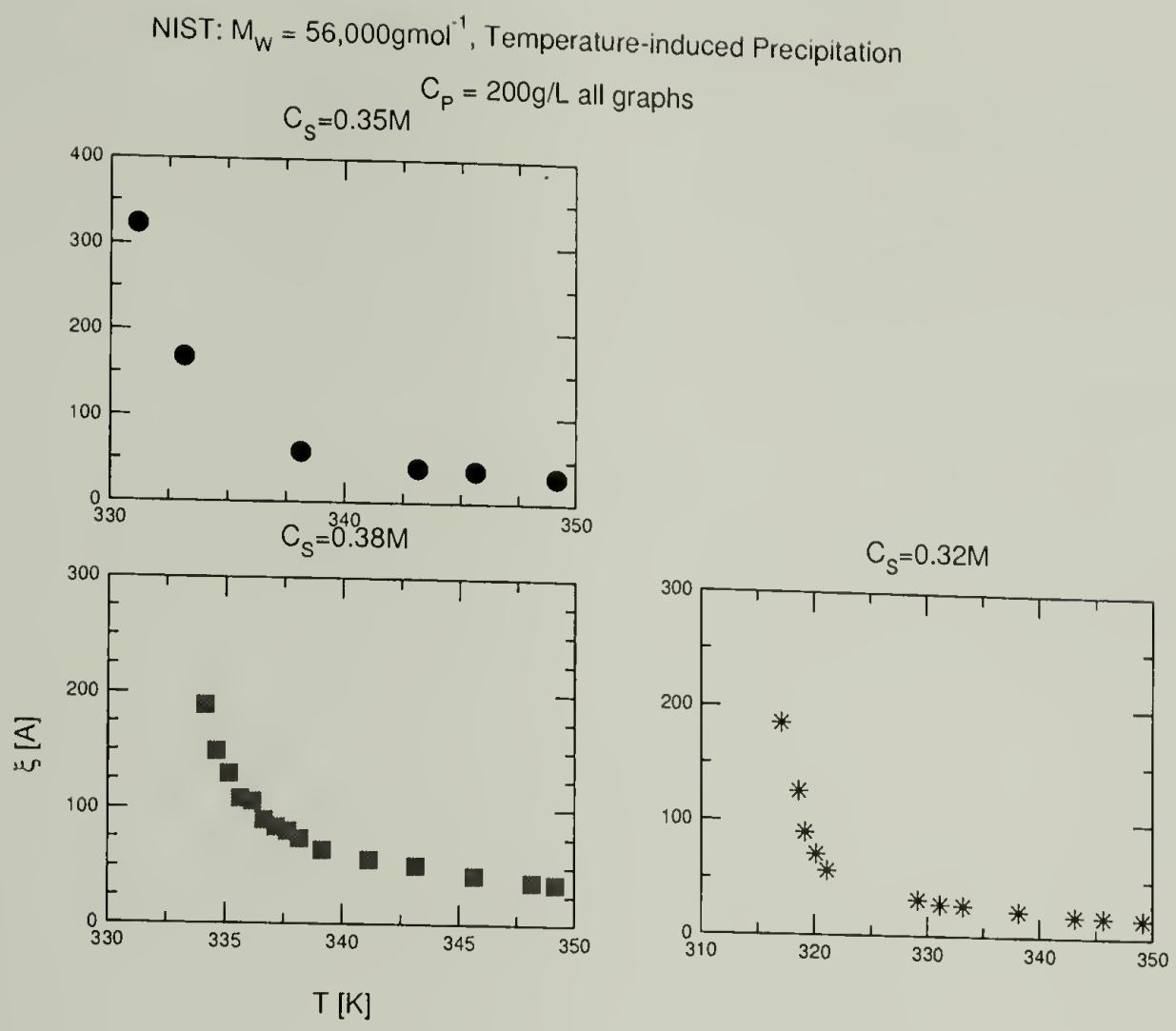

Figure 3.24: Summary of Divergence of ξ for molecular weight 56,000gmol^{-1} and three salt concentrations given above each figure.

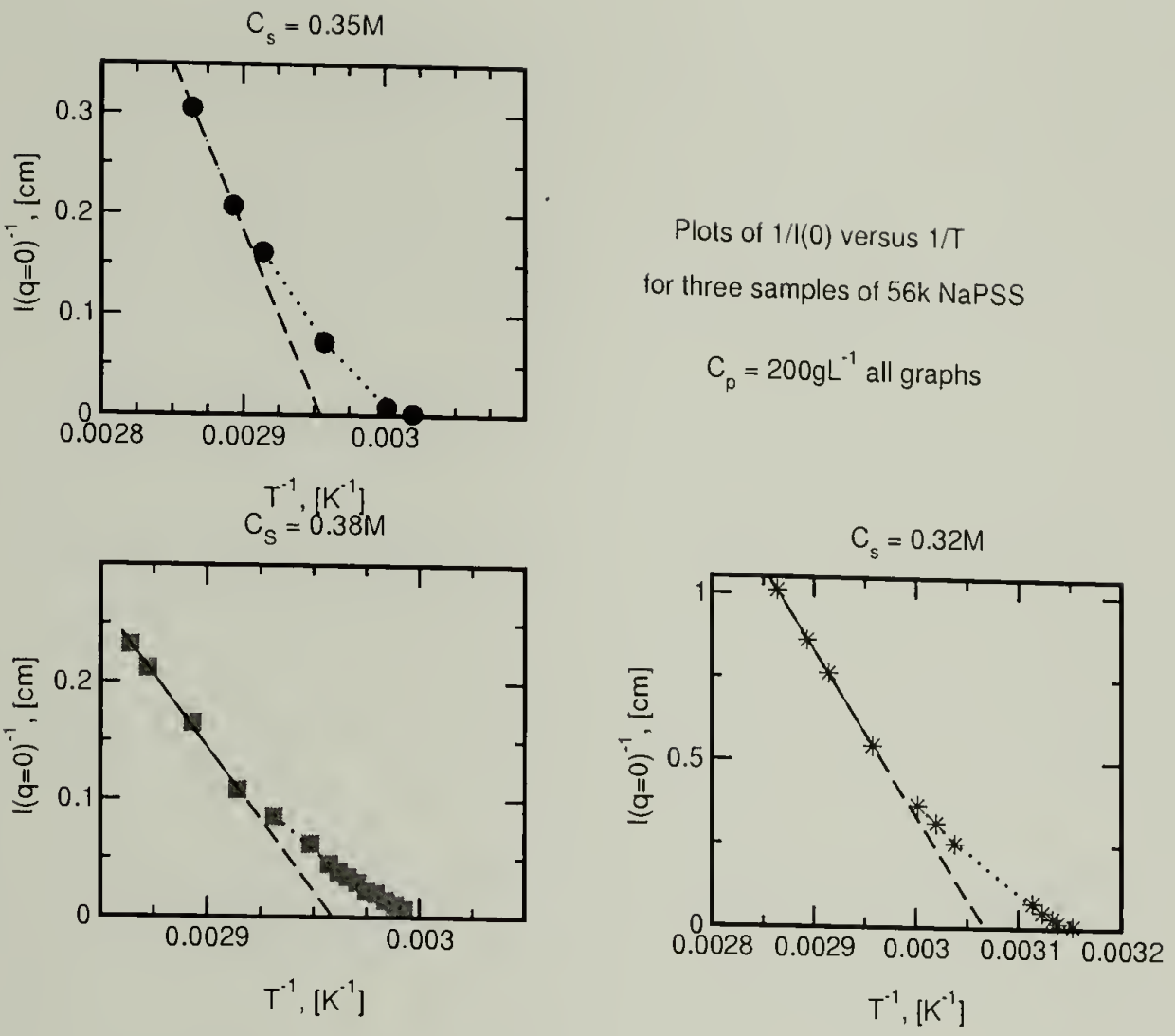

Figure 3.25: Summary of Mean Field-Fluctuation Regime, I(0) for molecular weight 56,000gmol^{-1} and three salt concentrations given above each figure.

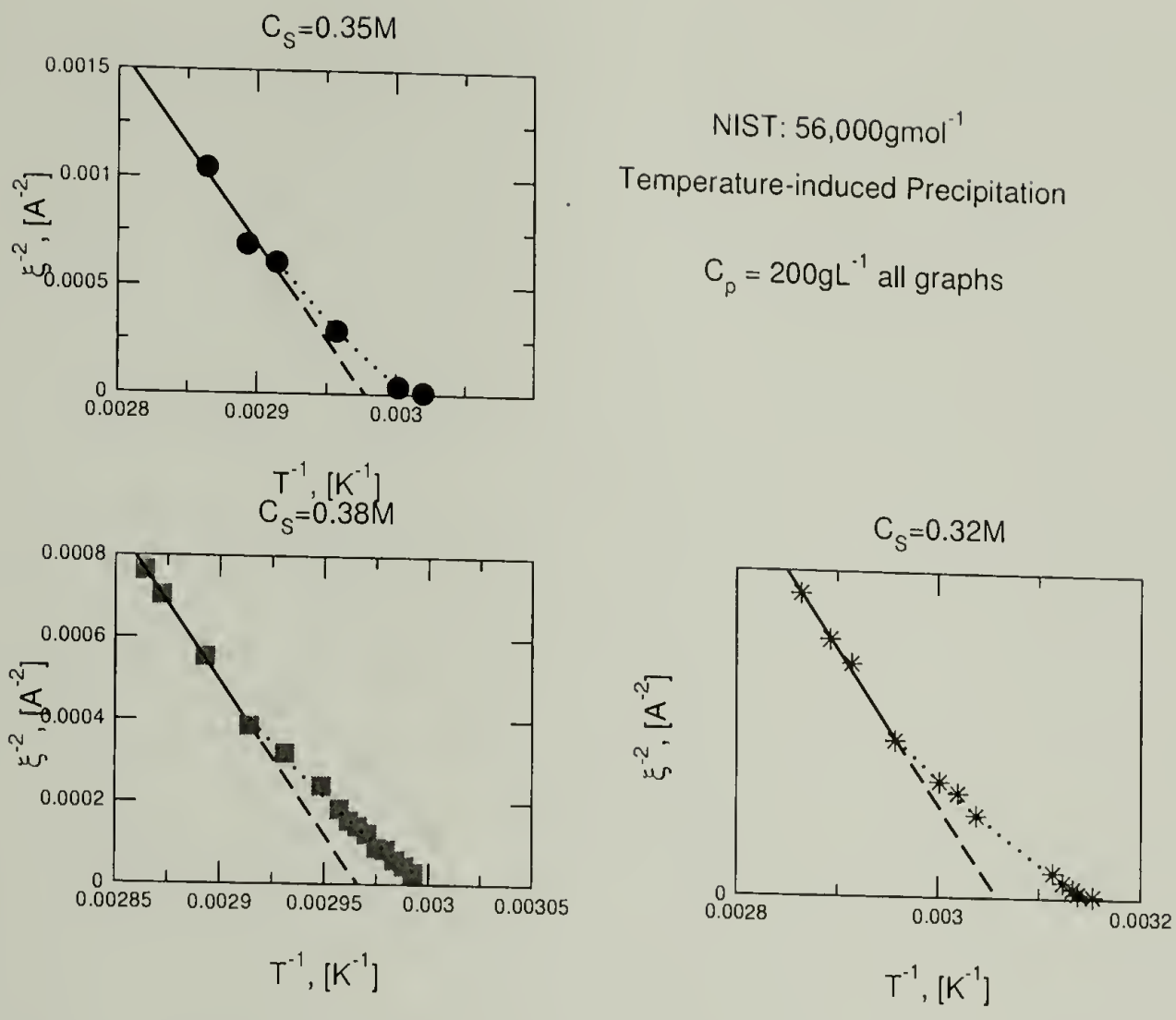

Figure 3.26: Summary of Mean Field-Fluctuation Regime, ξ for molecular weight 56,000gmol^{-1} and three salt concentrations given above each figure.

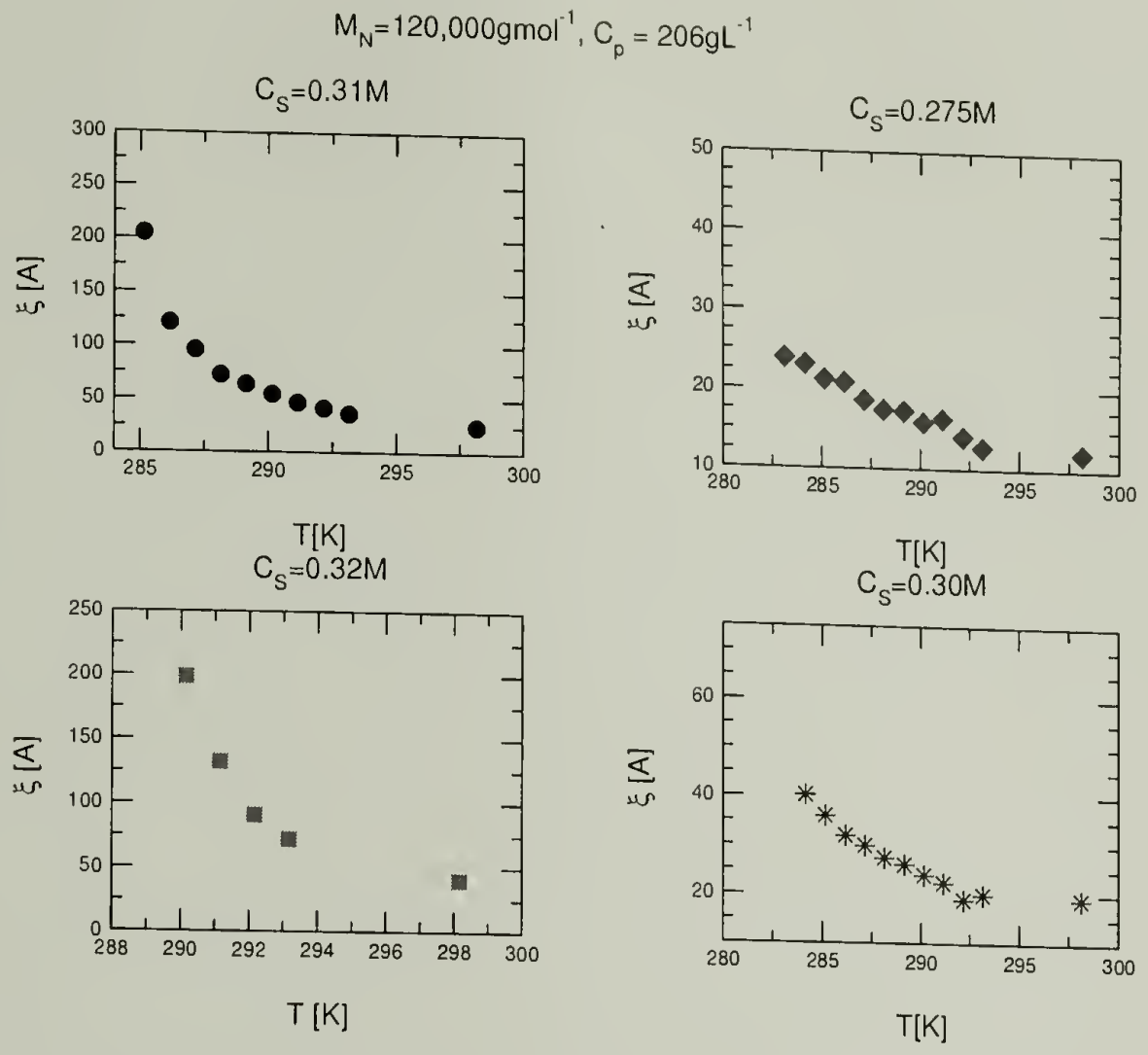

Figure 3.27: Correlation length versus temperature for M = 120,000 gmol^{-1}, C_p = 206gL^{-1}. Experiments performed below room temperature. Divergence observed for two samples C_s = 0.32 and 0.31M; samples C_s = 0.275 and 0.30M had to be stopped due to the problem of dew point, in which condensation of water from the air would influence the measured scattered intensity.

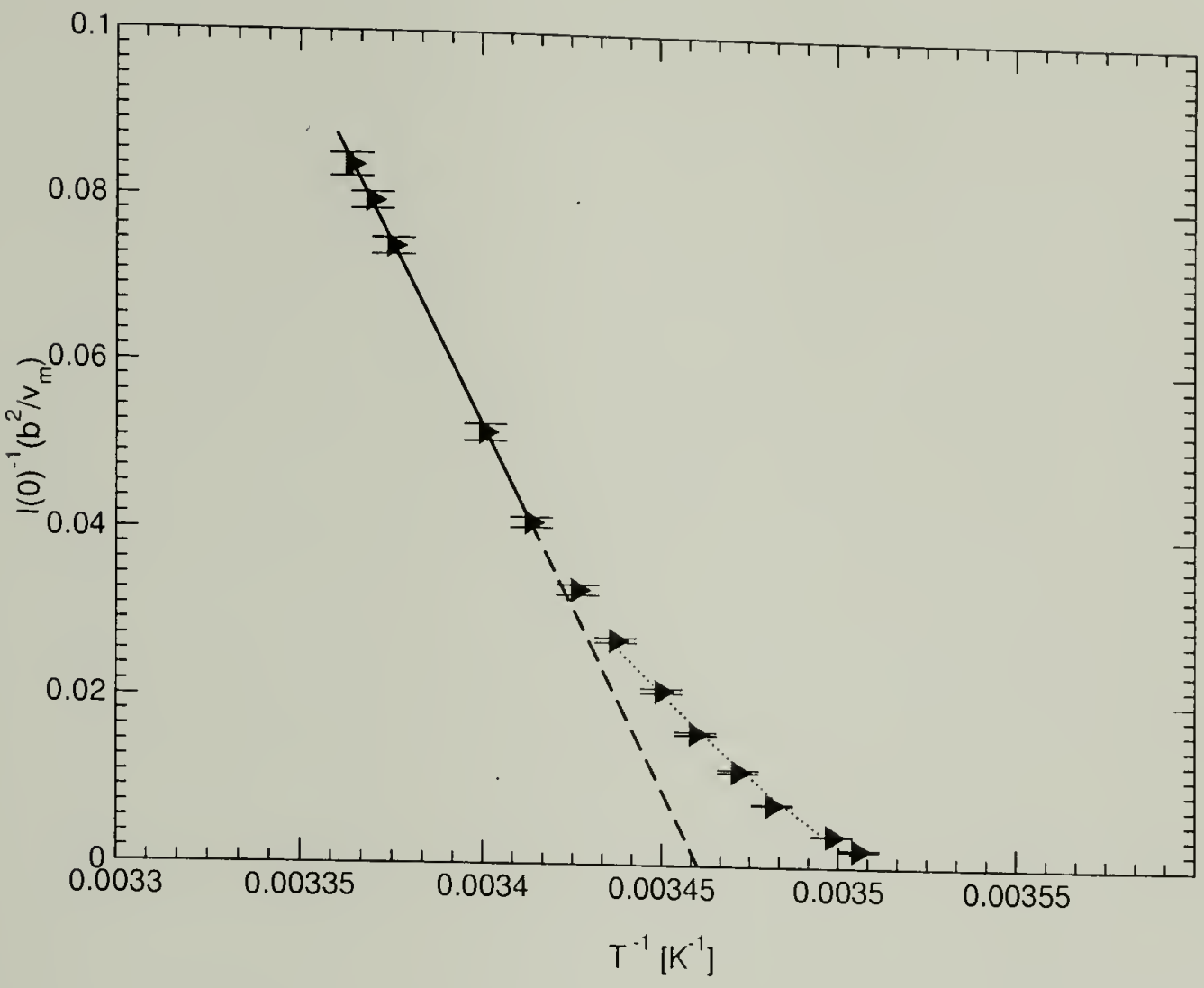

Figure 3.28: Inverse extrapolated scattered intensity to zero angle versus inverse absolute temperature for 200,000gmol^{-1}, polymer concentration 154gL^{-1}, and fixed salt concentration of 0.19M. The solid line indicates the linear region of mean field behavior and extrapolated to the mean field spinodal temperature. The curvature indicated by the dotted line indicates the Ising fluctuation region.

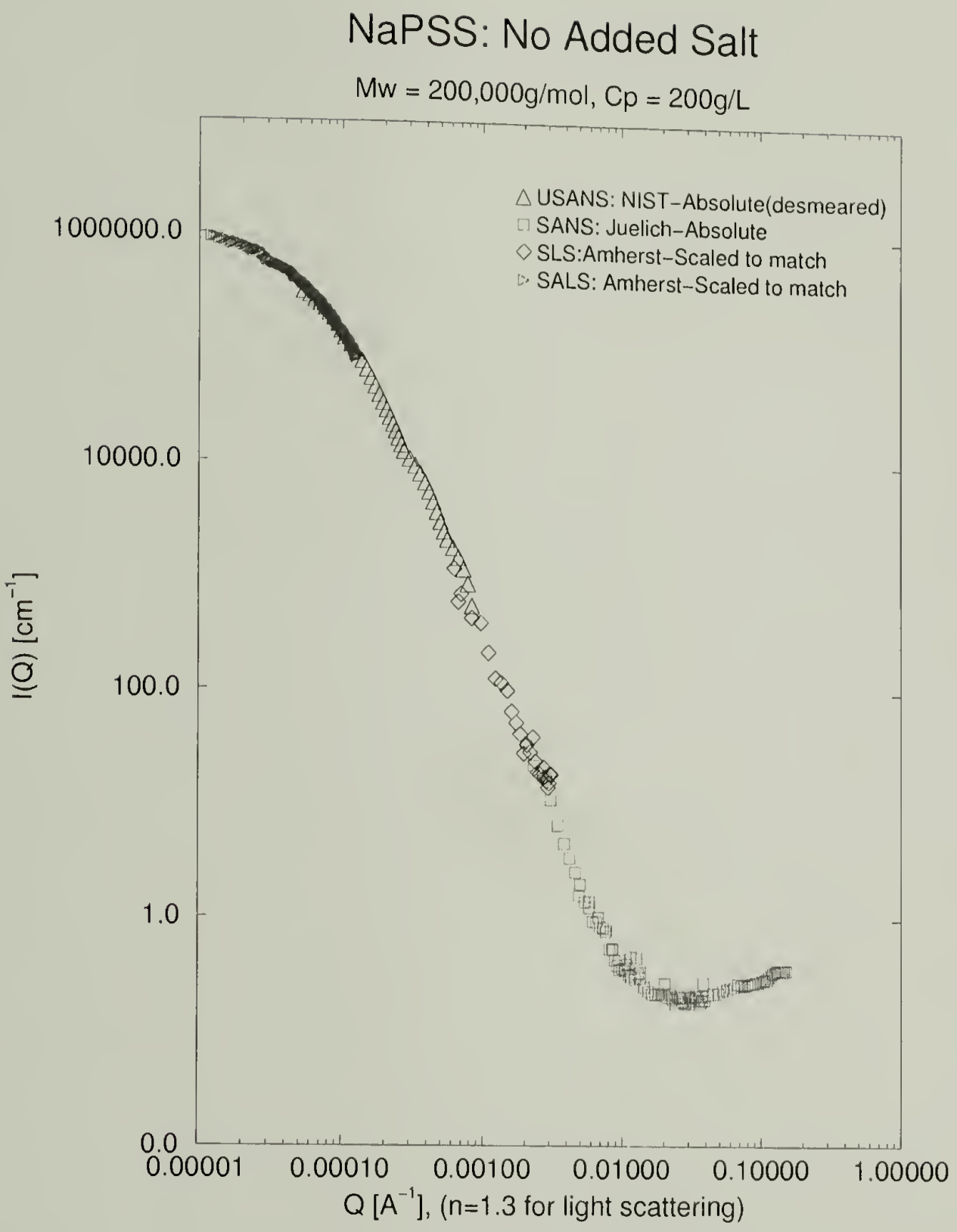

Figure 3.29: Experiments performed on a sample with molecular weight 200,000gL^{-1} with polymer concentration 206gL^{-1}(12 % by volume) and no added salt. A domain size of 4 microns is measured by Guinier analysis of the small-angle light scattering experiment.

CHAPTER 4

CONFIGURATIONAL PROPERTIES

4.1 Introduction

Having gained an understanding how the correlation length changes as the phase diagram is approached with temperature and added salt concentration, we now examine how the third length scale in the system, the radius of gyration, responds with a varying of the Debye length. It is known that in dilute solutions, without any complications of precipitation or phase diagrams, the chain dimensions measured by static light scattering are a strong function of the solution ionic strength[15]. As the ionic strength increases, the chain dimensions decrease due to the reduction of the range of the electrostatic interaction. This decrease was successfully quantified by using a variational procedure[13, 14, 15] to calculate the uniform expansion of chains, such that the model interaction between two Kuhn segments is of the form given in Eq.2.2.

Recent SANS experiments examined the variation of the persistence length as a function of the concentration of added multivalent salts. The experiments demonstrated that the persistence length decreases with increased ionic strength, in qualitative agreement with the role of κ^{-1} [50, 46]. Another recent set of experiments examined the influence of the valence of the counter-ion on the dimensions of labeled polymer chains. These experiments showed that the size of the chains are quantitatively smaller for multivalent cations in comparison to monovalent cations[51].

Unfortunately, no experiments have attempted to quantify the chain dimensions of polyelectrolytes in terms of concepts of excluded volume and electrostatic screening in the semidilute solution. We have attempted this analysis, as it will be shown, however, we have casting the influence of ion-pair formation into a renormalized degree of ionization that is a function of the added salt concentration. The results prove to be promising in comparison with the double screening theory. This complex problem that is burdened by specific interactions may be understood using coarse-grained theories.

For the problem under investigation, the room temperature $C_s - Cp$ diagrams were systematically probed using small-angle neutron scattering. A special labeling procedure is used to measure R_g as a function of molecular weight, polymer concentration, and added salt concentration. The motivation for these experiments is to measure the coupled length scales ξ and R_g as the phase boundary is approached. Since polymeric solutions have a characteristic dimension that is much larger than ξ, far from the phase boundary, it is interesting to measure the cross over in dominance as the phase boundary is slowly approached by increasing the ionic strength. Attempts will be made to quantify the chain dimensions by comparison to extended-chain and θ-coil dimensions as well as to the scaling and numerical results of the double screening theory in Table 4.1.

4.2 High Concentration Labeling

The high concentration labeling method [52, 53] has been used to follow single chain scattering for neutral polymeric systems, such as polymer/solvent[54, 55], polymer/polymer [56], and polymer/supercritical CO_2[57] mixtures. Here we apply the same formalism for aqueous polyelectrolyte solutions. Due to the dominant

neutron scattering contrast arising between monomer and solvent concentration fluctuations, the multi-component solution may be treated as an effective two-component system. This two component approximation has been successfully employed for sodium-poly(styrene sulfonate) without added salt[38, 46, 58, 51] and with added salt[59, 50, 60].

We refer to the main results of the high concentration methodology for the two component solutions,

$$I(q) = I_s(q) + I_t(q) \tag{4.1}$$

$$I_s(q) = KnN^2S_s(q) \tag{4.2}$$

$$I_t(q) = LnN^2S_t(q) \tag{4.3}$$

The prefactors are

$$K = [b_h - b_d]^2 x_h(1 - x_h)$$

$$L = [b_h x_h + b_d(1 - x_h) - b_s']^2$$

The absolute differential coherent scattering cross section, I(q), units of cm^{-1}, in this method is composed of a sum of two types of scattering; scattering associated with intra-chain monomer-monomer correlations(I_s) and total scattering from all monomer-monomer correlations(I_t), both intra and inter-chain. b_h and b_d are the scattering lengths of the protonated and deuterated monomers, respectively. b_s' is the scattering length of a solvent normalized via the ratio of the specific volume of the monomer and solvent molecule. b_s' may be adjusted by varying average scattering length of the solvent, by using an H_2O and D_2O mixture such that b_s' = $y_h b_{H_2O}$ + (1-y_h)b_{D_2O}, where y_h is the mole fraction of H_2O and b_{H_2O} and b_{D_2O} are the scattering lengths. n is the number of polymer molecules per unit volume

of solution and N the degree of polymerization. The essential physics remains in the single-chain structure factor (S_s), and the total scattering structure factor (S_t). The single chain scattering may be directly measured by making the prefactor L to the intensity of total scattering go to zero. We will refer to the matching point as the condition such that the average scattering length density[61] of the monomer matches that of the solvent which gives L=0.

4.3 Experimental Results

Samples were prepared by mixing dried polymer with the appropriate solvent mixture. Typical sample preparation and characterization are given in Appendix A and B. We have experimentally determined the matching point condition to extract the single chain scattering, based of the high concentration methodology. In order to make L=0 and yet retain a significant signal-to-noise ratio, we have chosen to fix the fraction of protonated chains at x_h=0.4 and tune the average scattering length of the mixed (H_2O,D_2O) solvent in such a way that $0.4b_h + 0.6b_d = b_s'$. The matching point utilizes a mass fraction of protonated chains, denoted x_h, of 0.40, with solvent of volume fraction H_2O, y_h, of 0.32. To accurately investigate varying salt concentrations, several stock salt solutions were prepared by dilution of a parent salty solution of $BaCl_2$ with $y_h = 0.32$. The absolute matching point conditions are increased to $y_h = 0.33$ due water content determined by TGA.

The experiments were performed at three different neutron scattering facilities; the National Institute for Standards and Technology (NIST) Center for Neutron Research[62] on the SANS beamline NG3, the Forchungszentrum Research Reactor FRJ-2[63] on beamline KWS-II, and at the W. C. Koehler SANS facility at the Oak Ridge National Laboratory[64]. The protocols performed at each reactor

are similar, we will describe the details for experiments performed at ORNL; the neutron wavelength was 4.75Å($\Delta\lambda/\lambda \approx 5\%$). The sample-detector distance was 5.8m and the data were corrected for instrumental backgrounds and detector efficiency on a cell-by-cell basis, prior to radial averaging to give a q-range of 0.008 $< q <$0.1Å^{-1}. The net intensities were converted to an absolute($\pm$4%) differential cross section per unit sample volume (in units of cm^{-1}) by comparison with precalibrated secondary standards, based on the measurement of beam flux, vanadium incoherent cross section, the scattering from water and other reference materials [65]. The efficiency calibration was based on the scattering from light water and this led to angle-independent scattering for vanadium, H-polymer blanks and water samples of different thicknesses in the range 1-10 mm. Procedures for calculating the incoherent background, arising largely from the protons in the sample, have been described previously [66].

4.3.1 No Added Salt: Evidence for Screening

For a fixed molecular weight the radius of gyration was measured as a function of polymer concentration in the semidilute regime without any added salt. Due to dissociated counter-ions and the presence of other chains, it is theoretically predicted that the size of the labeled chains decrease with increasing polymer concentration. This is experimentally observed. Fig.4.1 shows the result for the labeled chain scattering for four different polymer concentrations. The Z-averaged radius of gyration (R_g) was obtained from fits to the Debye structure factor, $S_D(q)$, Eq. 4.4, for all concentrations investigated,

$$S_D(q) = \frac{2}{q^4 R_g^4}(e^{-q^2 R_g^2} - 1 + q^2 R_g^2) \tag{4.4}$$

The details of the fits are left for Appendix D regarding the values of $I(0)$, R_g, and the incoherent background. It is observed in Fig.4.2 that the asymptotic behavior of the scaling of the radius of gyration with the polymer concentration follows with a scaling exponent is -0.24±0.01, in agreement with the double screening theory,Table 4.1. We do not observe any deviation from this measurement due to the fact that the concentrations examined are in the semidilute regime as experimentally verified in Chapter 3; this is self-consistent result. Further experimentation is necessary to examine the clear distinction between the semidilute and concentrated regimes.

The radius of gyration was also measured at a fixed polymer concentration in the semidilute regime as a function of the molecular weight, again without any added salts. The anticipated scaling was given in Table 4.1. For the three molecular weights examined we find a result which is in agreement with scaling theory, shown in Fig.4.3. These data were taken from three different laboratories, namely ORNL,NIST, and FZ-Jüelich. Additionally prepared samples of higher molecular weight were not able to be run at our most recent experimental trip, which would have improved the statistics.

We now describe the main results with the addition of barium chloride salt and merge the results with the correlation length.

4.4 Labeled Chain Results for 56,000gmol^{-1}

The method of data fitting was performed with the non-linear regression package from Mathematica 3.0 using the weights from the experimental errors in the measured I(q). A flat incoherent-scattering background was estimated from the scattering by a protonated polymer in the identical D_2O/H_2O mixture. This estimated background at high wavevectors is 0.341cm^{-1} and was subtracted from all data sets prior to fitting. Thus, the experiment measured the scattering behavior given by Eq.4.2, where S_s is modeled by Eq.4.4. This analysis works well as nearly the entire wavevector range may be fit. Particular exceptions may be made for the three highest salt concentrations where the scattering tends to deviate at low wave-vectors, to obtain good fits the first five data points were not fit. The experimental origin for this deviation may be two-fold; (1) these data are of low statistic due to averaging over less than 9 detector pixels, and (2) there remains a finite contribution from the total scattering. All the data-fits are shown in Fig. 4.4. The R_g and ξ for varying salt concentration are shown in Fig.4.5.

The size of the labeled chains decreases from 80±2Å to 54±1Å when the salt concentration is increased from 0.0M to 0.3375M. This is a decrease in the size of labeled chains by 33%. The coil shrinkage is consistent with the increased screening of repulsive intra-chain monomer-monomer electrostatic interactions by the mediating ions as the Debye length decreases from 9.57Åto 3.04Å (taking the degree of ionization to be 0.21). The numerical results are left for Appendix D which includes the degree of polymerization obtained from the scattered intensity to zero angle, which agrees well with the characterization data..

To gain an understanding of the size of the labeled chains, we compare to the rod-like limit and unperturbed theta-coil dimensions. The measured radius of

gyration, with no added salt, is smaller than that of a calculated fully extended rod-like conformation which is on the order of 200Å . Thus in comparison, the experimental data, are not properly described by a fully rigid rod-like conformation. The approach to the semi-dilute and concentrated solutions leads to an increased excluded volume screening by the presence of other monomers and electrostatic screening by the presence of dissociated counter-ions, explaining the smaller chain dimensions as theoretically predicted[14, 19].

The measured R_g of 54Å, at the highest salt concentration is larger than the theta dimensions calculated for fully sulfonated sodium-poly(styrene sulfonate) and polystyrene. Hirose et al.[67] have determined an empirical law of $< Rg^2 >_z = 0.030\text{Å}^2 M_W$ under experimental theta solvent conditions from dilute solution light scattering at 4.17M NaCl and 16.4°C. This law calculates a z-average radius of gyration of 42.2Å for our system using a weight average molecular weight as (0.4x52,400 + 0.6x54,900)x1.1g/mol = 59,290g/mol. Wignall et al.[68] determined an empirical law of $< Rg^2 >_z = 0.0729\text{Å}^2 M_W$ for atactic polystyrene in the melt. This calculates 46.7Å for our parent polystyrene system averaged as (0.4x29,800+0.6x28,500)x1.03g/mol = 29,890g/mol.

Neither of these estimates for the true theta-dimensions of poly(styrene) or poly(styrene sulfonate) match our measured chain dimensions, under high salt conditions. Even though both systems are under experimental theta-conditions by displaying the scaling criteria for flexible polymers of $< R_g^2 > \sim N$, they may not reflect identical local stiffness realized in this system, characterized by the characteristic ratio, C_∞[69].

4.4.1 Coupling of Length Scales

We have demonstrated the key experimental results of the R_g and ξ variation with added salt. In order to bring some physical insight into the coupling, R_g,ξ, and κ^{-1} are shown on Fig.4.6 with respect to the dimensionless parameter (κ_c^2/κ^2-1). However, the experimental estimate for the critical salt concentration differs by 6.6% between the two types of experiments: 0.335M and 0.357M for ξ and R_g, respectively. So, the critical κ_c^2 used was 11.38nm^{-2} and 10.773nm^{-2} for the R_g and ξ experiments, respectively.

Far from the phase boundary the size of the labeled chains is smaller than calculations for rod-like conformations. As argued earlier, this departure from rod-like conformations is consistent with excluded volume screening and electrostatic screening. The excluded volume screening is a result of the semidilute solution nature and the electrostatic screening is provided by dissociated polymer counter-ions. As salt is added to the solution, the radius of gyration decreases. The origin of this decrease is electrostatic in nature and may be theoretically related to the increased electrostatic screening, quantified by the decreasing Debye length, shown as the dashed line. As this electrostatic screening length decreases, monomers of the same chain are no longer influenced by the long-ranged Coulombic repulsion. Notice that the magnitude of the Debye screening length is always much less than the radius of gyration and less than the intrinsic persistence length of 6.9 Å. Yet, significant coil contraction is observed. This stresses the importance of electrostatics, even though the calculated theoretical range becomes less than the bare-persistence length of the polymer. Such behavior may be strongly coupled to an additional contribution from ion-pair formation, this influence is realized in Chapter 5.

Simultaneously, in the limit of screened electrostatics, the measure of all monomer-

monomer correlations ξ is extracted from the experimental data by the Ornstein-Zernike equation. ξ increases as the phase boundary is approached and begins under low salt as a measure of short-ranged inter-chain correlations[70]. However, as the phase boundary is approached the correlations become longer-ranged due to the diverging behavior with $(\kappa_c^2/\kappa^2\text{-}1)$. Eventually the microscopic correlations on the order of the radius of gyration are not important, as the correlation length diverges beyond R_g, such that $\xi \gg R_g$. The crossing of ξ past R_g is observed for critical neutral polymer solutions as the critical temperature is approached. However, in our case the system is not known to be of critical composition, nor approaching a critical point. Even in a complex electrolyte solution similar salient features are observed regarding monomer-monomer correlations, except that the intensive thermodynamic variable tuned is the salt concentration, not temperature.

Figures 4.7 through 4.13 are the main results for R_g and ξ variations for 120,000gmol^{-1} and 200,000gmol^{-1} samples. The comparison to the theta-coil and extended chain conformations are given in the respective figure captions. It can be seen that the ideal chain dimensions are never achieved. The onset of precipitation precludes any such ideal solution behavior-as measured via chain statistics.

4.5 Double Screening Theory Applied to R_g data

In collaboration with Kingshuk Ghosh, we have applied the double screening theory to calculate the radius of gyration for arbitrary values of the ionic strength and polymer concentration. The equations are not given here, but are coupled non-linear equations which were solved numerically by successive substitution. The input variables required to make the comparison of theory and experiment were polymer concentration, Bjerrum length, bare Kuhn length, degree of polymeriza-

tion, Kuhn segment valence, salt concentration, and the following form for the degree of ionization $\alpha = \alpha_o$-(Constant)C_s. The excluded volume parameter used was estimated from the total scattering data[60]. Hence, the comparison remains to be made with only two parameters and the trial form for the degree of ionization.

The main results are shown in Fig.4.14 in which the sample of molecular weight 120,000gmol^{-1} is shown as functions of polymer concentration and added salt concentration. These results show considerable agreement with the experimental data in the magnitude of the change in the expansion factor as a function of the added salt concentration. The chosen form of the degree of ionization was made in order to observe better agreement in terms of magnitude on coil contraction and curvature. The α_o which would be the degree of ionization under no added salt was set to 0.90 in order to realize the significant expansion factors measured experimentally, values are given in Table 4.2. The use of the uniform expansion and polyelectrolyte model was applied quantitatively from dilute solution results of Beer et al.[15].

It should be noted that such form of the salt concentration dependence of the degree of ionization is not treated within the theory. However, it does direct us to the significance of the effect of the added salt. One would expect in the case of strong binding between two monomers and a divalent ion, or one monomer and one divalent ion does reduce the charge density of the chain(assuming a uniform charge). The capacity for binding has been established experimentally by Francois et al.[72, 28] using EPR and fluorescence measurements in which an equilibrium is satisfied between the free and bound ions. Such recent advances, however, remain to be understood with respect to the loss in entropy of the polymer for enthalpic loss in forming hairpins or ionic cross-links between chains. Such scenarios can be found routinely in biology from zinc finger motifs in which one tetravalent zinc cation is bound among four residues[73]. The stabilization of the configuration via

ionic coordination allows for transcription factors to bind to DNA[74]. Although, in this case the coordination also involves secondary structure which tends to stiffen the chain leaving the more relevant problem of semiflexible polymers.

4.6 Concluding Remarks

Under the semidilute solution conditions, we measured radius of gyration of labeled chains by fitting the single chain scattering with the Debye structure factor. We recovered the following result, for the first time, $R_g = 0.83 C_p^{-0.24\pm0.01} M_w^{0.53}$. Here, the exponents for the molecular weight and polymer concentration and in comparison with the theoretical values of $-1/4$ and $1/2$, respectively. With the addition of the multivalent salt, we observe significant coil contraction for all concentrations and molecular weights investigated. Only in the high polymer concentration of $400 \mathrm{gL}^{-1}$ does the influence of added salt have a negligible effect as measured for the $200{,}000 \mathrm{gmol}^{-1}$ sample. The analysis performed was to compare the measured dimension with those of the two limiting cases, extended-chain conformation and unperturbed theta-dimensions. It appears that even with the addition of salt, precipitation always occurs before the onset of the theta dimensions. Compared to neutral polymer solutions prepared at the critical composition, the theta dimensions are reached and persist down to the critical temperature[71]. The double screening theory was used to calculate the expansion factor for the experimental conditions measured. In order to obtain reasonable agreement it was found necessary to use a salt concentration-dependent degree of ionization.

Table 4.1: Double Screening Predictions

Low Salt	High Salt
$R_g \sim N^{1/2} C_p^{-1/4}$	$R_g \sim N^{1/2} C_p^{-1/4}$
$\xi \sim N^0 C_p^{-1/2}$	$\xi \sim N^0 C_p^{-3/4}$

Table 4.2: Parameters

C_p	$\alpha(C_s)$	α_{final} at C_s
200	0.90-1.90C_s	0.29 at C_s=0.32M
100	0.90-3.27C_s	0.18 at C_s=0.22M
50	0.90-5.35C_s	0.15 at C_s=0.14M

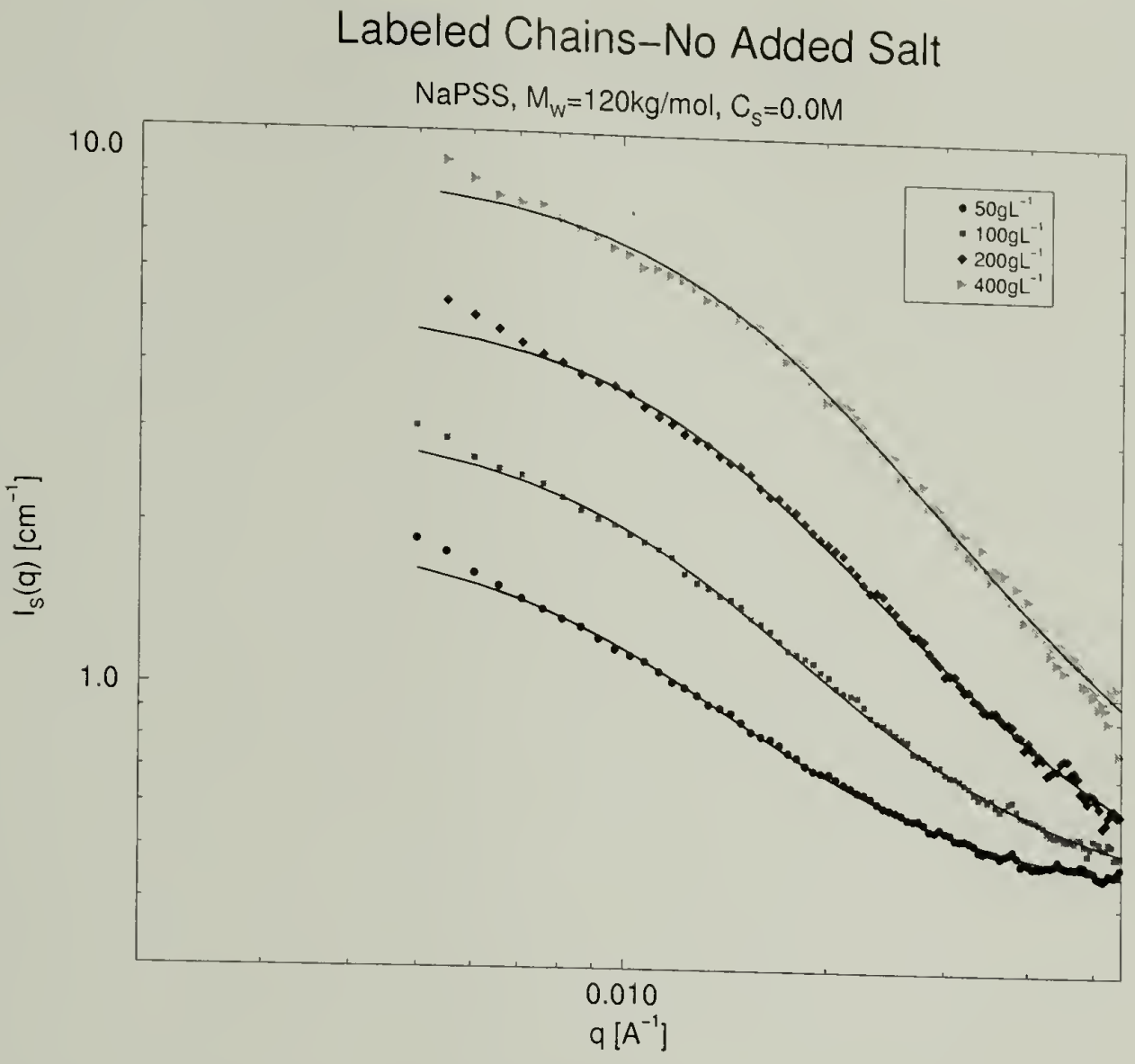

Figure 4.1: For a fixed molecular weight of 120kg/mol without added salt, the measured single chain scattered intensity as a function of wavevector is shown for four different polymer concentrations. Radius of gyration are extracted from fits to the Debye structure factor, shown as the dark lines.

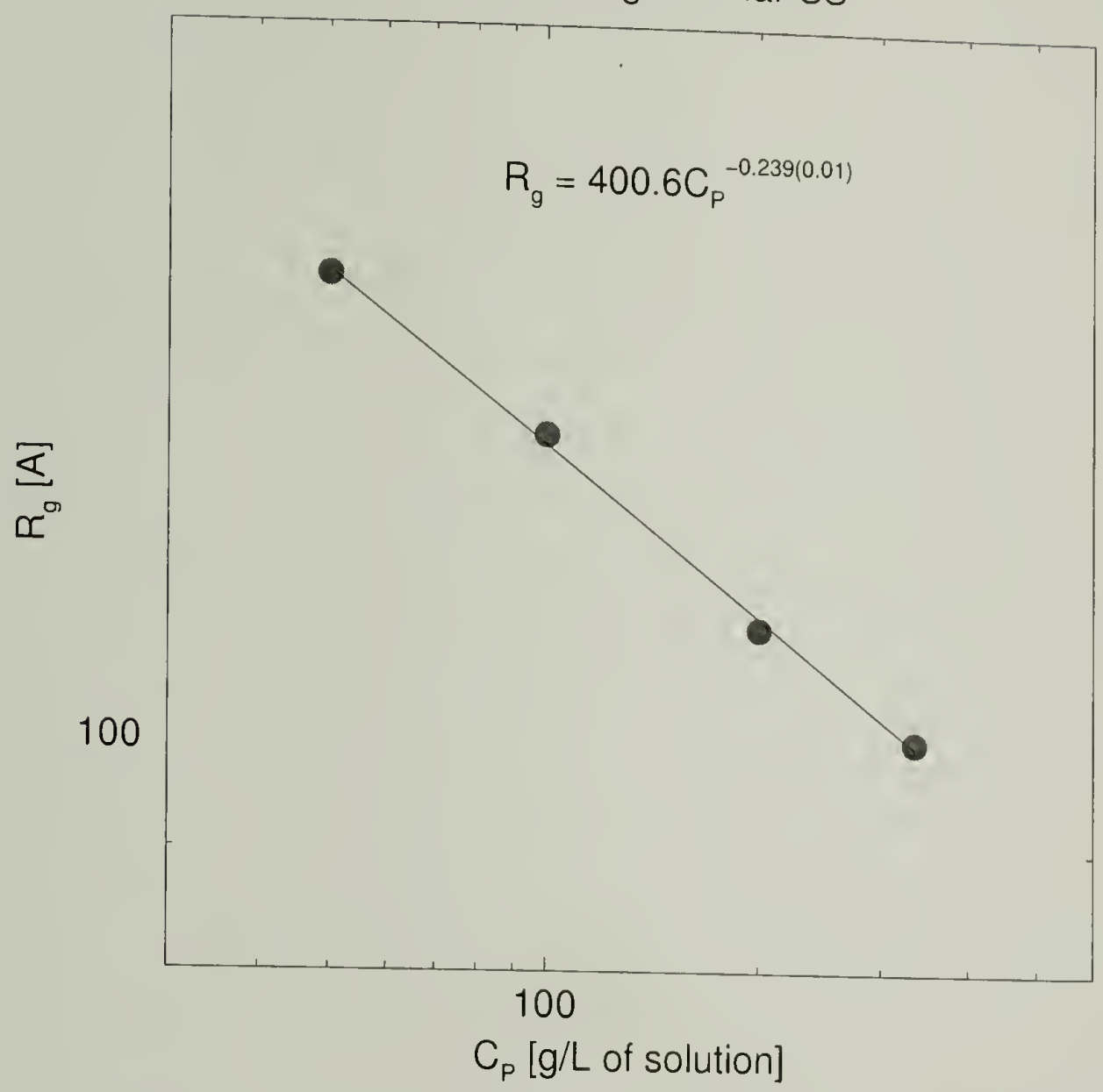

Figure 4.2: For a fixed molecular weight of 120kg/mol without added salt, the radius of gyration is found to decrease with increasing polymer concentration. The extracted scaling is in agreement with theoretical predictions for no added salt semidilute polyelectrolyte solutions.

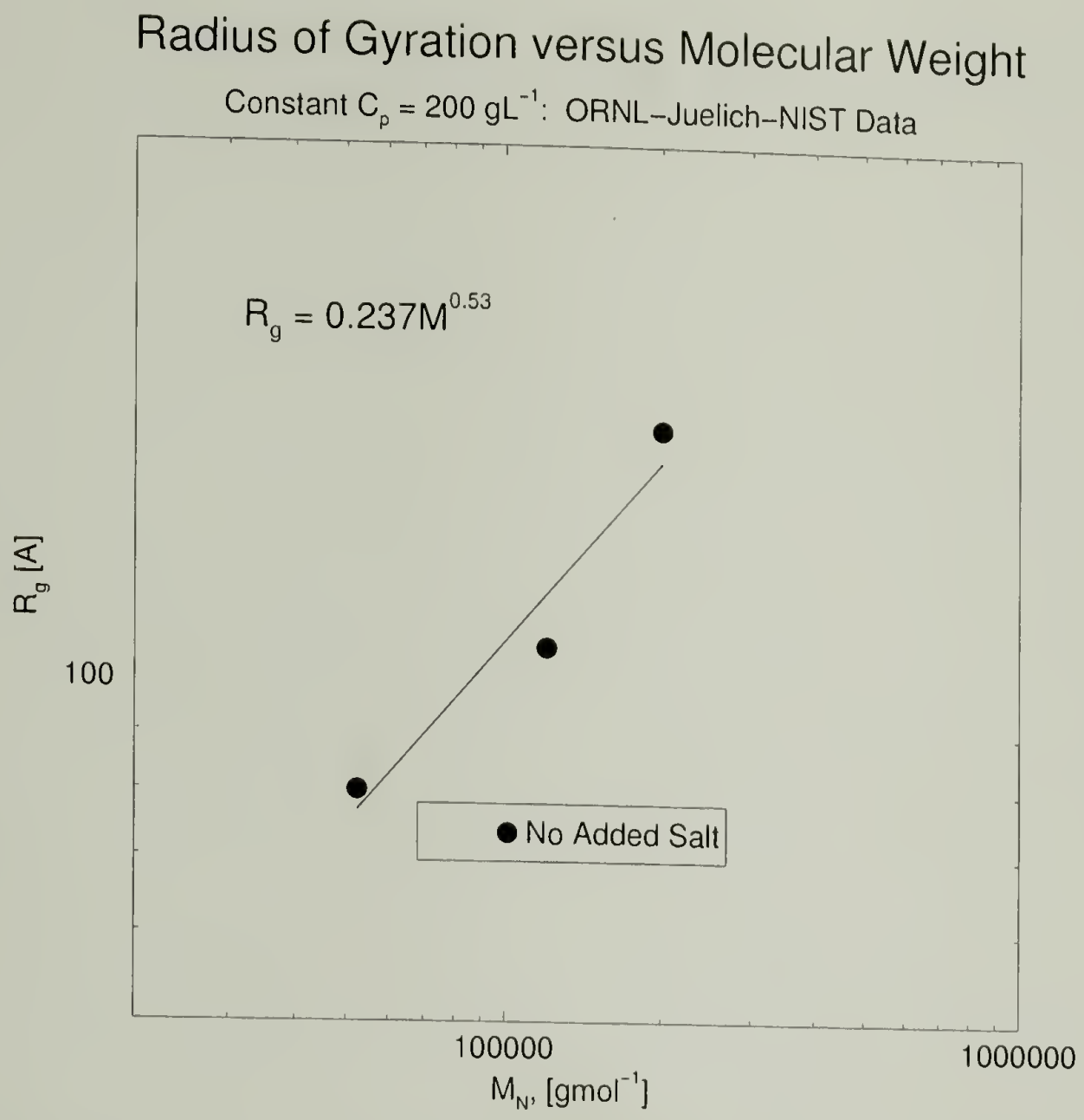

Figure 4.3: For a fixed polymer concentration of 200g/L without any added salt, the radius of gyration is found to increase with increasing molecular weight. A line is drawn which indicates a slope of 1/2, indicating agreement with predicted scaling for low ionic strength semidilute polyelectrolyte solutions. Data are from three neutron facilities.

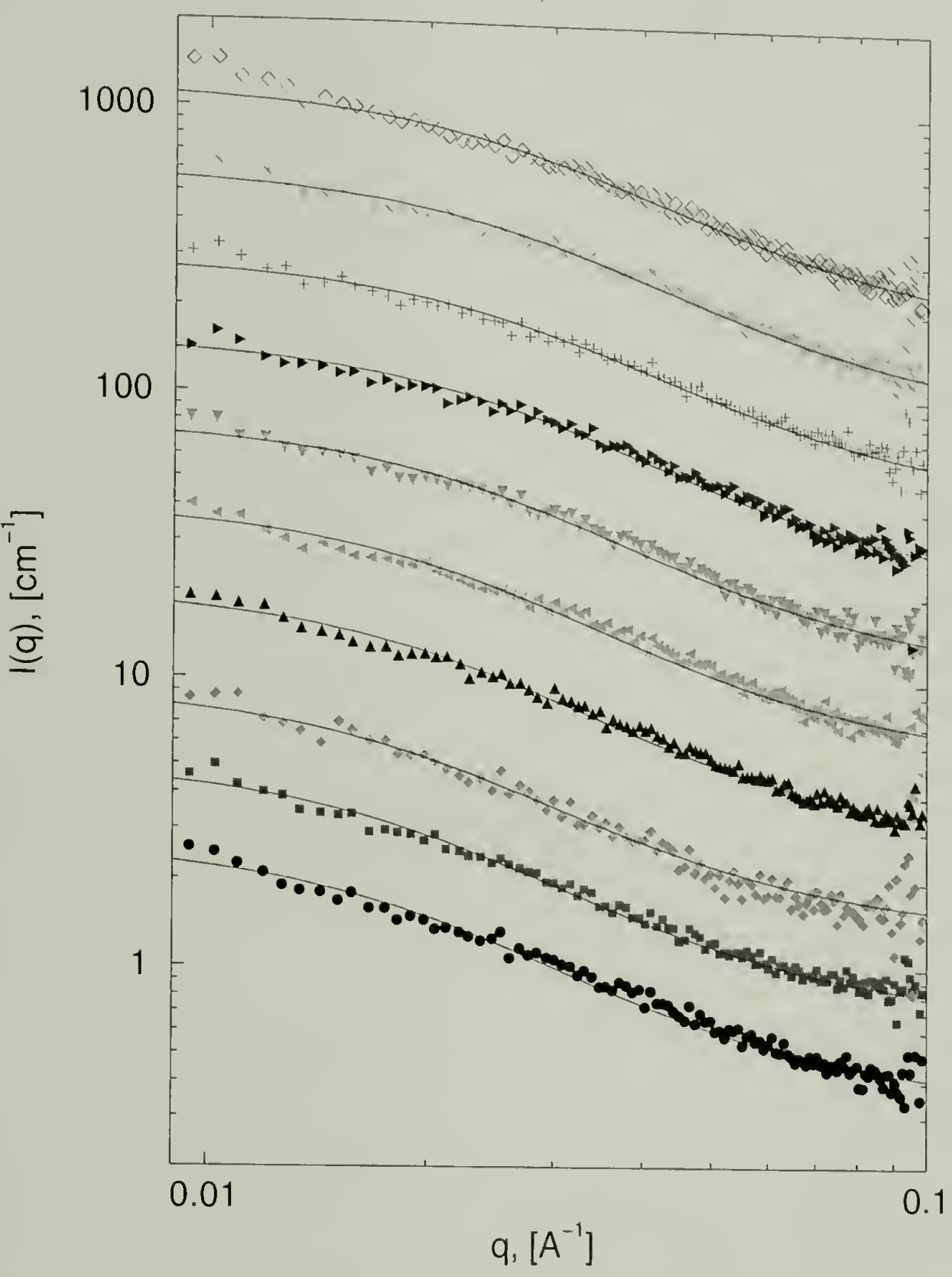

Figure 4.4: High concentration labeling for 56,000gmol^{-1}, experimental data fit with the Debye structure factor. Data sets are vertically shifted by a factor of 2 for increasing levels of barium chloride salt.

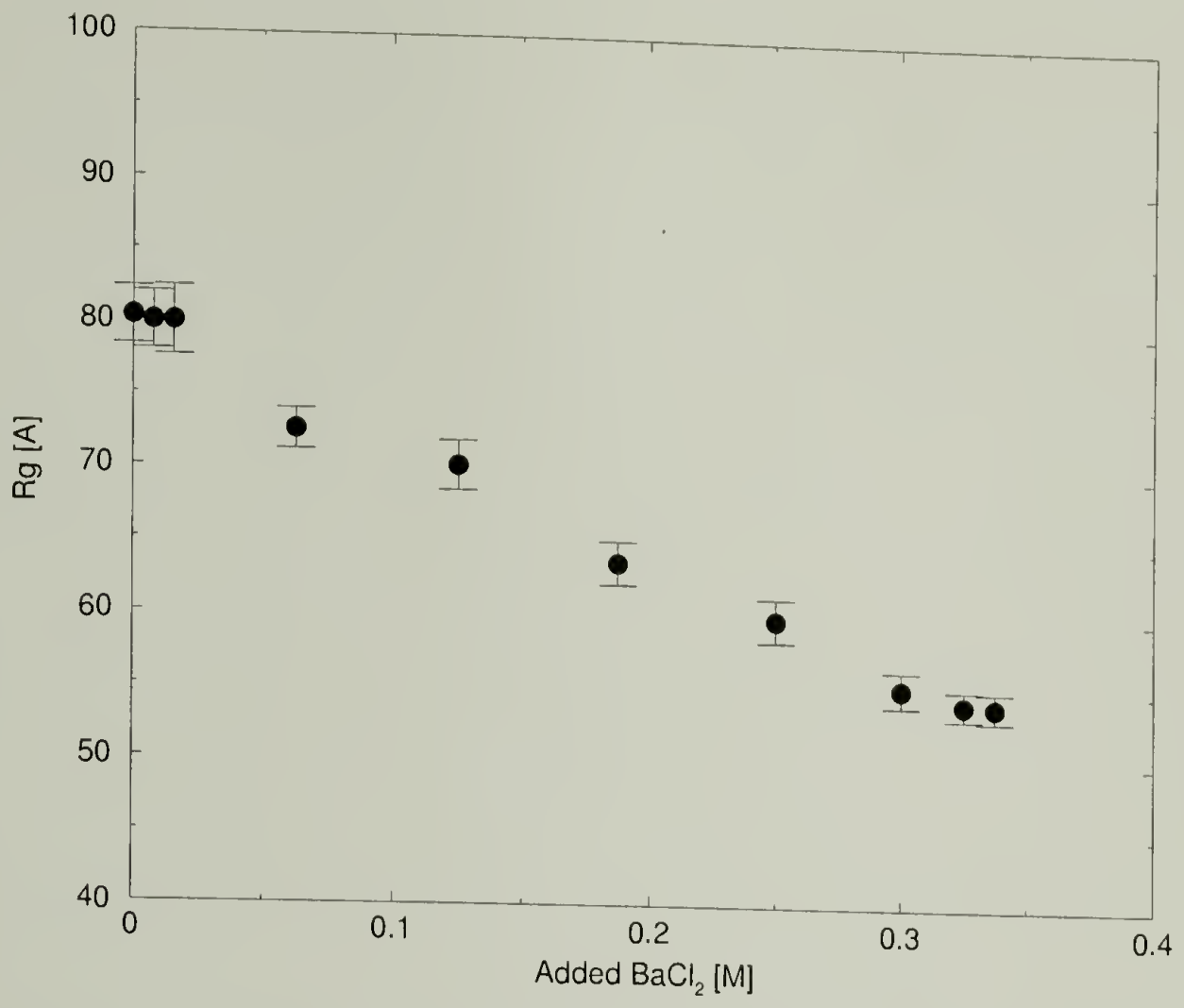

Figure 4.5: High concentration labeling, radius of gyration versus added barium chloride salt concentration for molecular weight 56,000gmol^{-1}.

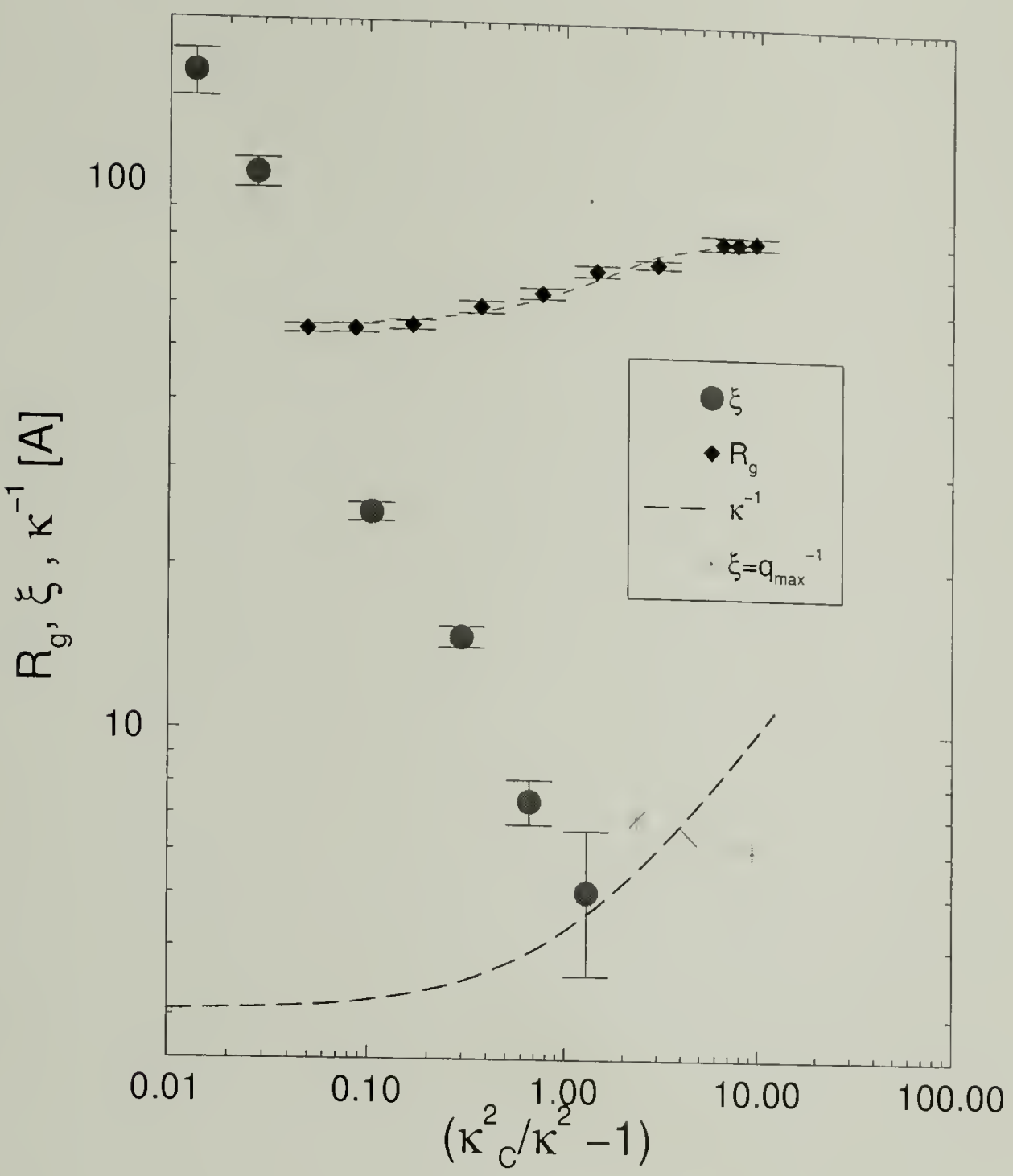

Figure 4.6: Composite plot of ξ, R_g, and κ^{-1} versus dimensionless depth from phase boundary. Critical conditions used are $\kappa^2_{c,\xi}$=10.773nm^{-2}, κ^2_{c,R_g} = 11.38nm^{-2}. The correlation length from the polyelectrolyte peak are also given.

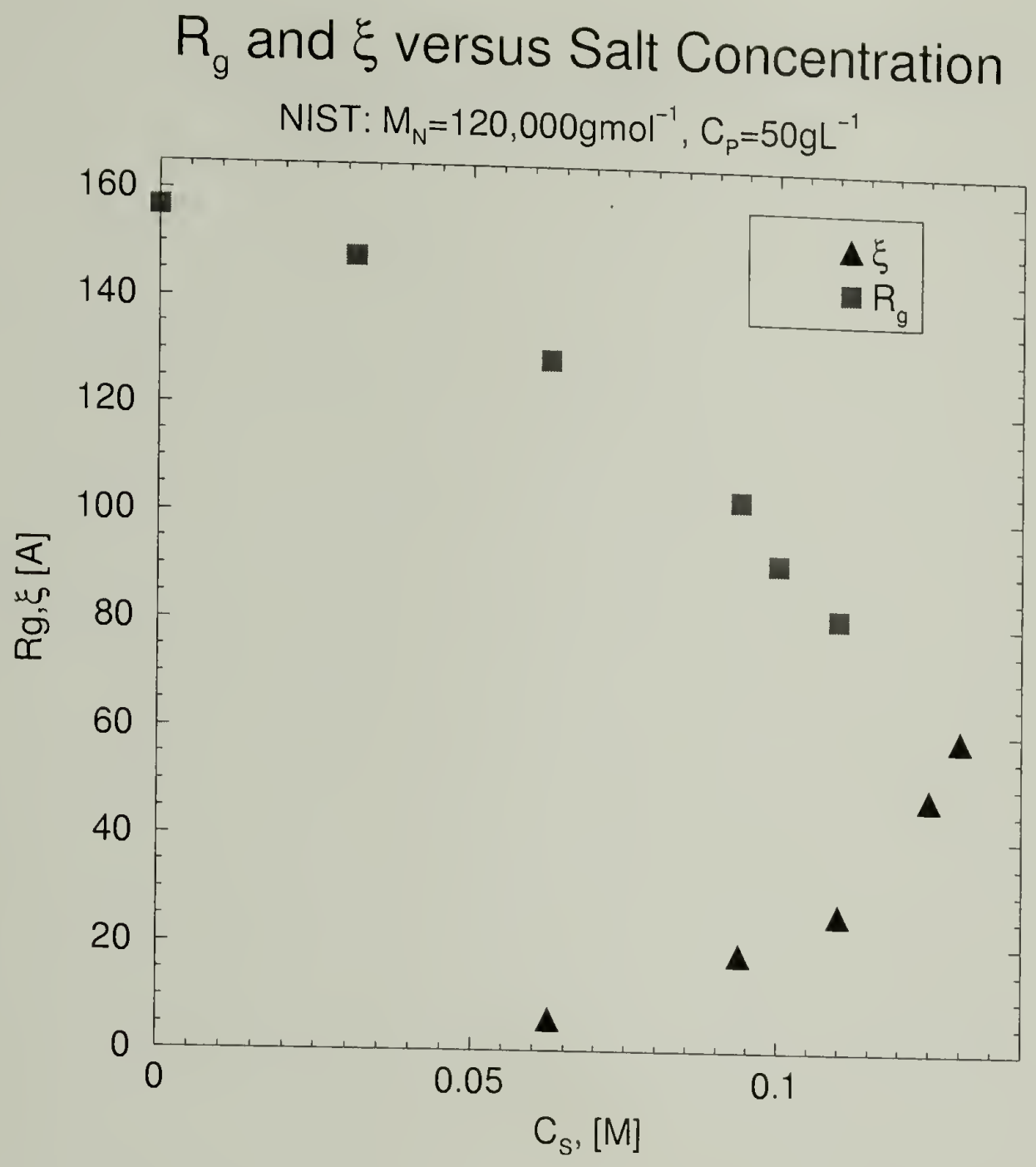

Figure 4.7: Overlap Concentration calculated is $12gL^{-1}$ and $88gL^{-1}$ for added salt levels of 0.0M and 0.11M, respectively. Estimated theta dimensions is 62Å. Estimated Rod-like dimensions is 420Å. An overall 48 % change in chain dimensions is observed.

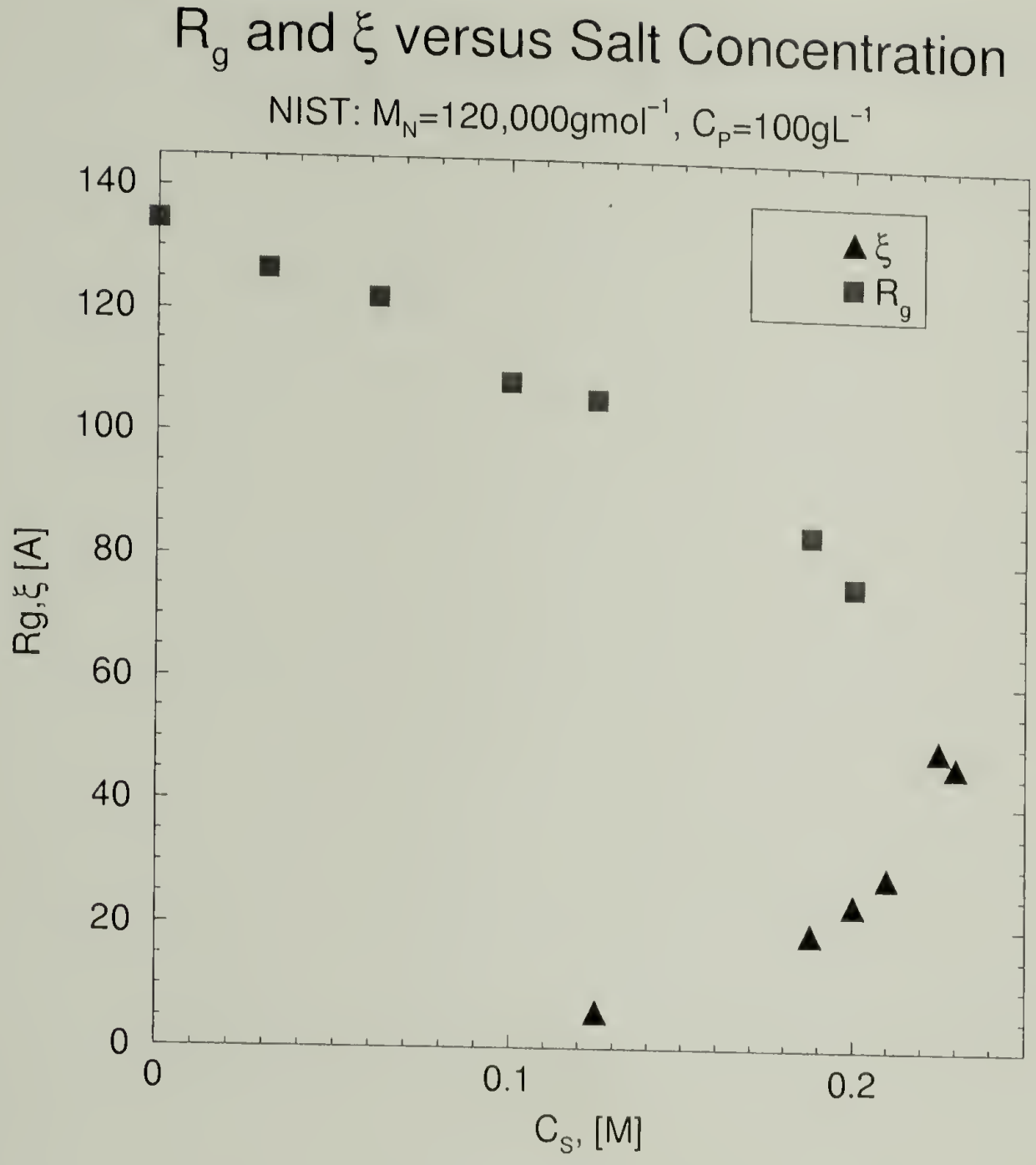

Figure 4.8: Overlap Concentration calculated is 20gL^{-1} and 108gL^{-1} for added salt levels of 0.0M and 0.2M, respectively. Estimated theta dimensions is 62Å. Estimated Rod-like dimensions is 420Å. An overall 44 % change in chain dimensions is observed.

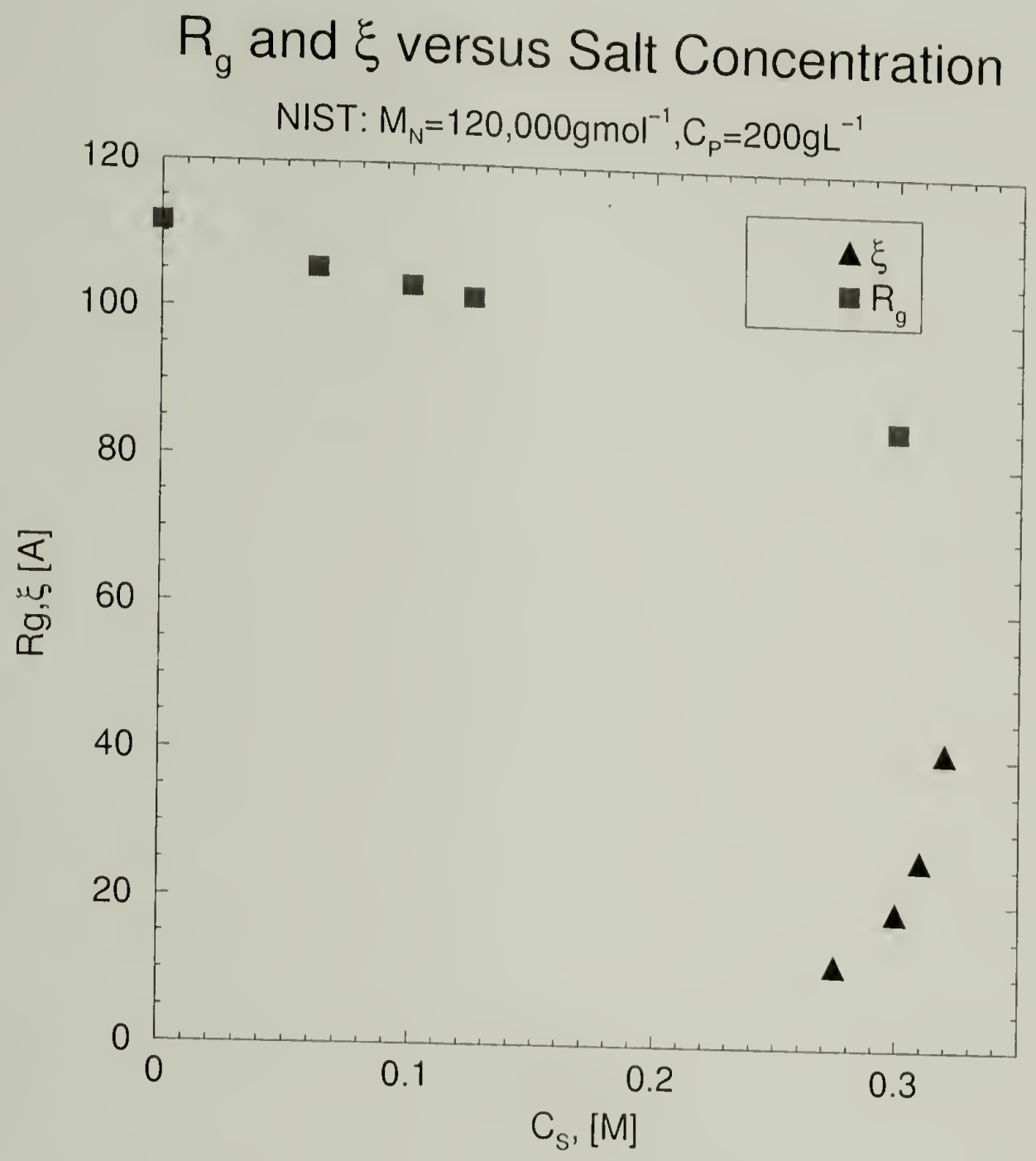

Figure 4.9: Overlap Concentration calculated is 34gL^{-1} and 77gL^{-1} for added salt levels of 0.0M and 0.30M, respectively. Estimated theta dimensions is 62Å. Estimated Rod-like dimensions is 420Å. An overall 24 % change in chain dimensions is observed.

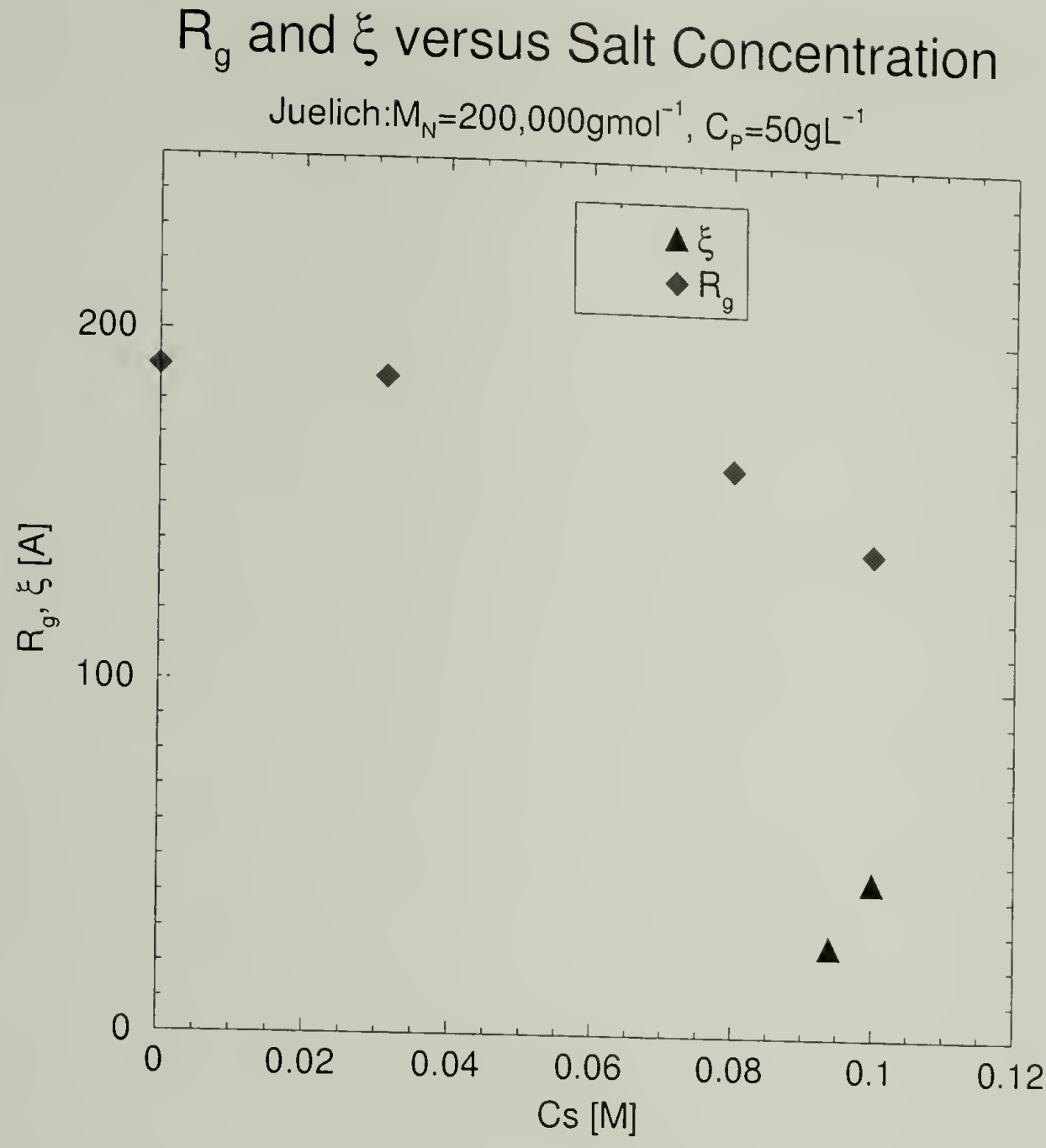

Figure 4.10: Overlap Concentration calculated is 12gL^{-1} and 30gL^{-1} for added salt levels of 0.0M and 0.10M, respectively. Estimated theta dimensions is 76 Å. Estimated Rod-like dimensions is 700 Å. An overall 26 % change in chain dimensions is observed.

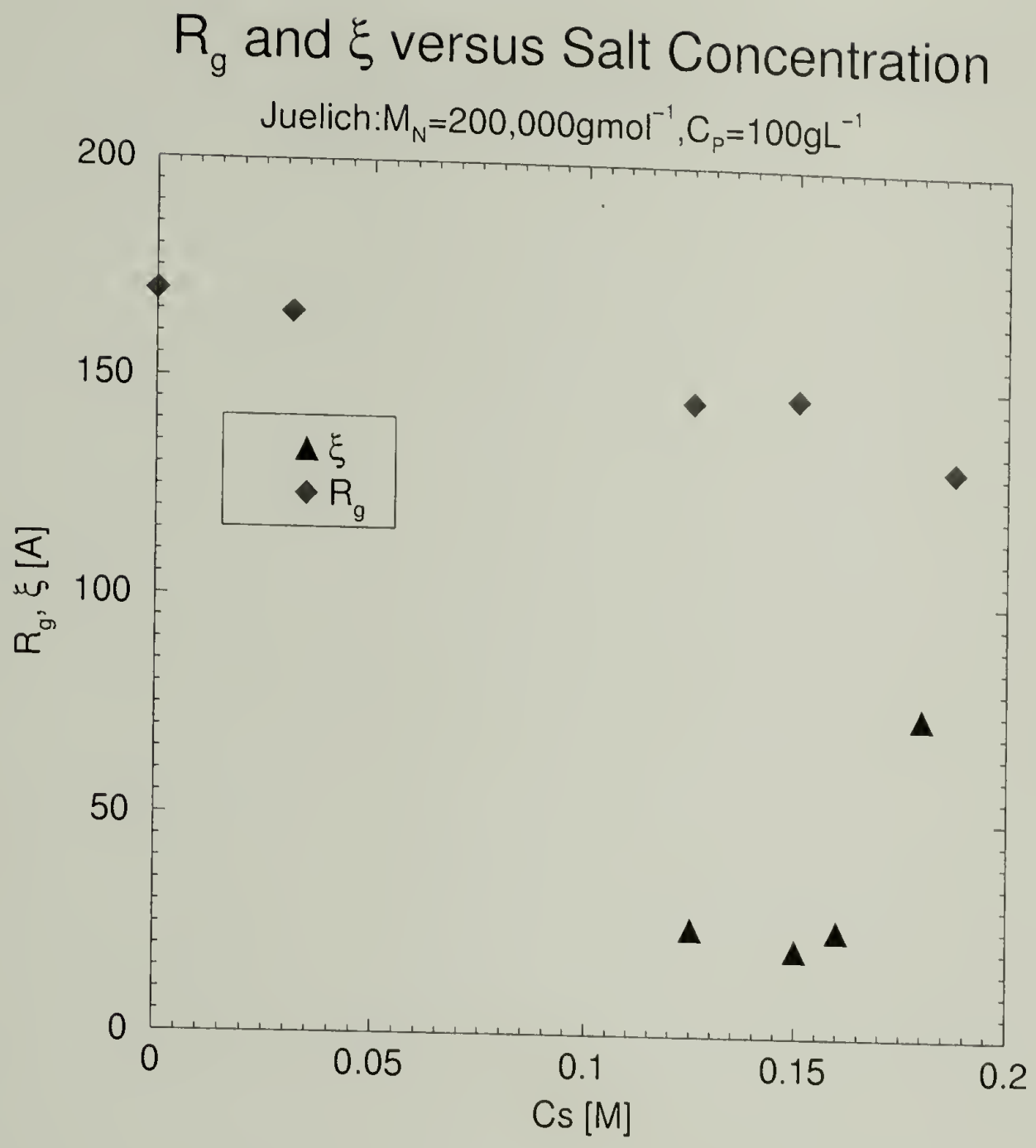

Figure 4.11: Overlap Concentration calculated is $16gL^{-1}$ and $35gL^{-1}$ for added salt levels of 0.0M and 0.1875M, respectively. Estimated theta dimensions is 76 Å. Estimated Rod-like dimensions is 700 Å. An overall 22 % change in chain dimensions is observed.

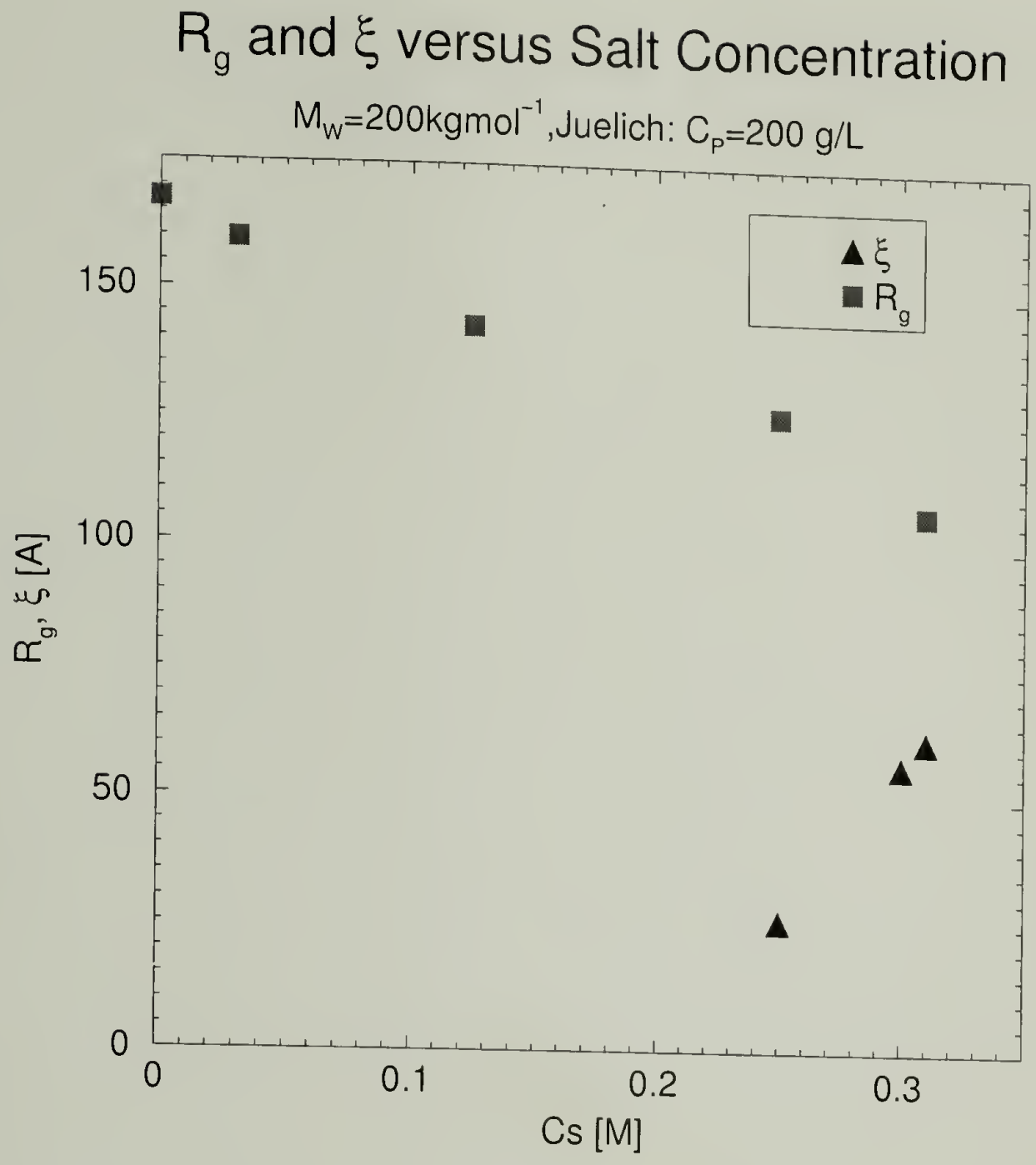

Figure 4.12: Overlap Concentration calculated is $17gL^{-1}$ and $65gL^{-1}$ for added salt levels of 0.0M and 0.31M, respectively. Estimated theta dimensions is 76 Å. Estimated Rod-like dimensions is 700 Å. An overall 36 % change in chain dimensions is observed.

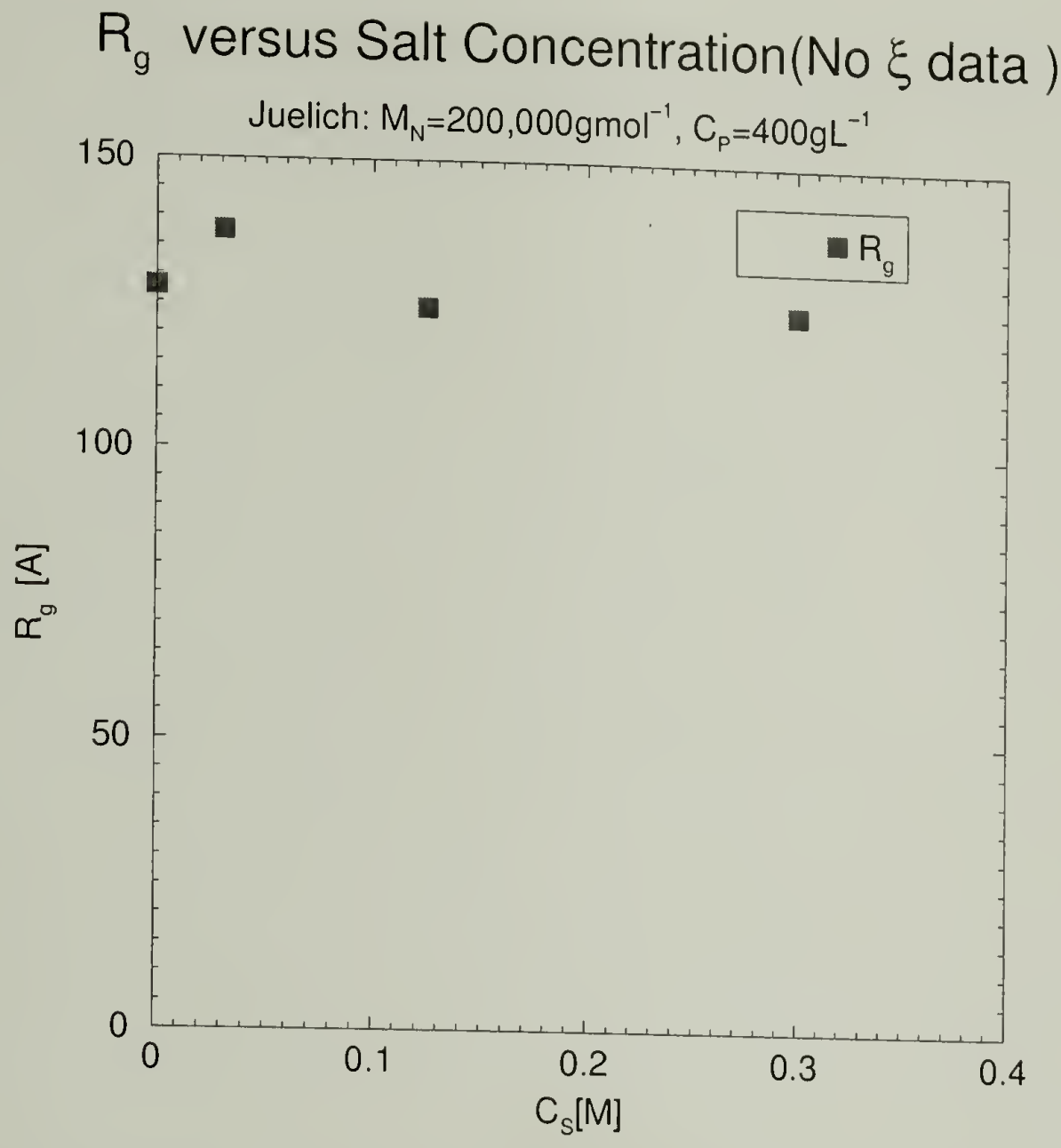

Figure 4.13: Overlap Concentration calculated is 38gL^{-1} and 41gL^{-1} for added salt levels of 0.0M and 0.31M, respectively. Estimated theta dimensions is 76 Å. Estimated Rod-like dimensions is 700 Å. An overall 3 % change in chain dimensions is observed.

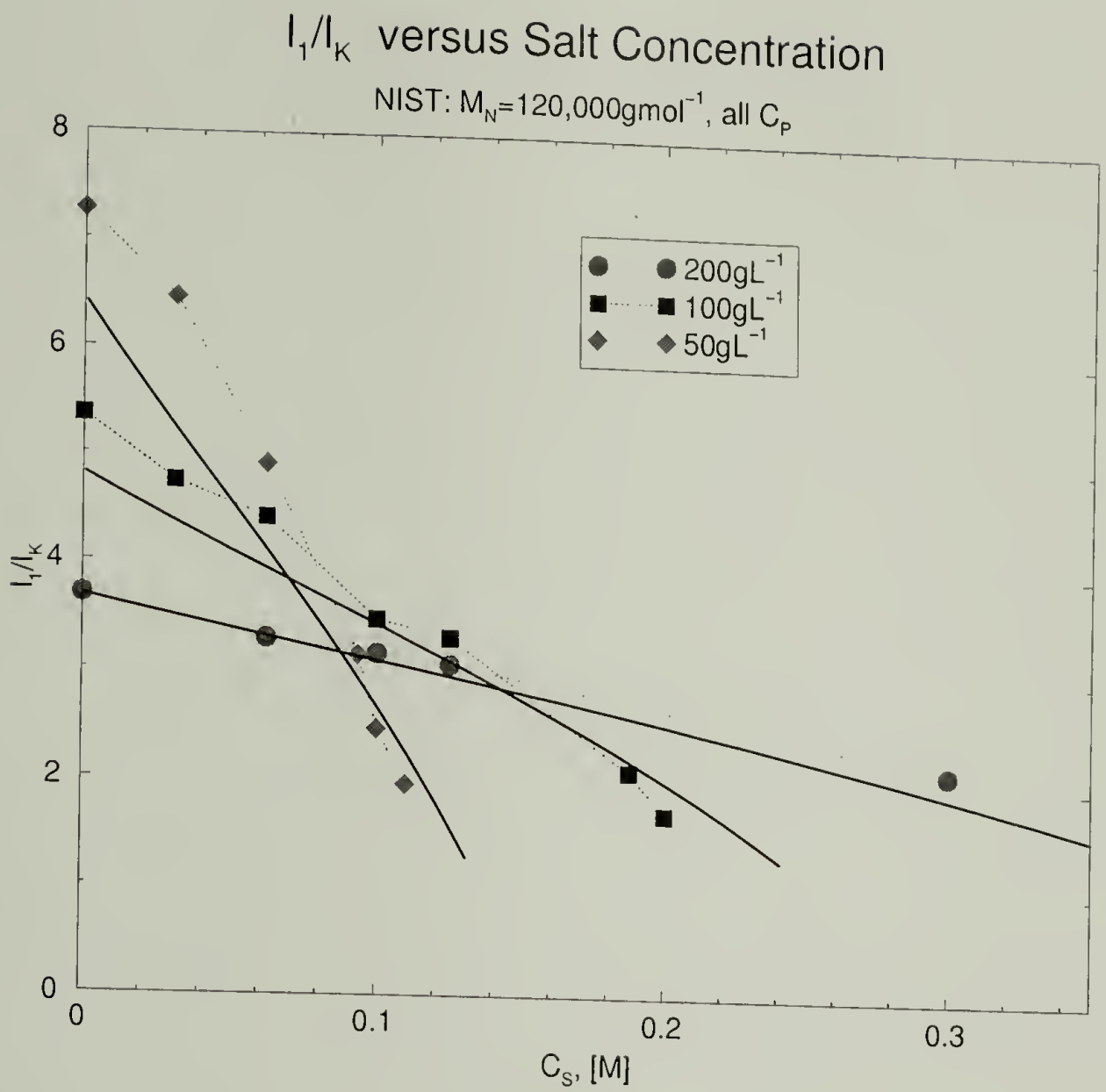

Figure 4.14: Double screening theory calculated using a salt-concentration dependence for the degree of ionization. $l_k = 1.38$nm, $a = 0.23$nm, $l_B = 0.715$nm.

CHAPTER 5

RECENT DEVELOPMENTS AND FUTURE WORK

Due to the presence of aggregation in the system, observed in the dilute solution, and the significant coil contraction observed in the experimental data for added multivalent salts, the specific effect of ion-bridging, or ion-pair formation is important and may help explain the observed experimental trends. A modification to the simple theory should account for the stable interaction between monomers mediated by the multivalent ion. To be consistent with the theory presented, any specific interaction will tend to reduce the charge density of the chain (α) and modify the ionic strength (κ^2).

This stable attractive effect of ion-pair formation modifies the Flory-Huggins χ-parameter,

$$\chi_{Eff} = \chi_o - \frac{w_c}{\kappa^2} + w_B \phi_s \tag{5.1}$$

The first two terms already treated earlier remain. However, the third term quantifies a net attraction between monomers mediated by a multivalent ion. The strength w_B is proportional to l_B, hence, inversely proportional to temperature. This effect can be introduced into the Edwards Hamiltonian via an additional two-body interaction,

$$H_{Bridge} = -|w_B| \sum_{\alpha,\beta=1}^{n} \sum_{\gamma=1}^{n_{Ba^{2+}}} \int_0^N ds \int_0^N ds' \delta[\vec{R}_\alpha(s) - \vec{r}_\gamma]\delta[\vec{R}_\beta(s') - \vec{r}_\gamma] \tag{5.2}$$

The attractive strength is denoted by w_B. The origin of this attractive term is due to the electrostatic energy of an ion-pair. The probability for the occurrence is the concentration of the multivalent ion, in our case the density of barium ions. By summing over the number of barium ions in solution, this term becomes simply a two-body short-range interaction that modifies the effective Flory-Huggins interaction parameter as denoted in Eq.5.1.

5.1 Complex formation

The types of ion-pair formation, illustrated in Fig.5.1, modeled are θ_1 fraction of monomers involved in an ion-pair between the counterion and monomer, θ_{21} fraction of monomers with a single multivalent ion and a single monomer, and θ_{22} fraction of monomers involved in an ion-pair between a single multivalent ion and two monomers. By properly accounting for fractions of bound species leading to the reduced ions contributing to the free solution ionic strength, the following is the adjusted degree of ionization,

$$\alpha = 1 - \theta_1 - 2\theta_{21} - \theta_{22} \tag{5.3}$$

and inverse-square Debye length,

$$\kappa^2 = 4\pi \left(\frac{l_B}{l}\right) \left(Z_c^2\rho_m + Z_+^2\rho_+ + Z_-^2\rho_- - Z_c^2\theta_1\rho_m - Z_+^2\theta_{21}\rho_m - \frac{1}{2}Z_+^2\theta_{22}\rho_m\right) \tag{5.4}$$

This approach does not provide an equilibrium relation between the fraction of ion-paired ions and the concentration of the polymer. This would arise in the form of an equilibrium constant. Such a constraint may yield more quantitative agreement between theory and experiment, but in this case the correct physics is given as an input.

The following spinodal phase diagrams have been constructed using the Flory-Huggins theory by replacing χ, by χ_{Eff} as given in Eq.5.1. The thermodynamic instability limit is solved numerically using Mathematica 4.0.

$$\left(\frac{\partial^2 \Delta F/k_B T}{\partial \phi^2}\right)\Bigg|_{Site} = 0 = \frac{1}{N\phi} + \frac{1}{1-\phi} - 2\chi_o + 2\frac{w_c}{\kappa^2} - w_B\phi_s \tag{5.5}$$

$$w_B = 3\frac{1}{2}\frac{l_B}{a}\frac{\epsilon_{bulk}}{\epsilon_{local}}\phi_s \tag{5.6}$$

ϕ_s is the volume fraction of the multivalent species. l_B is the Bjerrum length, a the separation distance of the ions, ϵ_{bulk} is the bulk dielectric constant of the solution, and ϵ_{local} is the local dielectric constant which may differ from the bulk. The origin of this strength comes from summing the total electrostatic energy for formation of a linear bridge between two negatively charged monomers and one positively charged divalent ion. In this case the separation between two adjacent ions is given by a and it is speculated that for such local interaction the characterization of the dielectric constant may be perturbed due to the high concentration of hydrophobic moieties in the nearby region. So, the strength, w_B is a collection of variables which have some uncertainty within the model.

5.2 Numerical Results

The following numerical results demonstrate the general phase behavior predicted from the above proposed model. We examine the effect of molecular weight(N), hydrophobicity(χ_o), fraction of ion bridging (θ_{22}), fraction of counter ion-monomer complexation (θ_1), and temperature(T). Due to the large variety of combinations of dominance each parameter may contribute to the overall physics, we will examine the roles of each parameter, keeping others fixed. The results demonstrated below do not correspond quantitatively with experimental data. The magnitudes of the parameters, especially χ_o, tends to adjust the magnitudes of complimentary variables to reach the unstable state. However, the general shapes of the phase diagrams remains similar. An attempt has been made to use experimental units, molar salt concentration and volume fraction for the polymer concentration. A quantitative mapping is not possible at this point, yet the general trends are in qualitative agreement with the experimental data of C_s-C_p and T-C_p and T-C_s diagrams presented in Chapter 3.

5.2.1 Effect of Molecular Weight

The influence of the molecular weight on the C_s-C_p diagram is demonstrated in Fig. 5.2. This plot shows that for low molecular weight, N = 100, leads to a curved spinodal with a minimum. A region of miscibility is found below the spinodal which extends into both the dilute and high concentration region. Since, the binodal curves have not been calculated here, the observed regions of miscibility need to be distinguished as stable or metastable. The high concentration region shows the familiar positive slope. However, a line representing the stoichiometric salting out between salt and polymer concentration is not found. However, by examining

higher molecular weights, this high polymer concentration region appears to be weakly dependent on molecular weight, consistent with experimental data.

As the molecular weight increases from 100 to 100000, the region of miscibility decreases, leading to a polymer concentration independent salting out line in the dilute solution region. This is observed similarly in experiments, for very low molecular weights a low polymer concentration region of miscibility is observed and secondly in the high polymer concentration region, the molecular weight dependence is similar to that observed in Fig.3.5.

5.2.2 Effect of Hydrophobicity: χ_o

In order to illustrate the qualitative features, we will use a molecular weight of 10000 and maintain a degree of ionization of the chain at $\alpha = 0.30$, with $\theta_{22} = 0.20$,$\theta_{21} = 0.05$, and $\theta_1 = 0.40$. The effect of the chemical mismatch (χ_o) between monomer and solvent is investigated and the results are in qualitative agreement with experiments. As χ_o increases, the region of miscibility decreases, as shown in Fig.5.3. We investigate a range of χ_o from 0.70 to 0.875. The shape of the spinodal curve is not changed, however, the spinodal shifts to lower salt concentrations with increasing χ_o. This indicates that if the solvent quality became poorer,a lower concentration of added salt would be required to precipitate the polyelectrolyte.

This behavior may also be interpreted as due to a change in temperature, since χ_o is typically inversely proportional to temperature. As the temperature decreases χ_o increases leading to a observed trends. However, the influence of temperature is not only within χ_o, but also in the strength w_B via the dependence on l_B. The model is in qualitative agreement with experimental trends in regards to temperature. As the temperature increases the phase boundary shifts to higher salt concentrations and lower polymer concentrations.

5.2.3 Effect of Ionic Bridging:θ_{22}

The fraction of monomers participating in an ionic bridge is defined as θ_{22}. By investigating this parameter the physics of enhanced immiscibility due to ion-bridging is probed. We now investigate the effect of this quantity on the C_s-C_p phase diagram keeping N=10000, $\theta_1 = 0.40$, $\theta_{21} = 0.025$, and χ_o=0.70. As the fraction of the monomers undergoing bridging increases, the region of miscibility decreases as shown in Fig. 5.4. This increased fraction of ionic bridges has two competing effects, the first effect is a large value of χ that favors immiscibility, while the other effect is a lower solution ionic strength because a larger fraction of ions are being removed from the free solution and localized on the polymer, which favors miscibility due to a larger screening length. In this case by increasing the fraction of ionic bridges the trend is to favor immiscibility, rather than miscibility due to larger screening length. This effect may be able to be tuned especially with different multivalent salts such as 1:3, where the valence of the salt can influence the screening length due to the Z^2 dependence.

5.2.4 Effect of Counter-ion Complexation: θ_1

The influence of the complexation between the counter ion and polymer is also investigated. Again, we investigate the effect on the C_s-C_p diagram, using N=10000, $\theta_{22} = 0.20$, $\theta_{21} = 0.025$, and χ_o=0.70. The model predicts that an increased fraction of bound counter-ions favors miscibility, as shown in Fig.5.5. The main effect of increasing θ_1 is to reduce the fraction of counter-ions in the free solution, which leads to a longer screening length-enhancing the miscibility particularly at high polymer concentrations. The scenario of θ_1 is coupled to two competing effects. By increasing the fraction of bound counter-ion the overall chain degree

of ionization is reduced, which actually decreases the miscibility. However, as the fraction of bound counter-ion increases, the overall solution ionic strength decreases leading to a larger screening length, which favors miscibility. Thus in this case the effect of ionic screening dominates as a larger quantity of added salt is required to precipitate the polymer due to the dominance of the effect of θ_1 on κ^2, rather than the effect of the lowered charge density α.

5.2.5 Spinodal Temperatures

The temperature-polymer concentration,$T - \phi_p$, phase diagram is also investigated, again only the spinodal curves. The general features are similar to neutral polymer solutions, but modified by the electrostatics. We demonstrate the results for two molecular weights, keeping all other parameters fixed; $\theta_{22} = 0.10$, $\theta_{21} = 0.05$,$\theta_{21} = 0.4$ and χ_o at 298K is equal to 0.70. Typically in neutral polymer solutions one examines χ versus ϕ_p. However, the formation of stable ion-pairs is also temperature dependent. So, we treat the system directly in the temperature dependence to illustrate the qualitative features clearer.

In Fig.5.6 we show for a molecular weight of N=100 the phase diagram appears similarly to neutral polymer solutions. For increasing levels of added salt the phase diagram shifts vertically to higher temperatures in qualitative agreement with the experimental trends given in Fig.3.6. The physical origin for this is due to both a reduced screening length that decreases the solvent quality and the increased formation of ion bridges with higher salt concentration that also decreases the effective solvent quality.

The effect of increasing molecular weight is similar to neutral polymer solutions, in the limit of very high molecular weight the critical composition approaches the zero polymer concentration limit as shown in Fig.5.7. Similar with the case of

$N = 100$, the influence of added salt is to increase the spinodal temperatures. These predictions should be compared with the experimental data in Figs. 3.6 and 3.19 in which similar temperature dependence is observed, however, the true liquid-liquid phase separation remains to be proven, yet with decreasing polymer concentration at fixed level of salt the precipitation temperatures increase.

The spinodal temperatures as a function of added salt concentration are shown for a fixed polymer concentration and ion-pair parameters. From this we will gain an understanding of the change in the spinodal temperatures. Fig.5.8 demonstrates the change in the spinodal temperatures for three fixed polymer concentrations of the critical composition, 5%, and 10% by volume fraction. The experimental data of Fig. 3.20 and 3.21 are in qualitative agreement.

5.3 Small-Angle Light Scattering: Kinetics

Using small-angle light scattering on dilute solutions reveals no significant scattering until the temperature is very close to the phase boundary. At which the small-angle intensity is time dependent, hence represents a kinetics of precipitation. Two samples about the maximum in the precipitation temperature were examined for a fixed salt concentration. Table 5.1 illustrates the relevant phase behavior data. The following are fits for the aggregate radius of gyration, scattered intensity to zero angle and fractal dimension using the following crossover formula,

$$I(q) = I(0)\left(1 + \frac{2}{3d_f}k^2R_g^2\right)^{-\frac{d_f}{2}}. \tag{5.7}$$

The advantage of this formula, as it is applied to polymer gels, is the generality and ability to capture the low and high kR_g limits of the Debye structure factor,

for a fractal dimension of 2, as well as a general form in which the fractal dimension as a fit parameter.

Data analyzes is for dark background subtracted scattering, calibration of the angular range using a diffraction grating of 100lines per mm, and have been corrected using the following form of I(q)=$I(q) * (1 + C_1$*q^2), with C_1 =1.0. This correction is due to the systematic discrepancy observed, at high angles, by measuring the two-dimensional scattering pattern on a flat screen. This form of data correction was determined comparison of experimental results and theoretical curves for diffraction by a single slit. This approximation is necessary for q 1.0μm.

These results demonstrate the large characteristic dimensions involved in the aggregation and kinetics of order 2 microns. It is interesting to note that the size of the radius of gyration of the aggregate tends to increase at very short times, yet remains constant in size as time progresses for both samples analyzed. The information on these length scales are typical of the length scale as observed under a microscope.

These experiments can lend to real time kinetics of aggregation which are properly characterized by a size and fractal dimension. However, it would be interesting to quantify the increase in number density of these fractal aggregates as a function of time. Once, the polarizability of the medium and aggregate can be estimated from their respective refractive indicies, one may quantitatively analyze[75] using a form of the scattering given by Eq.5.7 and model fractal particle with a pervading volume of R_g^3. By measuring the concentration of particles one can understand the driving force for aggregate formation as functions of temperature, polymer concentration, ionic strength, mixtures of salts, blends of polyelectrolytes, etc. Possibilities are endless, especially in a relatively simple experiment. Two experimental concerns would be using scratch-free quartz cells as it minimizes background which will in-

fluence the analysis. As the scattered intensity rises the interference of scratches will be magnified. Also be wary of the problem of sedimentation in these systems with micron-sized particles. It would be advised that large particles may sediment, which is interesting physics as well as practical matter[76].

SALS was also examined for semidilute polymer solutions. We observe scattering even under the conditions of homogeneous solutions, as indicated by visual inspection. One example of the result used to obtain the temperature dependent phase diagrams, is shown in Fig. 5.11. Here the SALS is shown as the temperature is lowered. At each temperature the scattering is weakly time dependent over a thirty minute waiting period. However, very close to the phase boundary the intensity rises significantly. For this particular sample, we did not observe a scattering peak, indicative of spinodal decomposition. However, we did observe a peak for a higher polymer concentration of $103 gL^{-1}$ as shown in 5.12. This peak was observed after a long waiting time in proximity to the anticipated precipitation temperature. In this case the waiting time was 18 hours and 30 minutes, thus the kinetics prove to be an exciting area to explore, in particular with the non-invasive method of small-angle light scattering.

5.4 Optical Microscopy

We also examined the precipitated mixture under optical microscope and observed the particulate nature. These particles are in the micron-scale an example of this is shown for a precipitate formed for a molecular weight of $56{,}000 gmol^{-1}$, $C_p = 0.00625M$ and $C_s = 0.25M$ in Fig.5.13. Upon mixing the stock polymer and salt solutions precipitation occurs immediately. This optical micrographs for 10x and 40x magnification were taken after the precipitate was shaken and a drop of

the cloudy solution was placed onto a glass slide with a cover slip. The evolution to form these particles have not been investigated, but as shown by the SALS data a study of the kinetics should prove useful.

5.5 Conclusions

By introducing the attractive interaction between two monomers, mediated by the multivalent salt a better qualitative understanding is made regarding the phase diagrams. Although, including this term modifies the phase diagram, the trends of the influence of added salt in the term of Coulombic repulsion is adequate to a first approximation. This is only the beginning in an attempt to understand the phase behavior of polyelectrolytes.

In attempts to quantify the phase boundary, strong time dependent small-angle light scattering is observed. These shallow quenches reveal no scattering wave vector peak, but fit the structure factor crossover formula. Fractal dimensions near 2 are obtained as well as a weakly varying radius of gyration of the aggregate as quantified by the fits.

Table 5.1: Summary of Phase Behavior:Kinetics

Table of Samples			
$\mathbf{C}_p$ [M]	$\mathbf{C}_s$ [M]	$\mathbf{T}_{clear}$[°C]	$\mathbf{T}_{SALS}$[°C]
0.006250	0.01563	48.5	39.5
0.003125	0.01563	51.9	44.0
0.001563	0.01563	52.8	45.0

Table 5.2: Crossover Fits:C_p = 0.00625M C_s = 0.01563M

Fit Results:C_p = 0.00625M C_s = 0.01563M					
$\mathbf{T}_{BATH}$	$\mathbf{T}_{RTD}$	**time [min.]**	$\mathbf{R}_g[\mu\mathbf{m}]$	**I(0) [counts/sec.]**	$\mathbf{d}_f$
40.0	39.1	5			
40.2	39.5	10	1.54	10578	2.10
40.2	39.5	12	1.81	22066	2.20
40.2	39.5	14	2.02	31857	2.07
40.2	39.5	15	2.20	43200	2.0
40.2	39.5	20	2.41	52800	1.87
40.2	39.5	25	2.61	63680	1.75
40.2	39.5	30	2.54	67445	1.80
40.2	39.5	35	2.57	68880	1.73
40.2	39.5	40	2.46	65433	1.74
40.2	39.5	45	2.35	64091	1.78
40.2	39.5	50	2.31	63470	1.80
40.2	39.5	55	2.27	62503	1.80
40.2	39.5	60	2.20	61920	1.86
40.2	39.5	65	2.21	62291	1.84

Table 5.3: Crossover Fits:C_p = 0.003125M C_s = 0.01563M

C_p = 0.003125M C_s = 0.01563M					
T_{BATH}	T_{RTD}	time [min.]	$R_g[\mu m]$	I(0)[counts/sec.]	d_f
45.0	44.0	11			
45.0	44.0	14	0.81	4293	600
45.0	44.0	15	1.14	9722	4.3
45.0	44.0	17	1.52	17912	2.61
45.0	44.0	25	1.88	32477	2.27
45.0	44.0	33	1.98	41993	2.23
45.0	44.0	40	2.00	45960	2.23
45.0	44.0	45	2.04	50388	2.21
45.0	44.0	50	2.05	53450	2.22
45.0	44.0	60	2.13	59031	2.16
45.0	44.0	70	2.15	62567	2.14

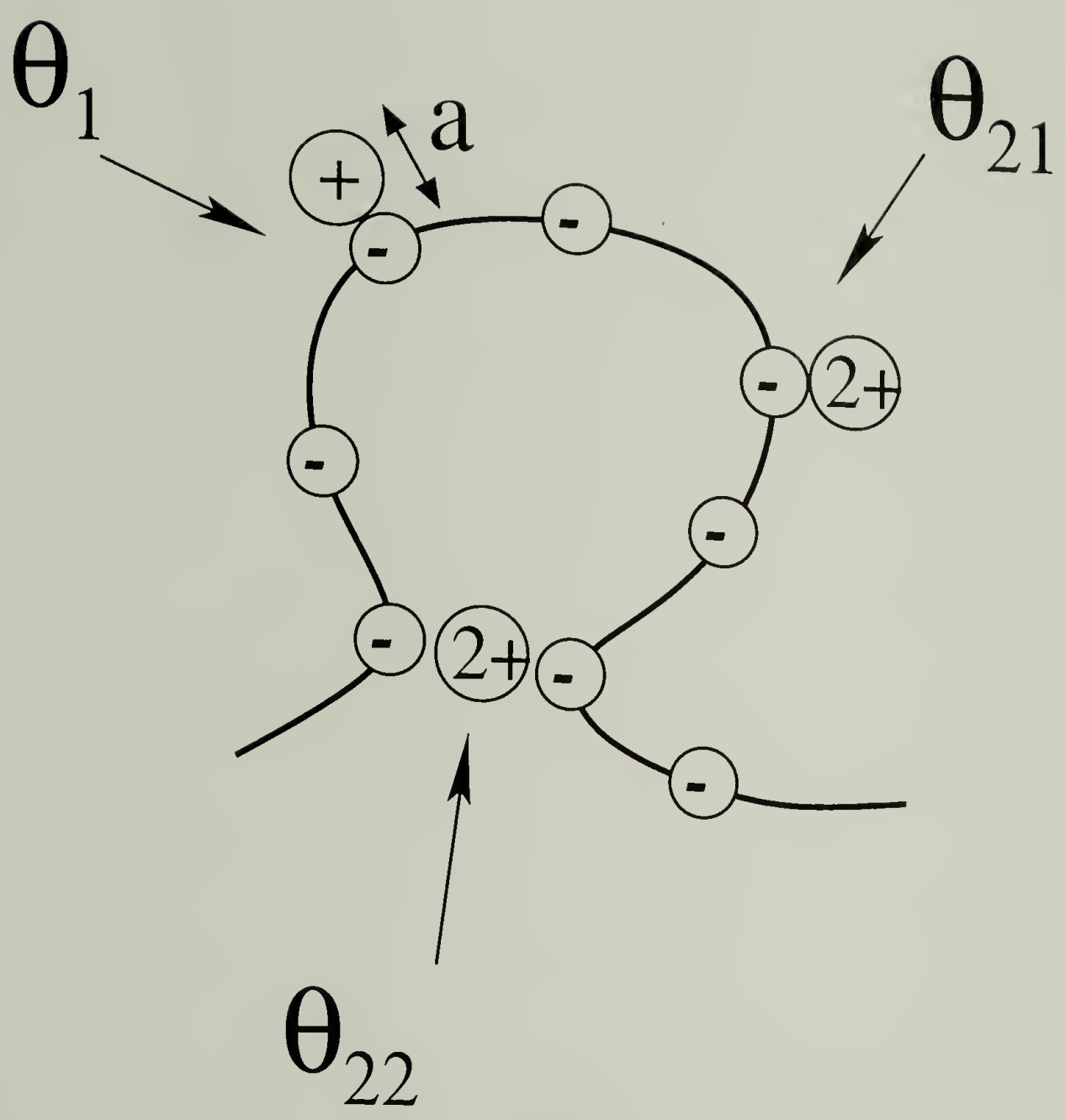

Figure 5.1: An example of the types of specific ion-pair formation modeled. θ_1 fraction of monomers have a bound counter ion of monovalent charge. θ_{21} have a fraction of monomers with a singly-bound multivalent ion and monomer. θ_{22} is the fraction of monomers maintaining an ion-bridge of two monomers and a singly multivalent ion. The remaining fraction of charged monomer is exactly the degree of ionization of the chain. a is the separation distance between the point charges.

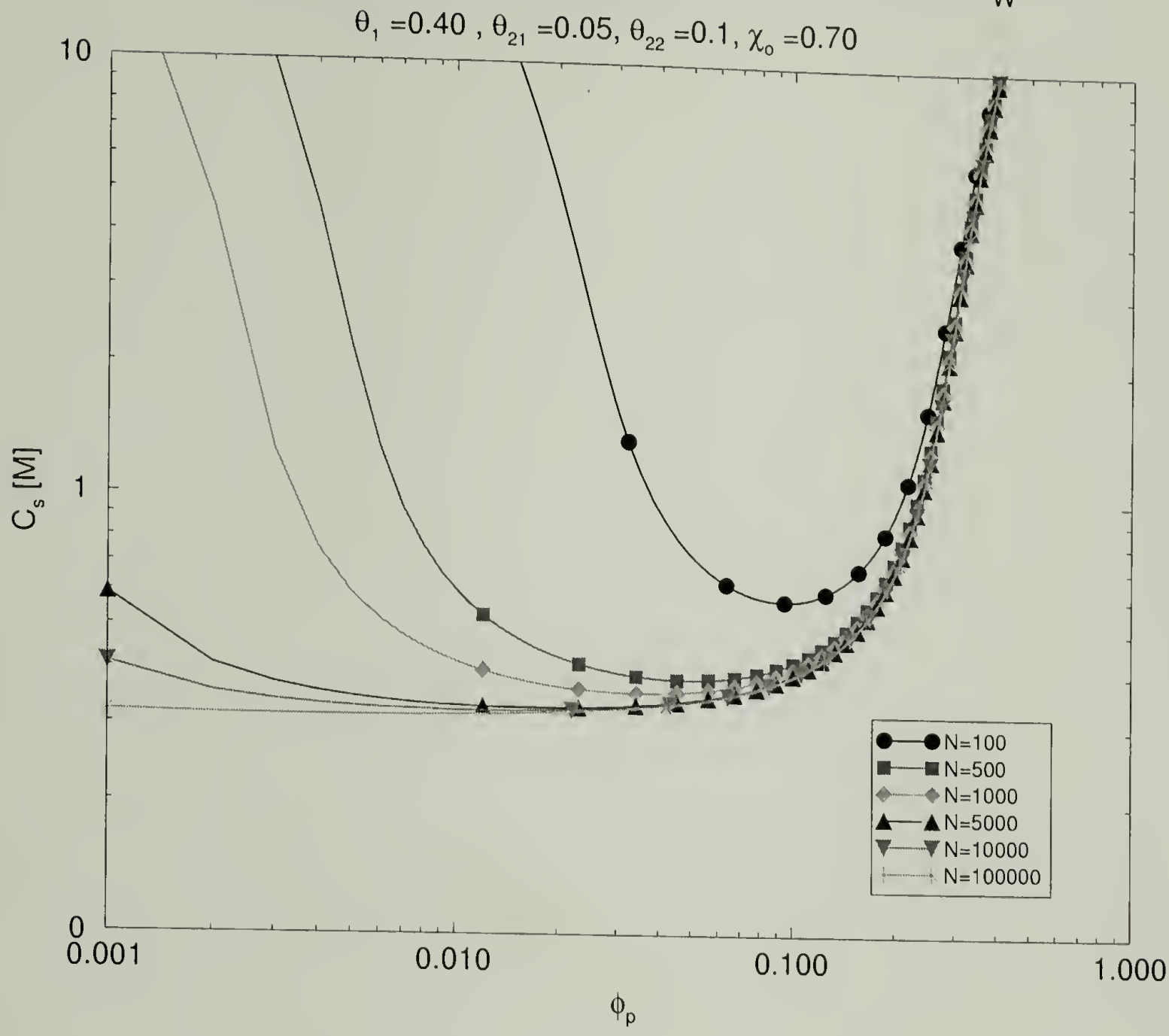

Figure 5.2: Numerical result: Influence of the molecular weight on the Cs-Cp diagram. The parameters are given in the heading of the figure.

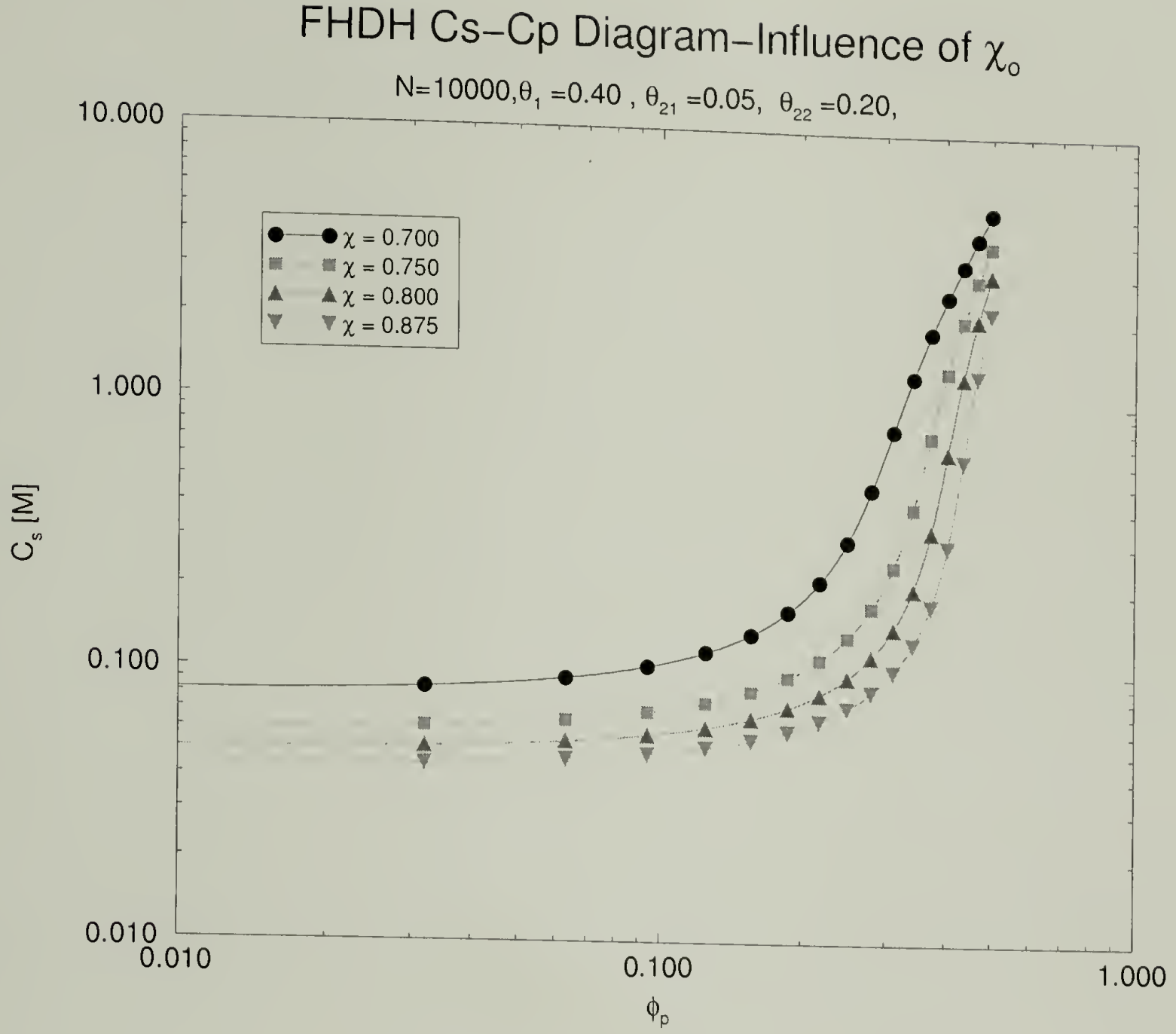

Figure 5.3: Numerical result:Influence of the chemical mismatch χ_o on the Cs-Cp diagram. The parameters are given in the heading of the figure.

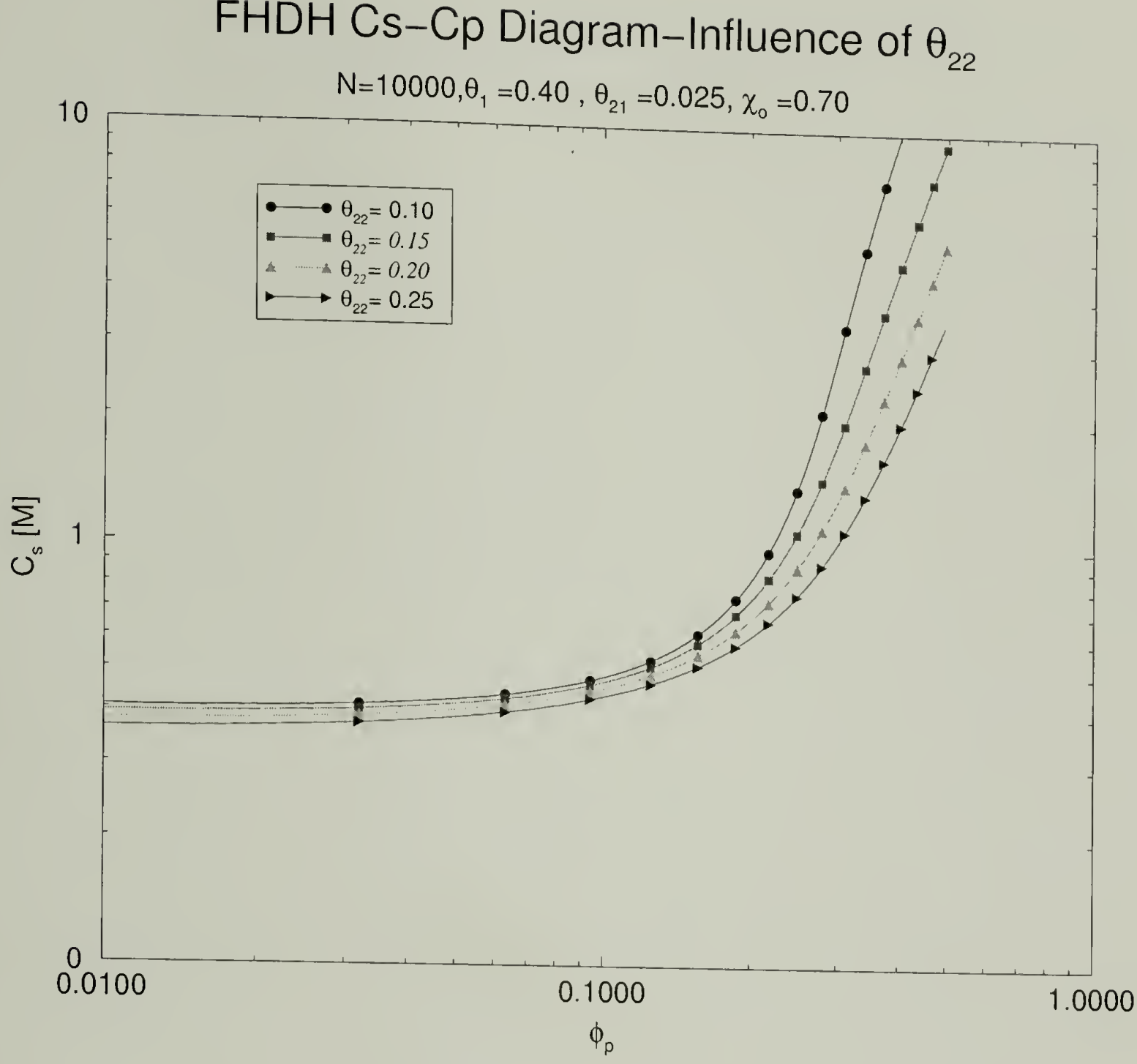

Figure 5.4: Numerical result: Influence of the fraction of monomers undergoing ion-pairs θ_{22}. The parameters are given in the heading of the figure.

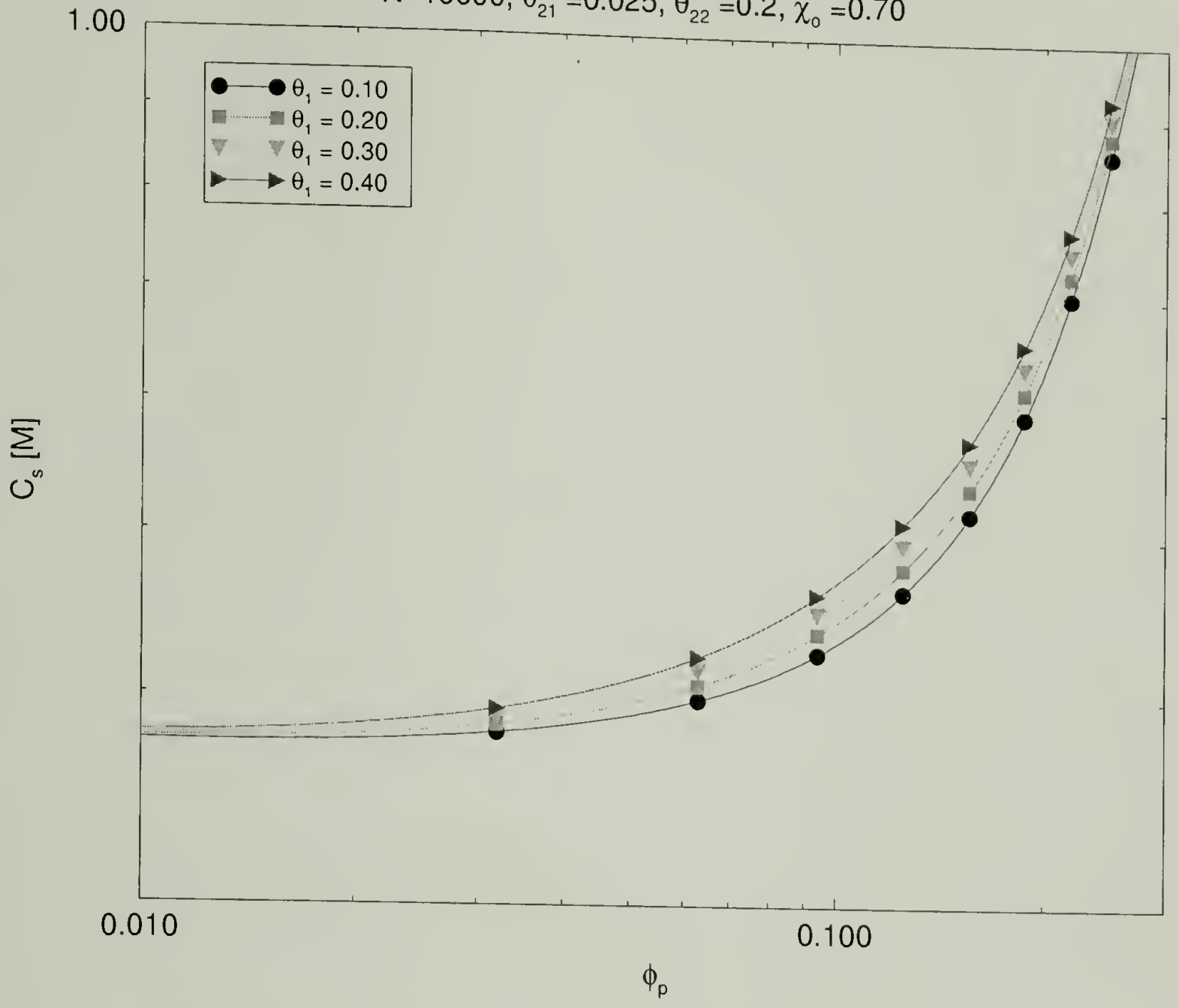

Figure 5.5: Numerical result: Influence of the fraction of monomers with condensed counter ions, θ_1. The parameters are given in the heading of the figure.

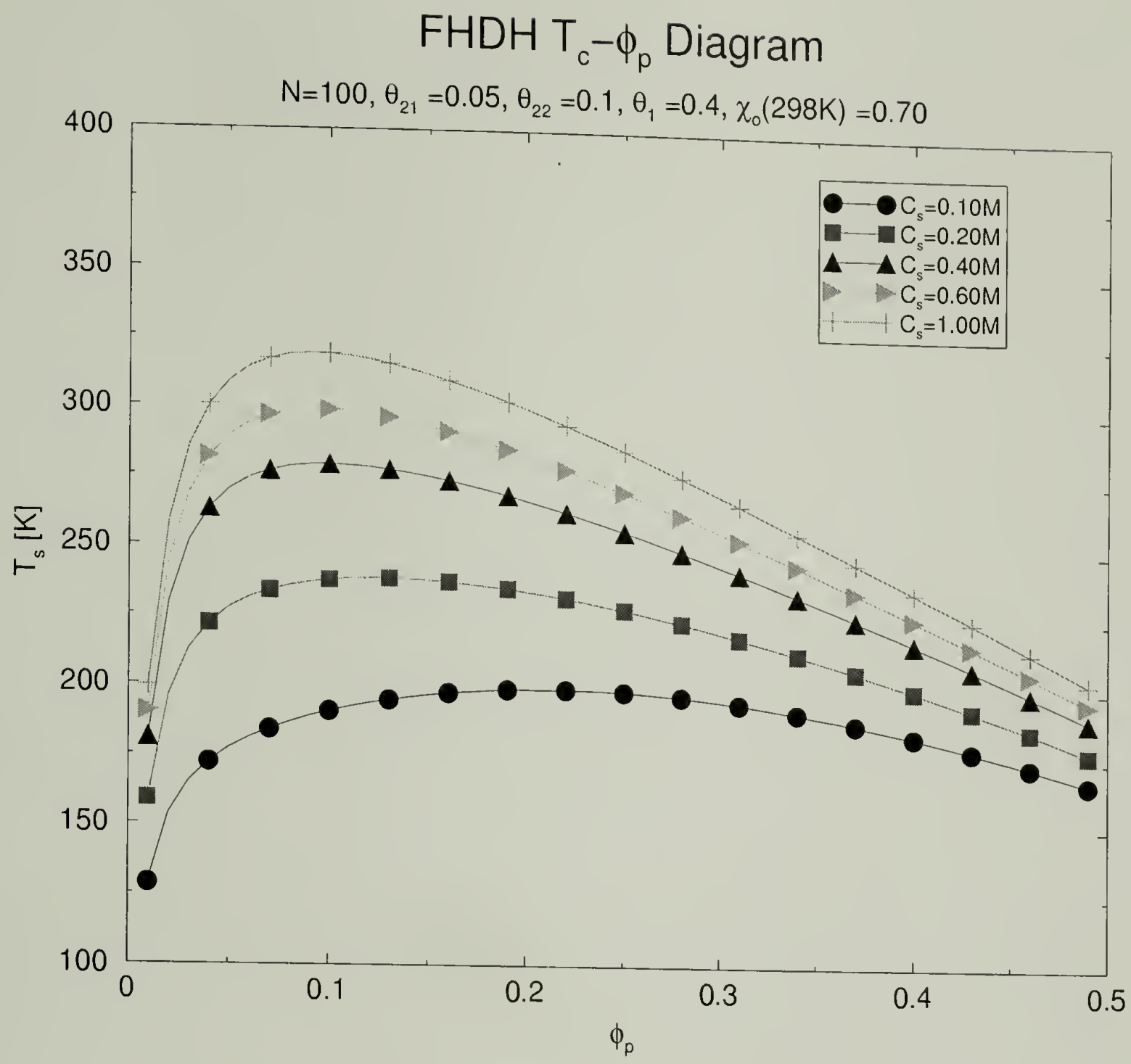

Figure 5.6: Numerical result: For a low molecular weight, N=100, Influence of added salt concentration of the temperature-polymer composition phase diagram. The values of the parameters are given in the heading of the figure.

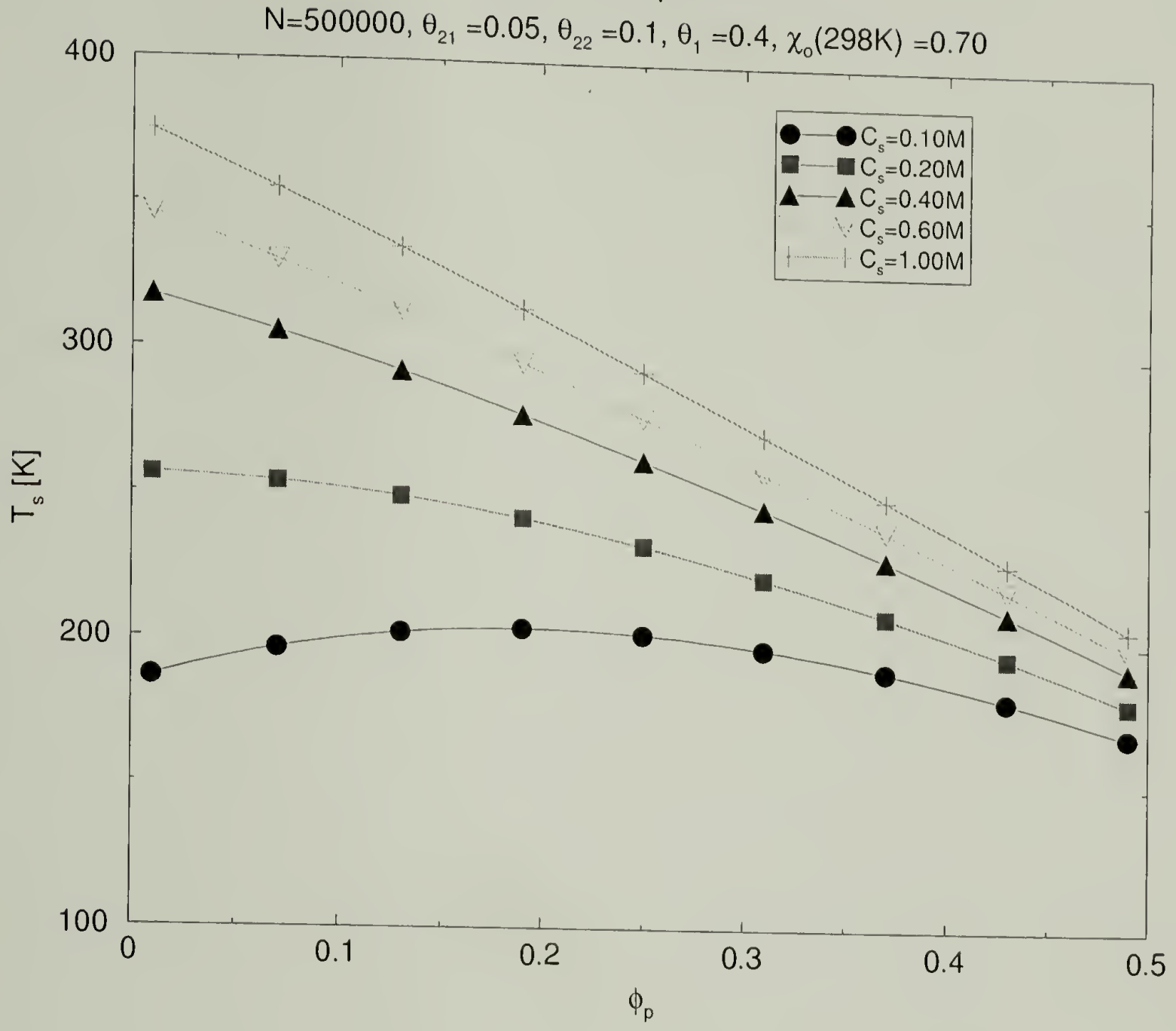

Figure 5.7: Numerical result: For a high molecular weight, N=500000, Influence of added salt concentration of the temperature-polymer composition phase diagram. The values of the parameters are given in the heading of the figure.

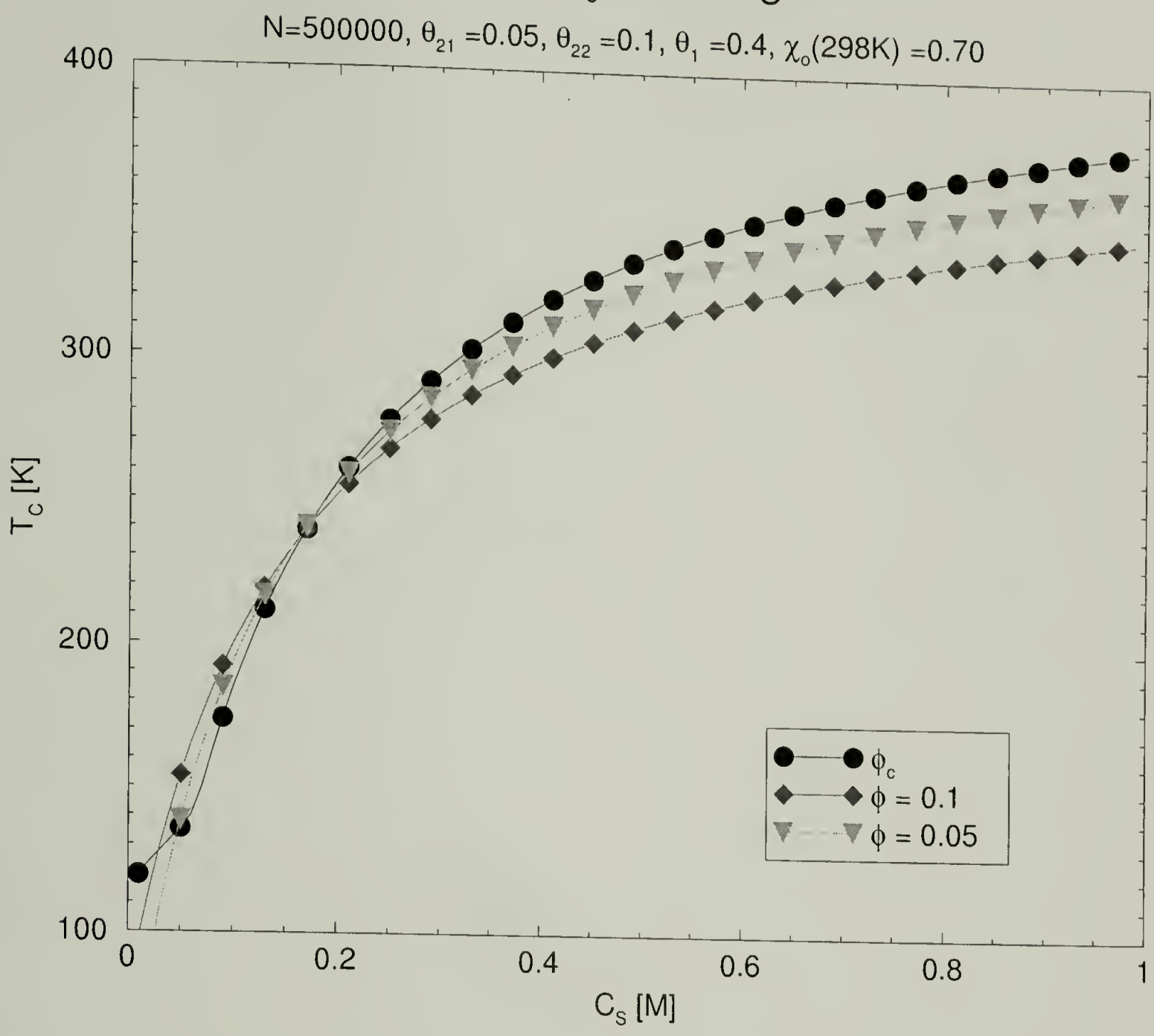

Figure 5.8: Numerical result: For a high molecular weight, N=500000, Influence of added salt concentration on the spinodal temperature, for three different polymer concentrations; the critical composition, 5% volume fraction and 10% volume fraction. The values of the parameters are given in the heading of the figure.

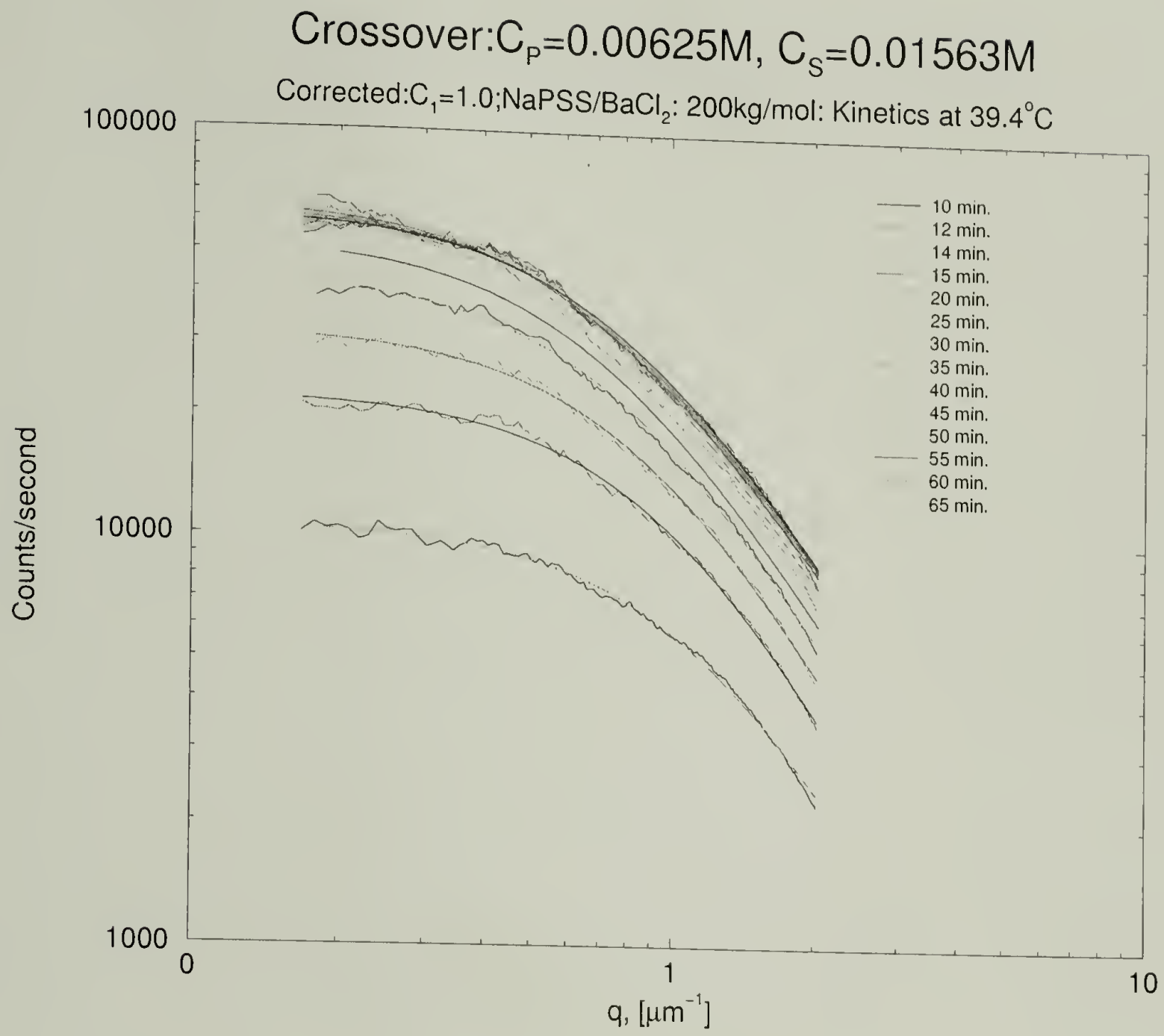

Figure 5.9: Time Dependent SALS for $C_p = 0.00625$M $C_s = 0.01563$M. Evolution of scattering at a fixed temperature of 39.4°C.

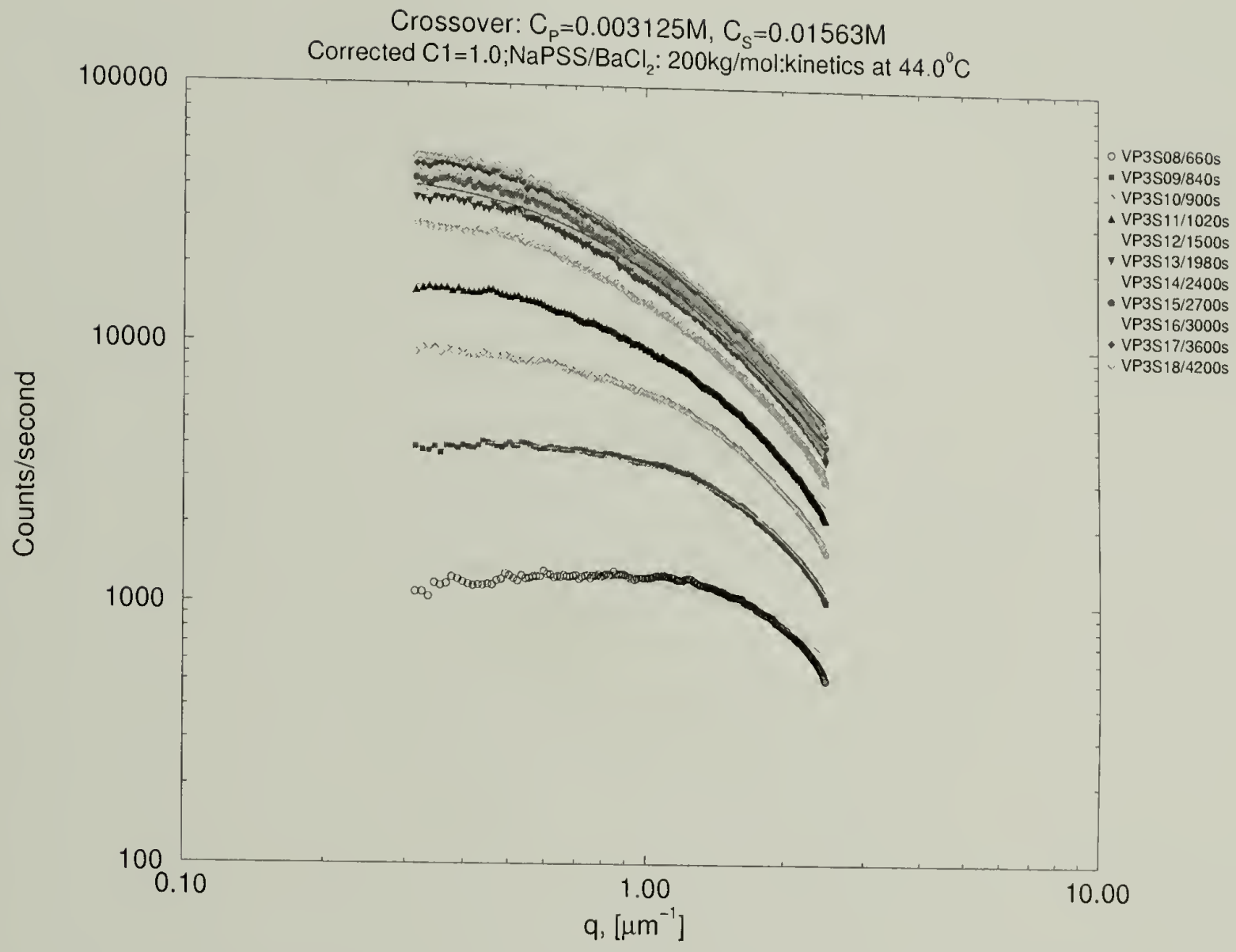

Figure 5.10: Time Dependent SALS for $C_p = 0.003125$M $C_s = 0.01563$M. Evolution of scattering at a fixed temperature of 44.0°C.

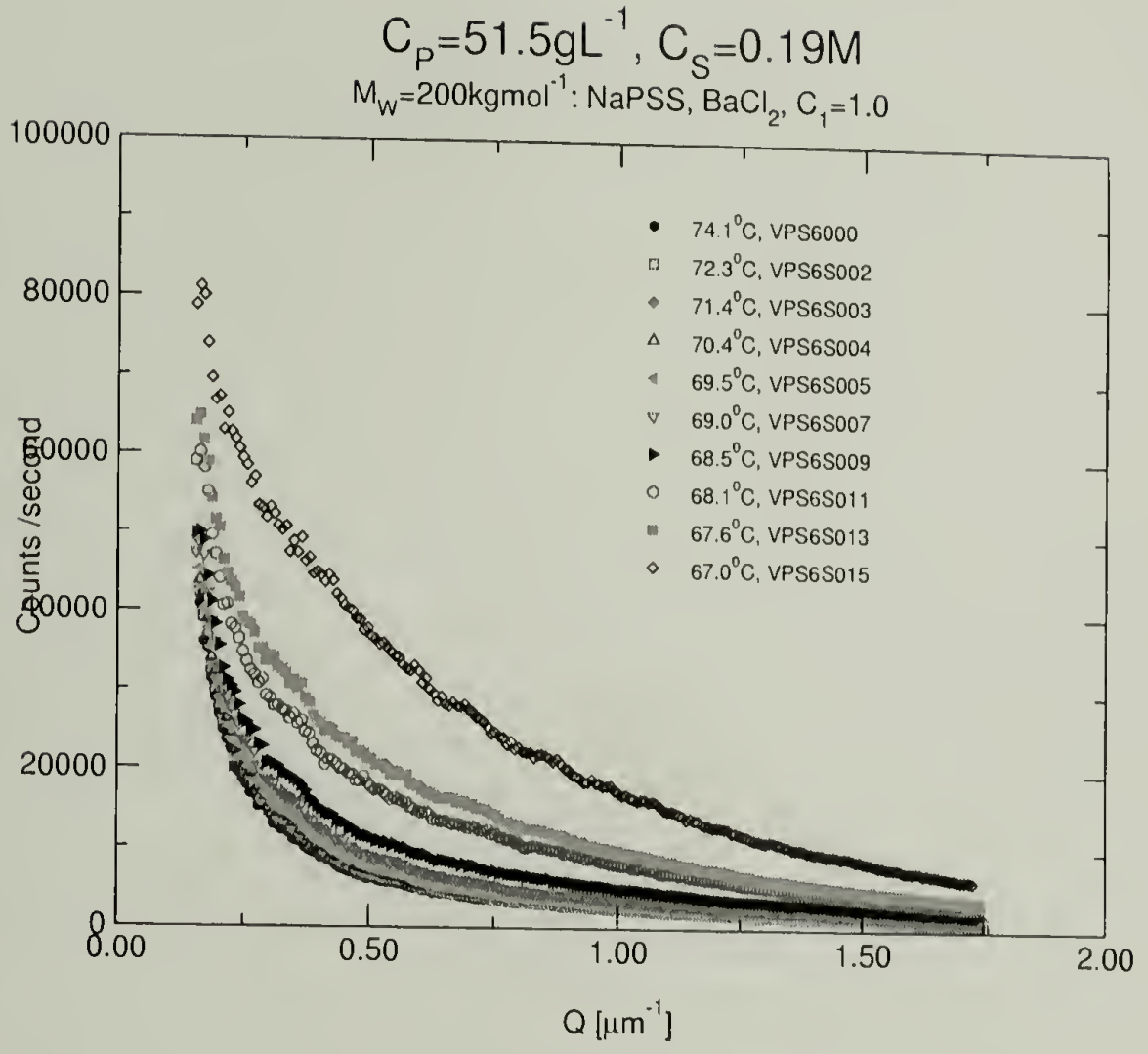

Figure 5.11: SALS observations for a fixed NaPSS concentration of 51.5gL^{-1}, barium chloride salt concentration of 0.19M and molecular weight of 200,000gmol^{-1}. These data indicate a large fluctuation even in the homogeneous phase. Systematic investigations of the long time dependence remain unexplored.

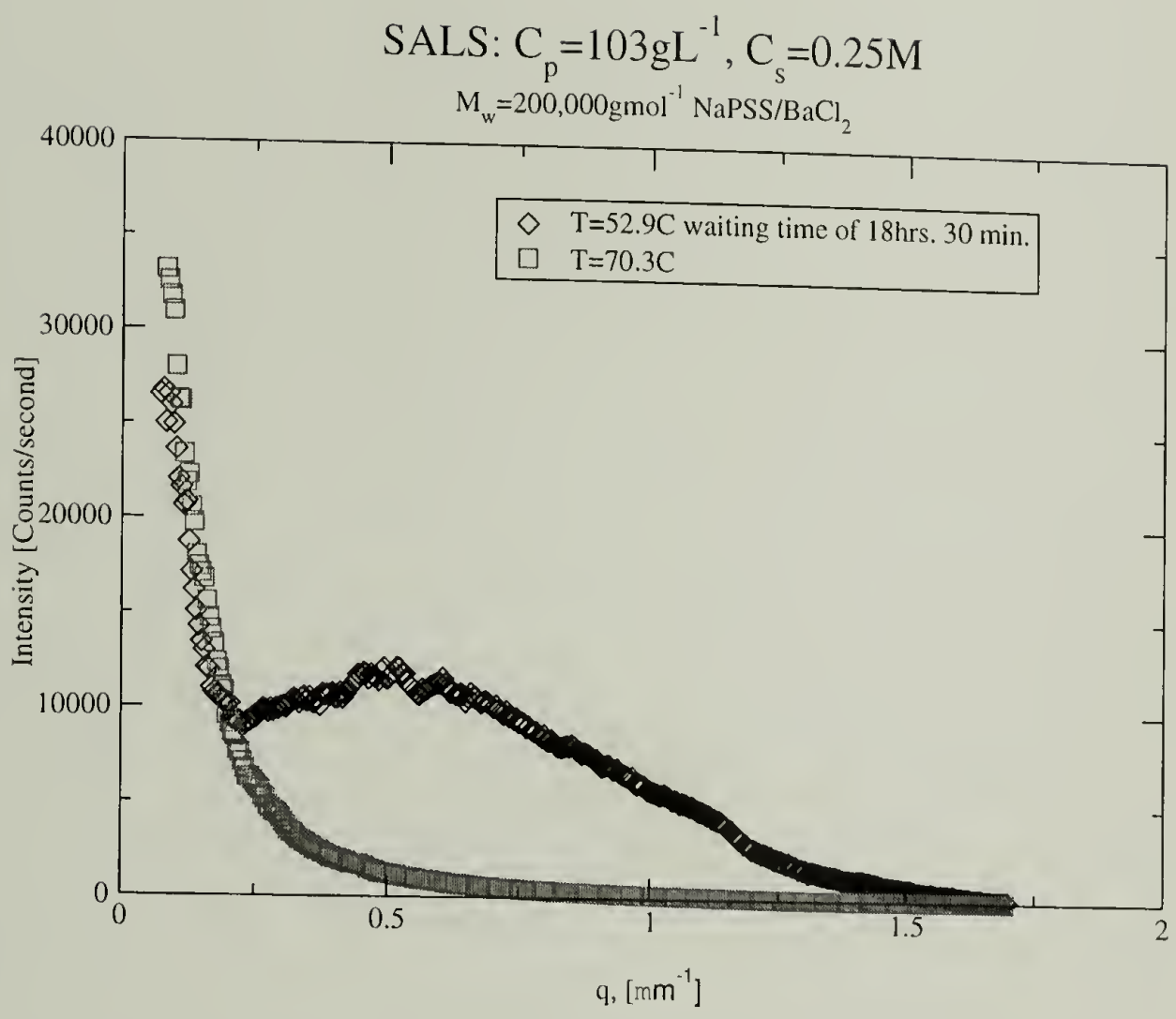

Figure 5.12: SALS observations for a fixed NaPSS concentration of 103gL^{-1}, barium chloride salt concentration of 0.25M and molecular weight of 200,000gmol^{-1}. Two temperatures are shown the high temperature limit of 70.3C and a temperature of 52.9C after 18 hrs. 30 min.. Notice the broad scattering peak, both at a finite wavevector and a continuous increase at the lower angle due to kinetics this kinetic phase behavior is unexplored in this system.

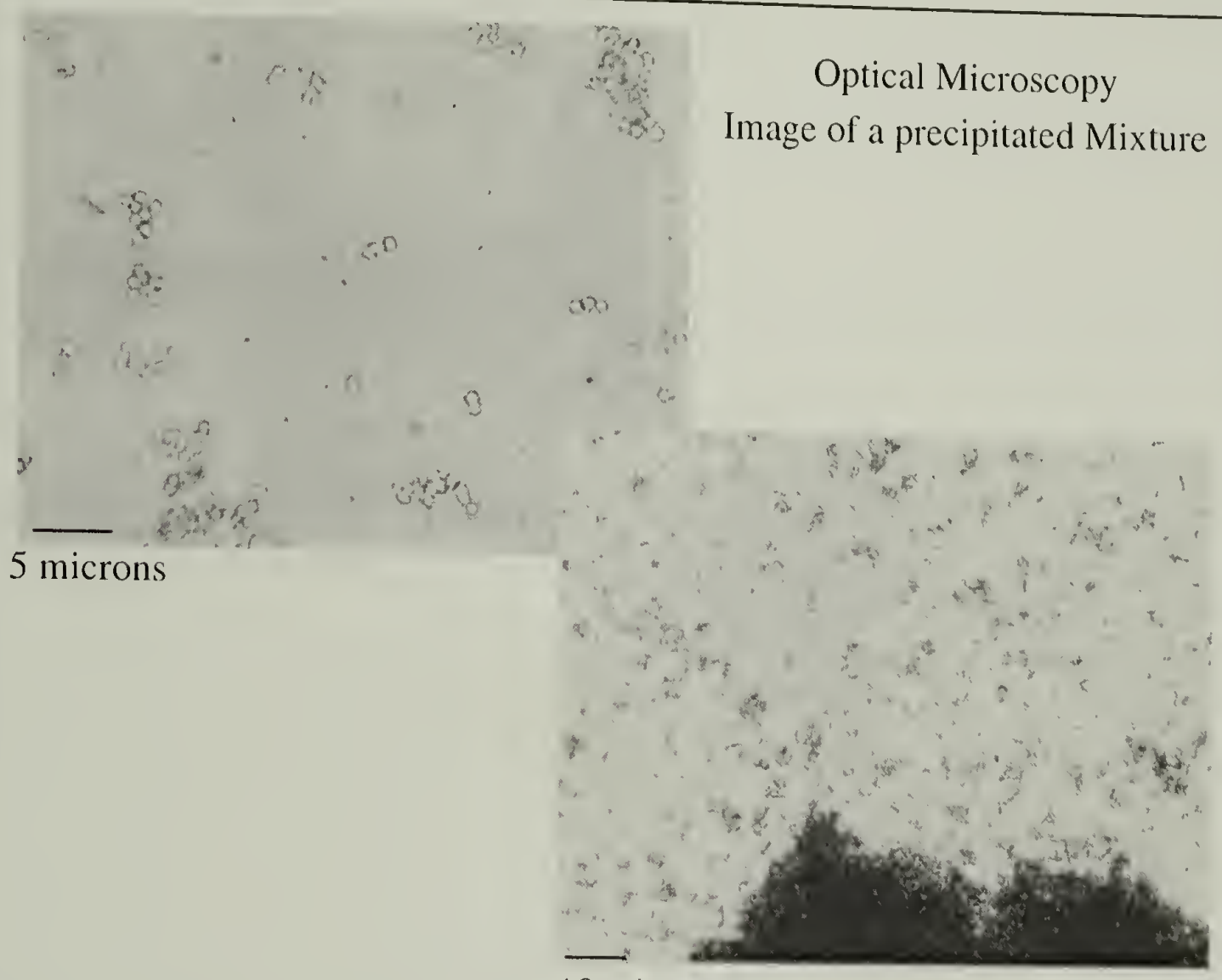

Figure 5.13: Optical Microscopy for an NaPSS / $BaCl_2$ solution with $M_w = 56{,}000$ $gmol^{-1}$, $C_p = 0.00625M$ and $C_s = 0.25M$. Two magnifications are shown along with the corresponding scale bars.

APPENDIX A

CHARACTERIZATION SUMMARY

18,000g/mol, Characterization Summary			
	Deuterated(R_g)	**Protonated(R_g)**	**Protonated(ξ)**
Expt No.	105	95	95
%S(E.A.)	95	97	97
PDI	1.05	1.03	1.03
M_1^{PS}g/mol	112	104	104
$M_{GPC,W}^{PS}$g/mol	8,800	8,822	8,822
$M_{GPC,N}^{PS}$g/mol	8,400	8,565	8,565
$N_{GPC,N}^{PS}$	81	82	82
%H_2O (TGA)	-	-	-

Molecular weight of sulfonated polystyrene is double the parent polystyrene, for high sulfonation degrees, so the identifying molecular weight used throughout for NaPSS is twice that of PS.

50,000g/mol, Characterization Summary	
	Protonated(ξ)
Expt No.	87
%S(E.A.)	100
PDI	1.02
M_1^{PS}g/mol	104
$M_{GPC,W}^{PS}$g/mol	24,850
$M_{GPC,N}^{PS}$g/mol	24,350
$N_{GPC,N}^{PS}$	234
%H_2O (TGA)	8.1

56,000g/mol, Characterization Summary			
	Deuterated(R_g)	**Protonated(R_g)**	**Protonated(ξ)**
Expt No.	119	108	109
%S(E.A.)	92	96	96
PDI	1.03	1.02	1.02
M_1^{PS}g/mol	112	104	104
$M_{GPC,W}^{PS}$g/mol	29,300	30,150	30,150
$M_{GPC,N}^{PS}$g/mol	28,500	29,800	29,800
$N_{GPC,N}^{PS}$	274	287	287
M_{GEL}^{NaPSS}g/mol	54,900	52,400	52,400
%H_2O (TGA)	8.6	7.5	8.8

120,000g/mol, Experiments Characterization Summary			
	Deuterated(R_g)	**Protonated(R_g)**	**Protonated(ξ)**
Expt No.	132	129	135
%S(E.A.)	86	89	-
%S(Titration)	-	-	95
PDI	1.05	1.02	1.02
M_1^{PS}g/mol	112	104	104
$M_{GPC,W}^{PS}$g/mol	65,900	61,000	61,000
$M_{GPC,N}^{PS}$g/mol	63,000	60,000	60,000
$N_{GPC,N}^{PS}$	563	577	577
%H_2O (TGA)	9.8	10.2	-

200,000g/mol, Characterization Summary			
	Deuterated(R_g)	**Protonated(R_g)**	**Protonated(ξ)**
Expt No.	131	133	134
%S(E.A.)	86	88	-
%S(Titration)	-	-	95
PDI	1.04	1.05	1.05
M_1^{PS}[gmol^{-1}]	112	104	104
$M_{GPC,W}^{PS}$[gmol^{-1}]	110,500	102,448	102,448
$M_{GPC,N}^{PS}$[gmol^{-1}]	107,300	100,085	100,085
$N_{GPC,N}^{PS}$[gmol^{-1}]	958	962	962
%H_2O (TGA)	9.0	11.1	10.3

400,000g/mol, Characterization Summary			
	Deuterated(R_g)	**Protonated(R_g)**	**Protonated(ξ)**
Expt No.	90	89	89
%S(E.A.)	-	-	-
PDI	1.04	1.05	1.05
M_1^{PS}g/mol	112	104	104
$M_{GPC,W}^{PS}$g/mol	217,600	217,000	217,000
$M_{GPC,N}^{PS}$g/mol	209,400	207,000	207,000
$N_{GPC,N}^{PS}$	1870	1990	1990
%H_2O (TGA)	17.5	-	-

APPENDIX B

SULFONATION OF POLY(STYRENE)S

The sodium-poly(styrene sulfonate) used in this study was prepared via sulfonation of protonated(h-PS) and deuterated(d-PS) polystyrene purchased from Polymer Laboratories and Polymer Source, Inc., respectively. These polystyrene standards were characterized by the manufacturers by gel permeation chromatography in tetrahydrofuran. Molecular weight details are given in Table I. The sulfonation method of Vink[77] was used with modification. The mass of polystyrene used was 400mg and 800mg for the protonated and deuterated reactions, respectively, the phosphorous pentoxide amount was increased by 50 percent as suggested by Smisek and Hoagland[78], and the amount of crushed ice required to precipitate the polymer was increased to 40g. The sulfonated polymer, recovered in de-ionized water, was titrated to a pH of 10 using sodium hydroxide solution purchased from Fisher Scientific, certified 0.201-0.199N, and subsequently filtered through a 0.22 μm Cellulose Acetate filter unit manufactured by Corning Costar. This clear solution was then dialyzed using Spectra/Por molecular-porous membrane tubing with molecular weight cut-off 3500 against water purified by a Milli-Q UF Plus system, a product of the Millipore Corporation, with resistivity 18MΩcm. Dialysis was performed with frequent change in the dialysis water. Once the conductance of the dialysis water remained constant over a 24 hour period and was below

0.6μS/cm the solutions were lyophillized. The lyophillized samples were characterized by elemental analysis for sulfur content and agarose gel electrophoreis. Gel electrophoresis was performed using a standard horizontal electrophoresis cell using sodium-poly(styrene sulfonate) from a Scientific Polymer Products Calibration Kit as mobility standards. Seakem LE Agarose of gel electrophoresis quality, distributed by FML Bioproducts, was used at a concentration of 0.9%, the balance buffer solution. The buffer solution used for gel setting as well as recirculating fluid was 0.01M reagent quality Na_2HPO_4. After electrophoresis with an applied field strength of 2V/cm for 2 hours the gel was stained with 0.01% methylene blue dye, de-stained with de-ionized water, and subsequently transfered to a flatbed scanner and digitized for analysis. The digitized bands were analyzed for the peak in the distribution and second moment, from which the polydispersity was obtained. [79]

Even after exhaustive drying of samples under high vacuum at 80°C, or heating for removal of water in an oven at 105°C, water was observed by thermal-gravimetric analysis. We find an average of 8% by mass of water content through our sample preparation.

APPENDIX C

NEUTRON SCATTERING CONSTANTS

Experimental Quantities.

$v_m(PSS^-)$[80]	$114.8 cm^3 mol^{-1}$
$v_s(H_2O)$[81]	$18.063\ cm^3 mol^{-1}$
$v_s(D_2O)$[81]	$18.137\ cm^3 mol^{-1}$
b_h(H-PSS^-)[82]	47.251 fm
b_d(D-PSS^-)[82]	120.124 fm
$b_s(H_2O)$[82]	-1.675 fm
$b_s(D_2O)$[82]	19.1458 fm

Experimental Quantities.

Formula	b_{COH} [fm]	b_{INC}[fm]	M_w [$gmol^{-1}$]	v_i [$cm^3 mol^{-1}$]
$C_8H_7SO_3$	47.251	176.924	183.2	114.8
$C_8D_7SO_3$	120.124	28.301	190.25	114.8
$NaC_8H_7SO_3$	50.883	180.514	206.19	108.2
$NaC_8D_7SO_3$	123.756	31.891	213.25	108.2
H_2O	-1.675	50.5498	18.01	18.063
D_2O	19.1458	8.086	20.023	18.137

APPENDIX D

LABELED CHAIN DATA

M_w=200,000gmol^{-1}, Radius of Gyration of labeled chains,T=25°C					
Cp[g/L]	**Cs[M]**	**$I_S(0)$, [cm^{-1}]Theory**	**$I_S(0)$, [cm^{-1}]**	**R_g,[Å]**	**I_{INC}, [cm^{-1}]**
400	0.0	15.06	12.3	128	0.52
400	0.03125	15.06	12.9	138	0.64
400	0.125	15.06	11.7	125	0.53
400	0.30	15.06	13.3	125	0.71
200	0.0	7.52	9.47	167	0.60
200	0.03125	7.52	7.66	160	0.56
200	0.125	7.52	7.38	143	0.527
200	0.250	7.52	7.06	126	0.614
200	0.31	7.52	7.00	107	0.610
100	0.0	3.76	4.11	169.7	0.331
100	0.03125	3.76	4.12	164.9	0.390
100	0.125	3.76	4.12	145.9	0.356
100	0.15	3.76	4.39	147.3	0.432
100	0.1875	3.76	4.08	131.5	0.387
50	0.0	1.89	2.05	189.6	0.381
50	0.03125	1.89	2.24	187.3	0.396
50	0.08	1.89	2.23	162.4	0.411
50	0.10	1.89	2.13	139.3	0.419

M_w=120,000gmol^{-1}, Radius of Gyration of labeled chains,T=25°C					
Cp[g/L]	**Cs[M]**	**$I_S(0)$, [cm^{-1}]Theory**	**$I_S(0)$, [cm^{-1}]**	**R_g,[Å]**	**I_{INC}, [cm^{-1}]**
200	0.0	4.46	4.73	112	0.366
200	0.0625	4.46	4.73	106	0.344
200	0.10	4.46	4.65	103	0.323
200	0.125	4.46	4.84	102	0.347
200	0.30	4.46	4.62	85	0.401
100	0.0		2.67	135	0.414
100	0.03125	2.23	2.65	127	0.409
100	0.0625	2.23	2.64	122	0.419
100	0.10	2.23	2.54	108	0.412
100	0.125	2.23	2.54	106	0.437
100	0.1875	2.23	2.52	84.3	0.447
100	0.20	2.23	2.56	76.0	0.402
50	0.0	1.11	1.49	157	0.421
50	0.03125	1.11	1.47	148	0.429
50	0.0625	1.11	1.46	129	0.438
50	0.09375	1.11	1.41	103	0.421
50	0.10	1.11	1.33	91.4	0.429
50	0.11	1.11	1.41	81.3	0.421

M_w=56,000gmol^{-1}, Radius of Gyration of labeled chains,T=25°C					
Cp[g/L]	**Cs[M]**	**$I_S(0)$, [cm^{-1}]Theory**	**$I_S(0)$, [cm^{-1}]**	**R_g,[Å]**	**I_{INC}, [cm^{-1}]**
200	0.0	2.10	2.30± 0.10	80.3±2.0	0.341
200	0.00078	2.10	2.17± 0.1	80.0±2.0	0.341
200	0.0156	2.10	1.96± 0.09	80.0±2.4	0.341
200	0.0625	2.10	2.18± 0.09	72.6±1.4	0.341
200	0.125	2.10	2.15± 0.10	70.2±1.7	0.341
200	0.1875	2.10	2.07± 0.09	63.6±1.5	0.341
200	0.250	2.10	2.04± 0.09	59.8±1.5	0.341
200	0.30	2.10	1.92± 0.08	55.2±1.2	0.341
200	0.325	2.10	1.98± 0.08	54.2±1.0	0.341
200	0.3375	2.10	1.94± 0.08	54.1±1.0	0.341

APPENDIX E

ORNL ORIGINAL PROPOSAL

Proposed Experiment

We propose to examine semi-dilute solutions of polyelectrolytes using small-angle neutron scattering. This work will lead to an understanding as to what happens to individual polyelectrolyte chains as a polyelectrolyte solution approaches an unstable phase boundary by changing the solution ionic strength. The polyelectrolyte and added salt we intend to investigate are sodium poly(styrene sulfonate) and barium chloride respectively with water as the solvent. We have constructed the phase diagram for this system. This system undergoes phase separation which can be seen visually. Such precipitation has also been observed by others.[1]

We intend to perform two different experiments. The first is to investigate one polymer concentration, approximately 2mg/mL and vary the salt concentration. This experiment is feasible with SANS by utilizing the scattering length contrast between heavy water and the hydrogenated poly(styrene sulfonate). In this experiment we will recover the chain statistics far from the unstable region. The data analysis should be straight forward, a Guinier plot from the radially averaged data should reveal the Rg^2.

In the second experiment we will investigate a higher polymer concentration approximately 20mg/mL with salt concentrations ranging between 0.002mg/mL to 200mg/mL. From these series of samples we will obtain a correlation length and Rg^2 as the system approaches the unstable region. We intend to utilize the high concentration labeling technique [2] by mixing deuterated and hydrogenated poly(styrene sulfonate) to provide the scattering length contrast and extract the two different length scales. For the high concentration labeling technique we will determine the details with Drs. Yuri Melnichenko and George Wignall at ORNL. We propose to purchase a perdeuterated poly(styrene) and perform a sulfonation reaction followed by counter-ion titration to obtain the sodium salt polyelectrolyte.

We have demonstrated the ability to sulfonate poly(styrene) in our laboratory and perform detailed purification. The samples which we intend to use will be well characterized with polydispersity less than 1.1. All sample preparation can easily be performed in our lab to produce a series of stock solutions. From these stock solutions, we can simply mix two test tubes at the SANS spectrometer into the required quartz cells.

1. A.Keller, K.A. Narh, J. Polym. Sci. Part B: Polym. Phys.,**31**, 231(1993).

2. Yu. Melnichenko, G. Wignall, Phys. Rev. Lett.,**78**, 686(1997).

Scientific Justification

Considering the phase diagram for a neutral polymer system which undergoes phase separation in the UCST type we understand the salient features as to the equilibrium properties of the single chain in dilute, semidilute, and concentrated solutions. Now if the same polymer were modified by the addition of a charged species we know that the phase diagrams are very different with different origins. The addition of new experimental parameters namely ionic strength, charge density, counter-ion valency, and added salt valency and concentration raises many more questions and opportunities for novel experiments to understand these systems. Many experiments have addressed the statics and dynamics of polyelectrolytes in dilute solution from low salt to high salt conditions using light scattering techniques[3]. However, with different labeling techniques now established, we now have the technology to investigate different length scales and separate the single chain structure factor from the total scattering. So, we wish to extend this effort to understand polyelectrolytes in non-dilute solutions with emphasis on understanding the connection between criticality and chain statistics in the context of the position of the system with respect to the phase diagram with constant temperature, charge density, and solvent type. We wish to answer the simplest question: What happens to the size of a labeled polyelectrolyte chain as an unstable region is approached by changing the ionic strength? To date no experiments have answered this question in the context of polymer's position in the polymer-salt phase diagram.

3. S. Förster, M. Schmidt, M. Antonietti, Polymer, **31**,781(1990).

Justification for Using Neutrons

We have examined these polyelectrolyte solutions with light scattering using an argon ion laser with wavelength 514nm. This does not allow us to probe simultaneously the various length scales of the monomer-monomer correlations and radius of gyration of the polyelectrolyte. The investigation of single chain statistics in non-dilute solutions by neutrons will hopefully clarify the pertinent length scales with knowledge of their origin using proper labeling techniques.

BIBLIOGRAPHY

[1] Muthukumar, M. *Pramana J. Phys.*, **1999**, 53,171.

[2] Alberts, B.;Bray, D.;Lewis, J.; Raff,M.;Roberts,K.;Watson, J.D. *Molecular Biology of the Cell*; Garland Publishing:New York, 1994.

[3] Cohen, F.E.; Prusiner, S.B. *Annu. Rev.*,**1998**, 67, 793.

[4] St George-Hyslop, P.H. *Scientific American*, **2000**, 283, 76.

[5] des Cloizeaux, J.; Jannink, G. *Polymers in Solution, Their Modelling and Structure*; Oxford University Press: Ney York, 1990.

[6] Janssen, S.; Schwahn, D.; Springer, T. *Phys. Rev. Lett.* **1992**, 68, 3180.

[7] Schwahn, D.; Schmackers, T.; Mortensen, K. *Phys. Rev. E* **1995**, 52, R1288.

[8] Chieux,P.; Sienko, M.J.*J.Chem.Phys.*, **1970** ,53, 566.

[9] Singh,R.R.; Pitzer,K.S. *J.Chem.Phys.*, **1990** ,92 6775.

[10] Fisher, M.E. *J. of Statistical Physics* **1994**, 75,1. and references there in.

[11] Narayanan,T.; Pitzer,K.S. *J.Chem.Phys.* **1995** ,102, 8118.

[12] Debye, P.; Hückel, E. *Phys. Z* **1923**, 24,185. McQuarrie, D.A. *Statistical Mechanics*; Harper Collins Publishers:New York, 1976.

[13] Muthukumar, M. *J.Chem. Phys.* **1987**,86,7230.

[14] Muthukumar, M. *J.Chem. Phys.* **1996**,105,5183.

[15] Beer, M.; Schmidt, M.; Muthukumar, M.*Macromolecules* **1997**,30,8375.

[16] Higgins, J.; Benoit, H. *Polymers and Neutron Scattering*; Oxford University Press:New York, 1996.

[17] de Gennes, P.G. *Scaling Concepts in Polymer Physics*; Cornell University Press:New York,1979.

[18] Borue, V.Yu.; Erukhimovich I.Ya. *Macromolecules***1988**,21,3240.

[19] Muthukumar, M. *Molecular Basis of Polymer Networks*, ed by A Baumgärtner. Springer:New York,1989(Vol 42, p 28).

[20] Joanny, J.-F.; Leibler, L. *J Phys Fr* **1990**, 51,545.

[21] Vilgis, T.A.; Borsali, R. *Physical Review A***1991**,43,6857.

[22] Olvera de la Cruz, M.; Belloni, L.; Delsanti, M.; Dalbiez, J.P.; Spalla, O.; Drifford M. *J Chem Phys* **1995**, 103,5781.

[23] Chaikin, P.M.; Lubensky, T.C. *Principles of Condensed Matter Physics* . Cambridge:Cambridge University Press, 1995.

[24] de Gennes, P.G.; Pincus,P.;Velasco,R.M.; Brochard,F. *J. de Physics* **1976** ,12, 1461.

[25] Delsanti, M.; Dalbiez, J.P.; Spalla, O.; Belloni, L.; Drifford, M. *ACS Symp. Ser.* **1994**, 548,381.

[26] Michaeli, I. *J.Polym.Sci.* **1960**, 48,291.

[27] Eisenberg,H.; Mohan, G.R. *J.Phys.Chem.* **1959** ,63,671.

[28] Heitz, C.; Francois, J. *Polymer* **1999**, 40,3331.

[29] Ikegami, A.; Imai, N.; *J. Polym. Sci.* **1962**,62,133.

[30] Narh, K.A.; Keller, A. *J. Polym. Sci., B: Polym. Phys.* **1993**,31,231.

[31] Axelos, M.; Mestdagh, M.; Francois J. *Macromolecules* **1994**,27,6594.

[32] Odijk, T. *Macromolecules* **1979** ,12, 688.

[33] Grimson, M.; Benmouna, M.; Benoit, H. *J.Chem. Soc., Faraday Trans.* **1988**, 84, 1563.

[34] Barrat, J.-L.; Joanny, J.-F. *Adv. in Chem. Phys.* **1996**, **XCIV**, 1.

[35] Yethiraj, A. *J.Chem.Phys* **1997**,108, 1184.

[36] Kaji, K.; Urakawa, H.; Kanaya, T.; Kitamaru, R. *J.Phys. France* **1988**,49, 993.

[37] Nierlich, M.; Williams, C.E.; Boue, F.; Cotton, J.P.; Daoud, M.; Farnoux, B.; Jannink, G.; Picot, C.; Moan, M.; Wolff, C.; Rinaudo, M.; de Gennes, P.G. *J. de Physique* **1979**,40, 701.

[38] Nierlich, M.; Boue, F.; Lapp, A.; Oberthur, R. *Colloid and Polymer Science* **1985**,263,955.

[39] Essafi, W.; Lafuma, F.; Williams, C.E.*ACS Symposium Series 548. Macroion Characterization from Dilute Solutions to Complex Fluids,* Schmitz, K.S., Ed.,1994.

[40] Essafi, W.; Lafuma, F.; Williams, C.E. *J. Phys. II France* **1995**,5, 1269.

[41] Ise, N., Okubo,T., Kungi, S.,Matsuoka,H., Yamamoto,K., Ishii,Y. *J. Chem. Phys.* **1984**,81, 3294.

[42] Matsuoka,H.,Ise, N., Okubo,T.,Kungi, S., Tomiyama,H., Yoshikawa,Y., *J. Chem. Phys.* **1985**,83, 378.

[43] Milas, M., Rinaudo,M., Duplessix,R.,Borsali,R.,Linder,P., *Macromolecules* **1995**,28, 3119.

[44] Ermi, B.; Amis, E.J. *Macromolecules* **1998**,31,7378.

[45] Borsali, R.; Nguyen, H.; Pecora, R. *Macromolecules* **1998**, 31, 1548.

[46] Boue, F.; Cotton, J.P.; Lapp, A.; Jannink, G. *J. Chem. Phys.* **1994**, 101,2562.

[47] Matsuoka, H.; Ise, N. *Adv. Polym. Sci.* **1994**, 114,187.

[48] Xie, Y.; Ludwig, K.F.; Bansil, R.; Gallagher, P.D.; Cao, X.; Morales, G. *Physica A* **1996**,232,94.

[49] Horkay, F.; Basser, P.J.; Hecht, A.-M.; Geissler, E. *Macromolecules* **2000**, 33, 8329.

[50] Dubois, E.; Boue, F.; *Macromolecules* **2001**, 34, 3684.

[51] Zhang, Y.; Douglas, J.F.; Ermi,B.D.; Amis, E.J. *J.Chem.Phys.* **2001**,114 ,3299.

[52] Williams, C.E.; Nierlich, M.; Cotton, J.P.; Jannink, G.; Boue, F.; Daoud, M.; Farnoux, B.; Picot, C.; de Gennes, P.G.; Rinaudo, M.; Moan, M.; Wolf, C. *J Polym Sci, Polym Lett Ed* **1979**, 17,379.

[53] Akcasu, A.Z.; Summerfield, G.C.; Jahansan, S.N.; Han, C.C.; Kim, C.Y.; Yu, H. *J Polym Sci, Polym Phys Ed* **1980**, 18,863.

[54] King, J.S.; Boyer, W.; Wignall, G.D.; Ullman, R. *Macromolecules* **1985**,18,709.

[55] Melnichenko, Y.B.; Wignall, G.D.; Van Hook, W.A.; Szydlowsky J.; Wikzura H.; Rebelo L.P. *Macromolecules* **1998**, 31,8436.

[56] Wignall, G.D.; Hendricks, R.W.;Koehler, W.C.; Lin, J.S.; Wai, M.P.; Thomas, E.L.; Stein, R.S. *Polymer* **1981**, 22,886.

[57] Melnichenko, Y.B.; Kiran, E.; Wignall, G.D.; Heath, K.D.; Salaniwal, S.; Cochran, H.D.; Stamm, M. *Macromolecules* **1999**, 32,5344.

[58] Takahashi, Y.; Matsumoto, N.; Iio, S.; Kondo, H.; Noda, I. *Langmuir* **1999**,15,4120.

[59] Spiteri, M.N.; Boue, F.; Lapp, A.; Cotton, J.P. *Phys. Rev. Lett.* **1996**, 77,5218.

[60] Prabhu, V.M.; Muthukumar,M.; Melnichenko,Y.B.; Wignall,G.D. *Polymer* **2001**, 42, 8935.

[61] Wignall, G.D. "Neutron Scattering from Polymers," in Encyclopedia of Polymer Science and Engineering. 2nd Edition. Edited by M Grayson and J Kroschwitz. New York:John Wiley & Sons, Inc, 1987(Vol 10, p 112).

[62] Glinka, C.J.; Barker, J.G.; Hammouda, B.; Krueger, S.; Moyer, J.J.; Orts, W.J. *J. App. Cryst.* **1998**, 31, 430.

[63] Schelten, J., In *Scattering Techniques Applied to Supramolecular and Nonequilibrium Systems*; Chen, S.H., Chu, B., Nossal, R.,Eds., NATO Advanced Study Series 73. Plenum:New York, 35-48(1981).

[64] Koehler, W.C. *Physica (Utrecht)* **1986**,137B,320.

[65] Wignall, G.D.;Bates, F.S. *J. Appl. Cryst.* **1986**, 20,28.

[66] Dubner, W.S.; Schultz, J.M.; Wignall, G.D. *J. Appl. Cryst.* **1990**,23,469.

[67] Hirose, E.; Iwamoto, Y.; Norisuye, T. *Macromolecules* **1999**, 32,8629.

[68] Wignall, G.D.; Ballard, D.G.H; Schelten, J. *J. Appl. Cryst.* **1974**,7,190.

[69] Strobl, G., *The Physics of Polymers* . New York:Springer 1996.

[70] Cotton, J.P.; Nierlich, M.; Boue, F.; Daoud, M.; Farnoux, B.; Jannink, G.; Duplessix R.; Picot C. *J. Chem. Phys.* **1976**,65,1101.

[71] Melnichenko, Y.B.; Wignall, G.D. *Phys.Rev. Lett.* **1997**, 78, 686.

[72] Francois, J.; Heitz, C.; Mestdagh, M. *Polymer* **1997**, 38, 5321.

[73] Branden, C.; Tooze, J. *Introduction to Protein Structure.* New York:Garland Publishing, p. 176.

[74] Weaver, R.F. *Molecular Biology.* Boston:McGraw-Hill, p. 331.

[75] Koberstein, J.; Russell, T.P.; Stein, R.S. *J. Polym. Sci. Polym. Phys.* **1979**, 17, 1719.

[76] Allain, C.; Cloitre, M., Wafra, M.; *Phys. Rev. Lett.* **1995**, 74, 1478.

[77] Vink, H. *Makromol.Chem.* **1981**,182,279.

[78] Smisek, D.L.; Hoagland, D.A.; *Macromolecules* **1989**,22,2270.

[79] Smisek, D.L. Ph.D. Thesis, University of Massachusetts-Amherst, 1991.

[80] Ise, N.; Okubo, T. *J. Am. Chem. Soc.* **1968**,90,4527.

[81] Handbook of Chemistry and Physics, ed DR Lide, 74th Edition, 1993(pp 6-14).

[82] Sears, V.F. *Neutron News* **1992**, 3,26.

[83] Drews, A.R.; Barker, J.G.; Glinka, C.J.; Agamalian, M. *Physica B* **1998**,241-243, 189.

[84] Schwahn, D.; Miksovsky, A.; Rauch, H.; Seidl, E.; Zugarek, G.*Nuclear Inst. and Methods in Phys. Research* **1985**, A239, 229.